ABSTRACT OF THESIS

Name of Candidate DAVID J.R. HOUSTON

Address DEPARTMENT OF PHYSICS, JAMES CLERK MAXWELL BUILDING, EH9 3JZ.

Degree DOCTOR OF PHILOSOPHY *Date* APRIL, 1976.

Title of Thesis NUMERICAL STUDIES IN HYDRODYNAMIC STABILITY THEORY

An extensive study of the eigenstate spectrum of the Orr-Sommerfeld equation for Blasius flow has been carried out. Both spatially and temporally developing disturbances have been considered for a wide range of Reynolds numbers. Variation in frequency or wavenumber has also been investigated.

Numerical methods have been used to probe the structure of the eigenvalue spectrum and to compute the corresponding eigenfunctions. All these methods are based on a finite difference model of the differential equation. A more analytical approach using a straight line approximation to the boundary layer profile has also been successful.

The results indicate that in either space or time the Blasius spectrum is discrete and, in contrast to channel flows, finite. The much-studied fundamental state is different in many ways from the higher eigenstates which occur in pairs and whose number increases as the Reynolds number, frequency or wavenumber increases. The possibility of an additional continuous spectrum is not ruled out but is considered unlikely from the results of the more analytical approach which takes into account the entire semi-infinite flow.

For comparison, the same methods have been applied to plane Poiseuille flow and the results obtained are in excellent agreement with other authors using rather different methods.

Use other side if necessary.

NUMERICAL STUDIES IN HYDRODYNAMICS

STABILITY THEORY

Thesis

Submitted by

DAVID J.R. HOUSTON, B.Sc.

for the degree of

DOCTOR OF PHILOSOPHY

University of Edinburgh

April, 1976.

To my parents

DECLARATION

I declare that this thesis is of my own composition and that, except where acknowledgement is made by reference, the work described is entirely my own and was carried out in the Department of Physics between July 1973 and September 1975.

Publication Note

Much of the work described in Chapter 4 of this thesis is incorporated in the paper

"Higher Eigenstates in Boundary Layer Stability Theory"

D. Corner, D.J.R. Houston and M.A.S. Ross

which has been accepted for publication by the Journal of Fluid Mechanics.

ACKNOWLEDGEMENTS

The author gratefully acknowledges the help of his supervisors Dr. R. Jordinson and Dr. F.H. Barnes, and the financial assistance of the Ministry of Defence.

He would also like to thank Professor W. Cochran for use of the facilities of the Department of Physics, and Edinburgh Regional Computing Centre for providing an excellent computing environment.

A special thank-you is due to Dr. M.A.S. Ross, who first aroused the author's interest in Stability Theory, for many stimulating discussions. He is also grateful to Dr. A. Davey, Dr. M. Gaster and Dr. L.M. Mack for helpful advice and correspondence.

The typing of this thesis was cheerfully undertaken by Mrs. R. Chester whose help is deeply appreciated.

Finally, the author would like to thank his wife for her understanding and encouragement.

CONTENTS

C O N T E N T S (Contd.)

ABSTRACT

An extensive study of the eigenstate spectrum of the Orr-Sommerfeld equation for Blasius flow has been carried out. Both spatially and temporally developing disturbances have been considered for a wide range of Reynolds numbers. Variation in frequency or wavenumber has also been investigated.

Numerical methods have been used to probe the structure of the eigenvalue spectrum and to compute the corresponding eigenfunctions. All these methods are based on a finite difference model of the differential equation. A more analytical approach using a straight line approximation to the boundary layer profile has also been successful.

The results indicate that in either space or time the Blasius spectrum is discrete and, in contrast to channel flows, finite. The much-studied fundamental state is different in many ways from the higher eigenstates which occur in pairs and whose number increases as the Reynolds number, frequency or wavenumber increases. The possibility of an additional continuous spectrum is not ruled out but is considered unlikely from the results of the more analytical approach which takes into account the entire semi-infinite flow.

For comparison, the same methods have been applied to plane Poiseuille flow and the results obtained are in excellent agreement with other authors using rather different methods.

LIST OF SYMBOLS

The following symbols have the designated meanings unless otherwise indicated in the text.

A, B	arbitrary constants
b	Blasius constant (÷ 1.216780621614)
c	non-dimensional complex wave velocity
D	differential operator $(= \frac{d}{dz})$
d	differential symbol
F	non-dimensional frequency parameter $(= \frac{\beta}{R})$
F(z)	dependent variable of Blasius equation (3.1)
f(η)	dependent variable of Blasius equation (2.10)
h	net spacing, step length
Im	imaginary part
i	$(-1)^{\frac{1}{2}}$
M(λ)	complex penta-diagonal discretisation matrix
n	number of equal intervals of length h
O(m)	order of m (applied to quantity q where $\frac{q}{m} \rightarrow$ finite limit)
P(x,z)	mean flow pressure
p(x,z,t)	pressure
R	Reynolds number $(= \frac{U_o \delta_1}{\nu}$ for Blasius flow)
Re	real part
S_m	sector of complex z-plane (m = 1,2,3)
$\underline{s}$	normalisation vector
t	time
U_o	maximum mean flow velocity in x direction
U(x,z)	x component of mean flow velocity
u(x,z,t)	x component of flow velocity
$\underline{v}$	complex eigenvector of M(λ)

LIST OF SYMBOLS (Contd.)

$W(x,z)$	z component of mean flow velocity
$w(x,z,t)$	z component of flow velocity
x	downstream coordinate
y	spanwise coordinate
z	vertical coordinate
z_c	critical complex value of z (where $U(z) = c$)
z_{max}	outer limit (for numerical work on Blasius flow)
α	non-dimensional wave number (space: complex, time: real)
β	non-dimensional real frequency
γ	non-dimensional complex parameter ($\gamma^2 = \alpha^2 + iR(\alpha-\beta)$)
$\delta_1(x)$	boundary layer displacement thickness
η	non-dimensional independent variable of Blasius equation (2.10)
λ	complex eigenvalue (space: α, time: c)
μ	viscosity
ν	kinematic viscosity ($= \frac{\mu}{\rho}$)
π	constant ($\doteq 3.14159265$)
ρ	density
$\underline{\phi}$	complex vector (discretised version of $\phi(z)$)
$\phi(z)$	complex eigenfunction of Orr-Sommerfeld equation
$\chi(z)$	complex eigenfunction of adjoint Orr-Sommerfeld equation
$\Psi(z)$	parallel mean flow stream function
$\psi(x,z,t)$	stream function
∂	partial differential symbol
∇^2	$\frac{\partial^2}{\partial x^2} + \frac{\partial^2}{\partial z^2}$

as subscripts:		as superscripts:	
i	imaginary part	j	iteration number
j	net point, state in spectrum		
r	real part		

CHAPTER 1

INTRODUCTION

1.1 Historical Review of Hydrodynamic Stability Theory

The transition from laminar to turbulent flow is one of the most fascinating discontinuities of Nature. Although an obvious macroscopic phenomenon, it remains more of a mystery than the intangible science of quantum mechanics, for example, which governs the very structure of matter.

It was Lord Rayleigh[1] who, in 1880, made the first brilliant attempt to solve the transition problem. He proposed that all real laminar flows contained small perturbations which in unstable conditions might grow in energy and eventually change the whole nature of the flow. Rayleigh avoided the problems of three-dimensional analysis by considering a purely two-dimensional perturbation of a parallel incompressible flow and the small disturbances were assumed to be simple harmonic waves travelling downstream. This simple model is the basis of stability theory.

At about the same time, Osborne Reynolds[2] was conducting a series of meticulous experiments in order to study the onset of turbulence. He discovered that transition occurred at a critical value of a parameter R (now known as the Reynolds number) representing the ratio of the inertial to the viscous forces in a fluid. In fact, $R = \frac{UL}{\nu}$ where U and L are typical velocity and length parameters of the flow and ν is the kinematic viscosity of the fluid. This introduced the principle of dynamical similarity where physically different flows of the same geometry and Reynolds number could be considered equivalent.

Since the critical Reynolds number was known to be high (about 1000 in the case of plane Poiseuille flow) Rayleigh ignored the viscous terms in the Navier-Stokes equations. His other basic assumption was that the perturbation amplitude was very small so that terms non-linear in the perturbation could also be neglected. This reduced the problem to the solution of a second order linear differential equation.

By considering the energy of the perturbation, Lorentz[3] showed that the linearisation of the equations was a serious limitation of the Rayleigh model. Nevertheless the linearised theory continued to develop but the viscous terms which were neglected in the Rayleigh equation were reinstated to give the fourth order Orr-Sommerfeld equation (1907). The basic mathematical aspects of this equation will be fully discussed in Chapter 2.

After 1904, when Prandtl[4] introduced the boundary layer concept, stability theory was applied to nearly parallel flows like the boundary layer on a flat plate as well as the more traditional strictly parallel flows like plane Couette and plane Poiseuille flow. The brilliant work on centrifugal instability by G.I. Taylor[5] in 1923 should also be mentioned, but this is rather different from the stability of parallel flows.

In 1924, the method of asymptotic expansions was used by Heisenberg[6] to solve the Orr-Sommerfeld equation for plane Poiseuille flow. His controversial conclusion was that the flow was unstable in contrast to the theoretically stable plane Couette flow. A few years later, a similar approach was used by Tollmien[7] and Schlichting[8,9] who predicted the instability of the boundary layer on a flat plate (Blasius flow).

Taylor[10] questioned the validity of Tollmien and Schlichting's results considering the downstream growth in the thickness of the boundary layer but this doubt was removed by the independent calculations of Lin[11], and by the remarkable experiments of Schubauer and Skramstad[12] in 1947. Indeed, this was the triumph of linearised stability theory that the theoretical and experimental results for Blasius flow should agree so well. Attention was centred on the so-called neutral curve which determined under which conditions the flow was unstable (see Figure 1.1).

Improved asymptotic solutions were obtained by Tollmien[13] and the asymptotic theory of the Orr-Sommerfeld equation was thoroughly investigated by Wasow[14,15,16]. For an excellent discussion of the implication of these results, the reader is referred to Lin[17].

1.2 The Influence of the Computer

The rapid growth in the technology and availability of digital computing in the 1950's had a tremendous effect on all branches of scientific research. Calculations which had been too tedious to perform by hand or desk calculator suddenly became relatively effortless. This opened up completely new avenues of research and the great power of numerical analysis was apparent.

Since only the leading terms of asymptotic expansions could be considered, the analytical theory of the Orr-Sommerfeld equation was limited in accuracy and so it was obvious that a purely numerical solution should be attempted. This was accomplished by L.H. Thomas[18] who, at Lin's instigation, obtained accurate solutions for plane Poiseuille flow in 1953. Most of these results

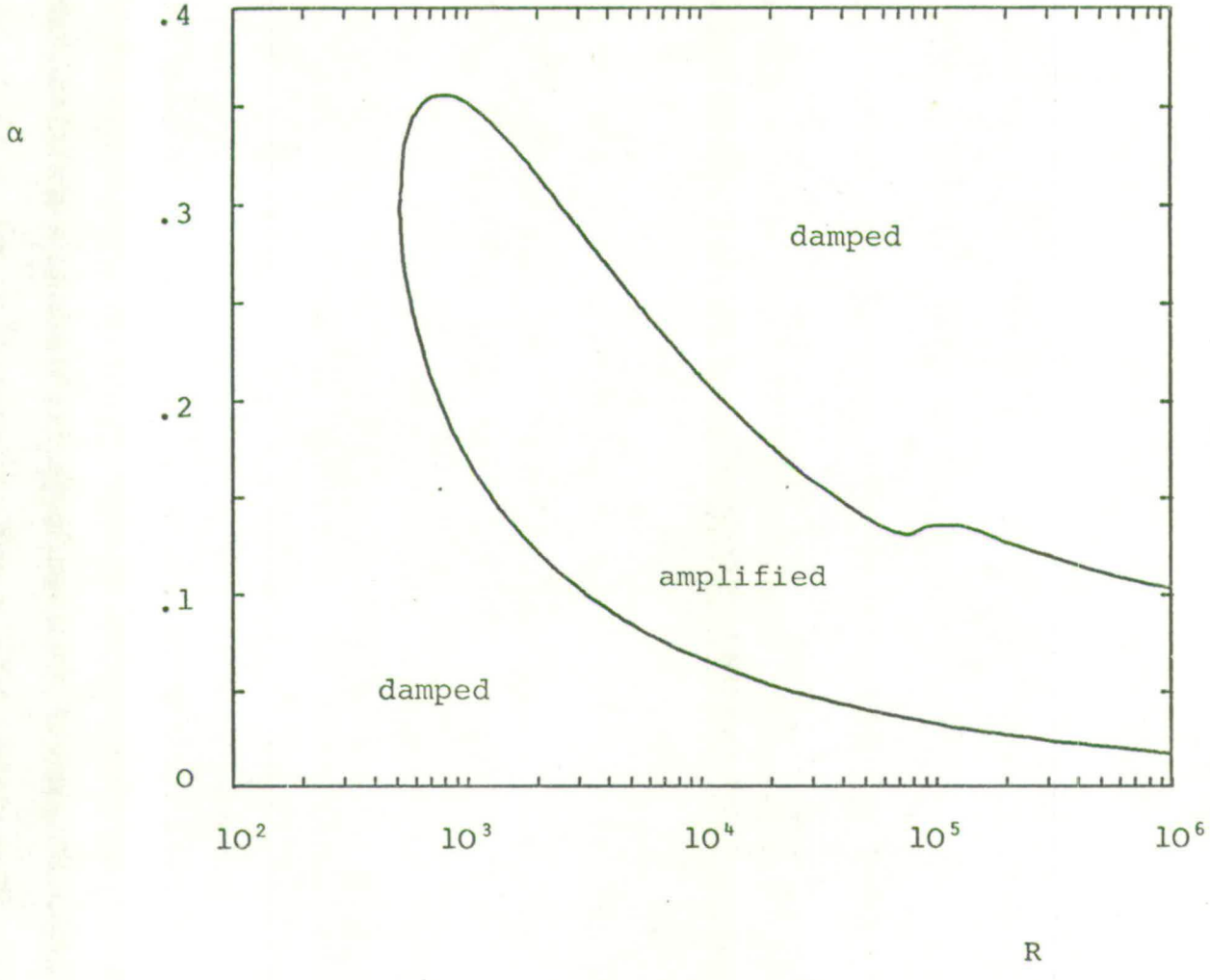

Figure 1.1 Neutral Stability Curve.
(Computed by the author).

did not correspond to neutral disturbances and so could not be directly compared with the neutral curve of Lin[11]. However, Shen[19] produced further curves of constant amplification using analytical methods and there was some discrepancy with the results of Thomas.

The first numerical study of boundary layer stability was completed in 1961 by Kurtz[20] who used the implicit finite difference method of Thomas. Three years later, Kaplan[21] employed an explicit shooting method to tackle the same problem, solving separately for the viscous and non-viscous solutions. In spite of the difference in approach, the results of Kurtz and Kaplan were in good agreement.

In all the theoretical and numerical work so far discussed, only the temporal development of disturbances was considered. This is because the temporal eigenvalue appears linearly in the Orr-Sommerfeld equation and so the analysis is relatively straightforward. However, in experiments (e.g. those of Schubauer and Skramstad), it is convenient to measure the spatial development of the perturbation but the corresponding eigenvalue is non-linear. Since the numerical solution for a non-linear eigenvalue is not much more difficult to obtain, it became attractive to produce spatial solutions for direct comparison with experiment. For near-neutral disturbances, however, the space-time transformation of Gaster[22] could be used instead.

Spatially developing disturbances in plane Poiseuille flow were investigated theoretically by Watson[23] in 1962. Michalke[24,25] made an excellent numerical study of both temporal and spatial stability in a shear flow. Spatial solutions for Blasius flow were obtained by Jordinson[26] for direct comparison with experiments carried out by Ross et al.[27]. These

experiments were similar to those of Schubauer and Skramstad[12] but rather more refined, including computer control of the wind tunnel and its instruments. Agreement between theory and experiment was good, and was further improved by Barry and Ross[28] who solved an extended form of the Orr-Sommerfeld equation which took some account of the change in thickness of the boundary layer.

For a description of other experimental results, the reader is referred to the review of Stuart[29]. The excellent survey of numerical methods by Ross[30] is also recommended.

1.3 Non-Linear Theory

In 1951, a non-linear stability model for plane Poiseuille flow was devised by Meksyn and Stuart[31] and developed by Stuart[32] and Watson[23]. It took account of the following second order effects - distortion of the mean flow, generation of the second harmonic of the perturbation, and distortion of the perturbation itself.

The Stuart model was extended by Pekeris and Shkoller[33] to include third order effects, where the perturbation and its harmonics were expanded in eigenfunctions of the Orr-Sommerfeld equation and the mean flow distortion was expanded in cosine functions. Despite the enormous amount of numerical analysis involved, the problem was solved successfully and it was found that the amplitude of high order eigenstates (heavily damped by linear theory) suddenly increased in 'a cascade' of energy. This behaviour was found at Reynolds numbers far below the critical Reynolds number for plane Poiseuille flow according to linearised stability theory.

Since plane Poiseuille flow has a constant Reynolds number, non-linear theory in this case is much easier to apply than in the case of the boundary layer where the Reynolds number increases downstream. There is much controversy over the best way of dealing with this effect, as is apparent from the recent work of Bouthier[34], Ling and Reynolds[35], and Gaster[36]. A completely numerical approach to the non-linear stability of the Blasius boundary layer has been made by Corner et al.[37] with some success.

Meanwhile the Stuart model continues to develop. See, for example, Stewartson and Stuart[38].

1.4 The Spectrum of the Orr-Sommerfeld Equation

For many years, the least stable eigenstate of the Orr-Sommerfeld equation was the only one considered worth studying. However, after the complete asymptotic theory of Wasow[14], Morawetz[39] embarked on a study of the spectrum of eigenvalues for three flows, plane Couette, plane Poiseuille and Blasius flow. Her results will be discussed in Chapter 2.

In 1954, Grohne[40] investigated the eigenvalues of plane Couette flow but his results do not agree with later work[43]. In 1961, Schensted[41] made an extensive study of the spectrum in the case of plane parallel flows of finite width and axisymmetric Poiseuille flow. Some of her conclusions will be presented in Chapter 2. A further contribution to the mathematical theory of the Orr-Sommerfeld equation for plane parallel flows of finite width was made by Eckhaus[42].

Since 1964, several numerical investigations of the temporal eigenvalue spectrum have been carried out. Gallagher and

Mercer[43,44] have studied plane Couette flow. The plane Poiseuille spectrum has been tackled by Grosch and Salwen[45] and even more successfuly by Orszag[46] while the axisymmetric case has been studied by Davey and Drazin[47] and Salwen and Grosch[48].

In the case of unbounded flows like the boundary layer on a flat plate, very little work has been done. Jordinson[49] found some temporal and spatial Blasius eigenvalues and computed their eigenfunctions. Two higher spatial states were also found by Corner[50] who considered both the ordinary Orr-Sommerfeld equation and the extended form of Barry and Ross[28].

It was intended that the present work should fill the gap in knowledge which exists concerning the structure of the spatial and temporal spectrum of the Orr-Sommerfeld equation for Blasius flow. In addition to the computation of a considerable number of eigenvalues and eigenfunctions it was hoped that answers to the following questions might be obtained.

(1) Is there a continuous part of the spectrum due to the semi-infinite width of the flow?

(2) Is the discrete part of the spectrum finite or are there infinitely many states as in the case of bounded flows?

(3) Is it possible to classify the eigenstates in some way which is consistent with their behaviour?

(4) Is there any qualitative difference in the nature of the spatial and temporal eigenstates?

Since the present work was begun, results for the temporal Blasius spectrum have been obtained by Mack[51] and Davey[52] using rather different numerical methods. These will be compared with the present results in Chapter 5.

CHAPTER 2

MATHEMATICAL PRELIMINARIES

2.1 Basic Equations

This work is concerned with two-dimensional, viscous, incompressible fluid motion. A rectangular coordinate system is used with the x-axis pointing downstream and the z-axis perpendicular to the basic flow. It is assumed throughout that there is no variation in the y-direction.

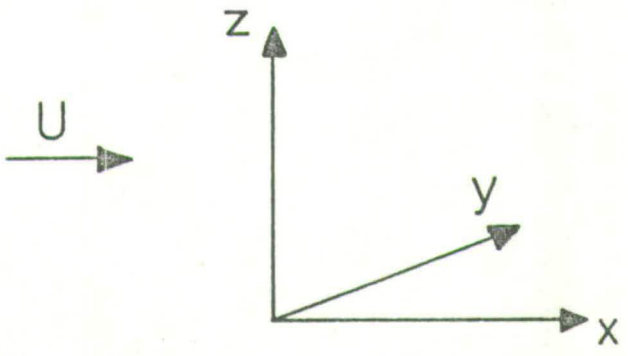

The equations of motion are the Navier-Stokes equations

$$\frac{\partial u}{\partial t} + u\frac{\partial u}{\partial x} + w\frac{\partial u}{\partial z} + \frac{1}{\rho}\frac{\partial p}{\partial x} = \nu \nabla^2 u \qquad (2.1a)$$

$$\frac{\partial w}{\partial z} + u\frac{\partial w}{\partial x} + w\frac{\partial w}{\partial z} + \frac{1}{\rho}\frac{\partial p}{\partial z} = \nu \nabla^2 w \qquad (2.1b)$$

and the continuity equation

$$\frac{\partial u}{\partial x} + \frac{\partial w}{\partial z} = 0 \qquad (2.2)$$

which is automatically satisfied by defining a stream function $\psi(x,z,t)$ such that

$$u = \frac{\partial \psi}{\partial z}, \qquad w = -\frac{\partial \psi}{\partial x}.$$

Since the only component of vorticity $h(x,z,t)$ is

$$h = \frac{\partial u}{\partial z} - \frac{\partial w}{\partial x} = \nabla^2 \psi,$$

by eliminating the pressure, equations (2.1) may be written in the form

$$\frac{\partial \nabla^2 \psi}{\partial t} + \frac{\partial \psi}{\partial z}\frac{\partial \nabla^2 \psi}{\partial x} - \frac{\partial \psi}{\partial x}\frac{\partial \nabla^2 \psi}{\partial z} = \nu \nabla^4 \psi \qquad (2.3)$$

which is known as the vorticity equation.

2.2 Parallel Mean Flow

Suppose that the flow is steady and unidirectional so that the equations of motion are independent of t and W is identically zero. Equation (2.2) implies $\frac{\partial U}{\partial x} = 0$ and (2.1b) gives $\frac{\partial P}{\partial z} = 0$. Equation (2.1a) then reduces to

$$\frac{dP}{dx} = \mu \frac{d^2 U}{dz^2} \quad . \qquad (2.4)$$

Since U is independent of x, $\frac{dP}{dx}$ is constant and the general solution of (2.4) is the quadratic

$$U = \frac{1}{2\mu}\frac{dP}{dx} z^2 + Az + B \quad . \qquad (2.5)$$

Two special cases of (2.5) are of particular importance, both being flows between parallel walls. It is convenient to make all quantities non-dimensional with respect to the Reynolds number $R = \frac{U_o H}{\nu}$ where H is half the width of the channel and U_o is the maximum flow velocity.

Assuming this non-dimensionalisation, consider flow between the planes $z = 0$ and $z = 2$ in the following cases.

(i) Plane Couette Flow

There is no pressure gradient so that $\frac{dP}{dx} = 0$ and the profile is linear. The plane $z = 0$ is stationary but the

plane $z = 2$ moves parallel to itself with unit velocity so that the boundary conditions are

$$U(0) = 0, \qquad U(2) = 1$$

so that (2.5) reduces to

$$U = \frac{1}{2}z. \tag{2.6}$$

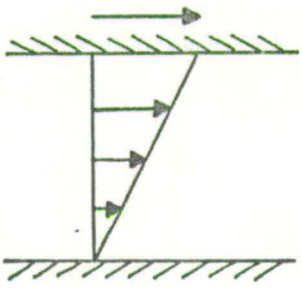

(ii) Plane Poiseuille Flow

The pressure gradient is favourable and both planes are stationary. The boundary conditions are

$$U(0) = U(2) = 0$$

giving the parabolic profile

$$U = z(2 - z) \tag{2.7}$$

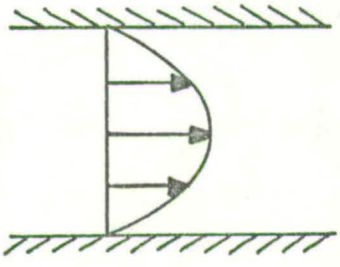

2.3 Blasius Mean Flow

Consider the flow over a semi-infinite flat plate lying in the plane $z = 0$ with its leading edge along the y-axis. The flow is uniform and parallel to the x-axis except in the

immediate vicinity of the plate where the fluid velocity is affected by the no-slip requirement on the surface. This region of intense vorticity where viscous and inertial forces are of comparable magnitude is called the boundary layer. Since it is very thin in comparison with the downstream distance from the leading edge, some simplification of the equations of motion is possible by neglecting terms of small order.

In this way, equations (2.1) become

$$\frac{\partial u}{\partial t} + u\frac{\partial u}{\partial x} + w\frac{\partial u}{\partial z} + \frac{1}{\rho}\frac{\partial p}{\partial x} = \nu \frac{\partial^2 u}{\partial z^2} \qquad (2.8a)$$

$$\frac{1}{\rho}\frac{\partial p}{\partial z} = 0 \qquad (2.8b)$$

Equations (2.8) together with (2.2) are the boundary layer equations first derived by Prandtl[4] A full discussion of their validity is given by Jones & Watson[53] .

In the absence of a pressure gradient and under steady conditions equations (2.8) reduce to

$$U\frac{\partial U}{\partial x} + W\frac{\partial U}{\partial z} = \nu \frac{\partial^2 U}{\partial z^2} \qquad (2.9)$$

and the boundary conditions for flow over a flat plate are

$$U = W = 0 \qquad z = 0$$

$$U \to U_o \qquad z \to \infty .$$

The solution of (2.9) is of similarity type and was first obtained by Blasius[54] . The similarity variable η is non-dimensional and the stream function may be written:

$$\psi = (2\nu U_o x)^{\frac{1}{2}} f(\eta) \quad \text{where} \quad \eta = \left(\frac{U_o}{2\nu x}\right)^{\frac{1}{2}} z .$$

Thus

$$U = U_o f' , \qquad W = \left(\frac{\nu U_o}{2x}\right)^{\frac{1}{2}} (\eta f' - f),$$

$$\frac{\partial U}{\partial z} = U_o \left(\frac{U_o}{2\nu x}\right)^{\frac{1}{2}} f'', \qquad \frac{\partial U}{\partial x} = -\frac{U_o}{2x}\, \eta f'' ,$$

and

$$\frac{\partial^2 U}{\partial z^2} = \frac{U_o^2}{2\nu x} f''' \qquad \text{where } ' \text{ denotes } \frac{d}{d\eta} .$$

Substitution of these expressions into (2.9) yields the ordinary differential equation

$$f''' + ff'' = 0 \tag{2.10}$$

with boundary conditions

$$f = f' = 0 \qquad \eta = 0,$$

$$f' \to 1 \qquad \eta \to \infty .$$

Equation (2.10) is non-linear and must be solved numerically. With η defined as above and $f''(0) \doteq \cdot 4696$, a solution is obtained with $\lim_{\eta \to \infty} f' = 1$ as required (Jones & Watson[53]). The displacement thickness, δ_1, of the boundary layer is given by

$$\delta_1 = \int_0^\infty \left(1 - \frac{U}{U_o}\right) dz = \left(\frac{2\nu x}{U_o}\right)^{\frac{1}{2}} \int_0^\infty (1-f')\, d\eta$$

$$= \left(\frac{2\nu x}{U_o}\right)^{\frac{1}{2}} b \tag{2.11}$$

where b has the value $1 \cdot 21678$ (Jones & Watson[53]).

Equation (2.10) has the property that if $F(\eta)$ is a solution, so also is $f(\eta) = sF(s\eta)$ where s is an arbitrary scaling factor. Since the boundary layer Reynolds number is normally defined as $R = \frac{U_o \delta_1}{\nu}$ it is necessary to choose $s = \frac{1}{b}$ so that the non-dimensional z $(= \frac{\eta}{b})$ is the new

independent variable. Thus the Blasius equation (2.10) should be solved for $F(z)$ with $F''(0) \doteq .4696b^3$, where $'$ now denotes $\frac{d}{dz}$.

The non-dimensional velocity components are given by

$$U(z) = \frac{1}{b^2} F'(z) \qquad W(z) = \frac{1}{R}(zF'(z) - F(z)). \quad (2.12)$$

Note that since R is large $U >> W$ and the Blasius flow is almost parallel.

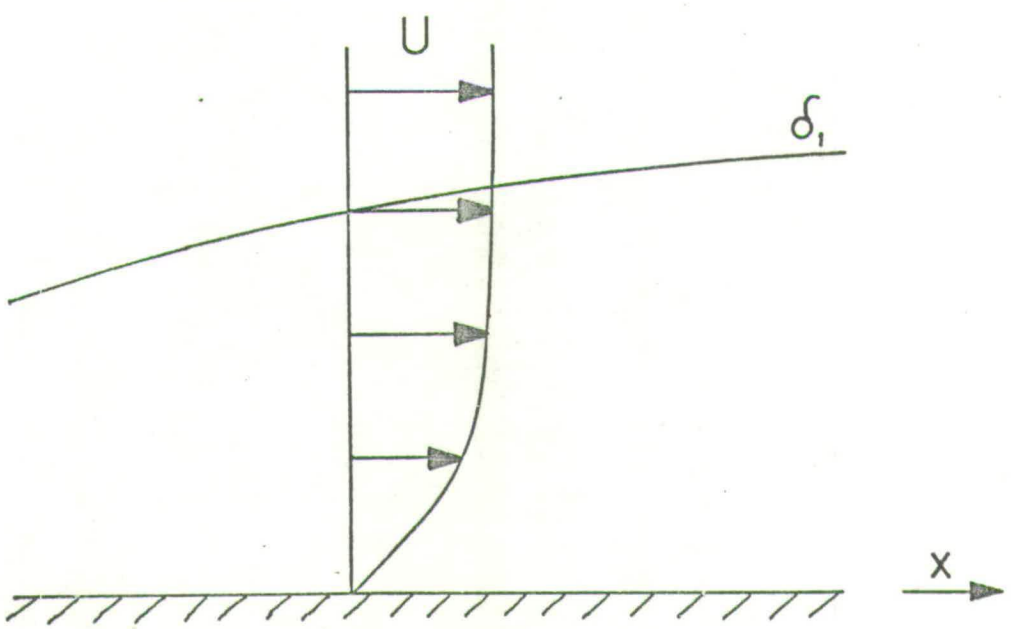

2.4 Orr-Sommerfeld Equation

Consider a general two-dimensional perturbation with stream function $\psi(x,z,t)$ imposed on a parallel mean flow $\Psi(z)$. The total stream function $\Psi + \varepsilon\psi$ (where ε is a small parameter representing the amplitude of the disturbance) must satisfy the vorticity equation (2.3) as, indeed, must Ψ itself. Subtraction of the equation for Ψ from the total equation eliminates $O(1)$ terms involving only the mean flow and, since ε is small, the $O(\varepsilon^2)$ terms which are non-linear in

the perturbation may be ignored. This procedure leaves the following equation to be solved:

$$\frac{\partial(\nabla^2\psi)}{\partial t} + \frac{\partial\Psi}{\partial z}\frac{\partial(\nabla^2\psi)}{\partial x} - \frac{\partial\psi}{\partial x}\frac{\partial^3\Psi}{\partial z^3} = \nu\nabla^4\psi \,. \qquad (2.13)$$

Assume now that all variables have been made non-dimensional with respect to an appropriate Reynolds number and that only wavy disturbances of the form

$$\psi(x,z,t) = \phi(z)e^{i(\alpha x-\beta t)} \,,$$

known as Tollmien-Schlichting waves, are considered. Then

$$\nabla^2\psi = e^{i(\alpha x-\beta t)}(D^2 - \alpha^2)\phi \,,$$

and (2.13) is reduced to the ordinary differential equation

$$\left[\frac{i}{R}(D^2 - \alpha^2)^2 + (\alpha U(z) - \beta)(D^2-\alpha^2) - \alpha U''(z)\right]\phi(z) = 0 \qquad (2.14)$$

where $D = \frac{d}{dz}$ and $U'' = \frac{d^2U}{dz^2}$.

Equation (2.14) is known as the Orr-Sommerfeld equation. It is important to note that this equation is not confined to strictly parallel flows of the form (2.5) but is still valid for almost parallel flows (like the Blasius) in the sense that the terms neglected in the derivation of (2.14) have little effect on the solution. This was shown by Pretsch[45].

The boundary conditions for (2.14) are that at a rigid wall

$$\phi = \phi' = 0 \qquad (2.15)$$

and that both these functions should be bounded at infinity. In the Blasius case, as $z \to \infty$, $U \to 1$, $U'' \to 0$ and (2.14) reduces to

$$(D^2 - \gamma^2)(D^2 - \alpha^2)\phi = 0$$

where $\gamma^2 = \alpha^2 + iR(\alpha - \beta)$ (2.16)

with general solution

$$\phi = Ae^{-\alpha z} + Be^{-\gamma z} + ae^{\alpha z} + be^{\gamma z} .$$

Assuming $\alpha_r, \gamma_r > 0$, ϕ will diverge at infinity unless $a = b = 0$. The appropriate outer boundary condition for Blasius flow is therefore

$$\phi \sim Ae^{-\alpha z} + Be^{-\gamma z} \qquad (2.17)$$

The solution of the Orr-Sommerfeld equation with appropriate boundary conditions leads to an eigenvalue problem involving three parameters α, β, and R (each of which can in general be complex) together with the complex eigenfunction ϕ. Two classes of solution are of particular physical importance.

(S) Spatially Developing Disturbances

R and β are given real, positive values and the problem is solved for α as complex eigenvalue. The disturbance may be written

$$\psi(x,z,t) = e^{-\alpha_i x} \phi(z) e^{i(\alpha_r x - \beta t)}$$

so that there is growth of the perturbation in space if $\alpha_i < 0$.

This type of solution is useful for comparison with experiment where the flow is often excited artificially by a ribbon or loudspeaker oscillating with prescribed frequency and the spatial development of disturbances is measured. The experiments of Schubauer & Skramstad[12] on the Blasius boundary layer and those of Freymuth[56] on a jet flow are typical examples.

(T) Temporally Developing Disturbances

R and α are given real, positive values and the problem is solved for $c = \frac{\beta}{\alpha}$ (the wave velocity) as complex eigenvalue. The disturbance may be written

$$\psi(x,z,t) = e^{\alpha c_i t} \phi(z) e^{i\alpha(x-c_r t)}$$

so that there is growth of the perturbation in time if $c_i > 0$.

This type of solution has been studied extensively in analytical work because c appears linearly in the equation (unlike α) and the problem is less complicated mathematically. Since R is a large parameter, asymptotic solutions of (2.14) are possible. This approach has been rigorously established by Lin [17].

2.5 Properties of the Orr-Sommerfeld Equation from Analytical Methods

In Lin's first method[17], equation (2.14) has the following formal asymptotic solutions:

$$\phi_1(z) = \phi_{10}(z) + (\alpha R)^{-1} \phi_{11}(z) + O(\alpha R)^{-2} \qquad (2.18a)$$

$$\phi_2(z) = \phi_{20}(z) + (\alpha R)^{-1} \phi_{21}(z) + O(\alpha R)^{-2} \qquad (2.18b)$$

$$\phi_3(z) = e^{-(\alpha R)^{\frac{1}{2}} Q(z)} \left[f_o(z) + (\alpha R)^{-\frac{1}{2}} f_1(z) + O(\alpha R)^{-1} \right] \qquad (2.18c)$$

$$\phi_4(z) = e^{+(\alpha R)^{\frac{1}{2}} Q(z)} \left[f_o(z) + (\alpha R)^{-\frac{1}{2}} f_1(z) + O(\alpha R)^{-1} \right] \qquad (2.18d)$$

where $\phi_{10}(z)$ and $\phi_{20}(z)$ are independent solutions of the Rayleigh equation

$$\left[(U(z) - c)(D^2 - \alpha^2) - U''(z) \right] \phi(z) = 0 \qquad (2.19)$$

and

$$Q(z) = \int_{z_c}^{z} [i(U(z) - c)]^{\frac{1}{2}} dz, \quad f_o(z) = (U(z) - c)^{-5/4} .$$

Wasow[14] has shown that the region of validity of the expansions (2.18) on the complex z-plane is determined by the curves $Re(Q(z)) = 0$ which emanate from the critical point z_c where $U(z) = c$. Near z_c, $U-c \doteq k(z - z_c)$, where k is a constant, and hence

$$Q = (ik)^{\frac{1}{2}}(z - z_c)^{3/2} .$$

Thus, there are three such curves with an angular spacing of $2\pi/3$ which satisfy

$$\arg(z-z_c) = \frac{4n-3}{6}\pi - \frac{1}{3}\arg k \qquad n = 1,2,3. \tag{2.20}$$

These curves divide the z-plane into three sectors, as shown in the diagrams.

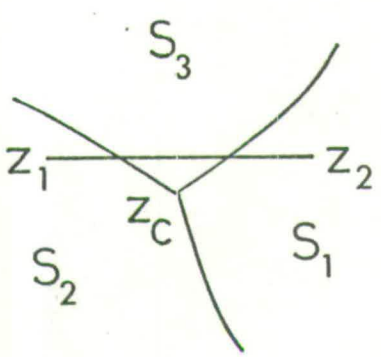

damped eigenstate

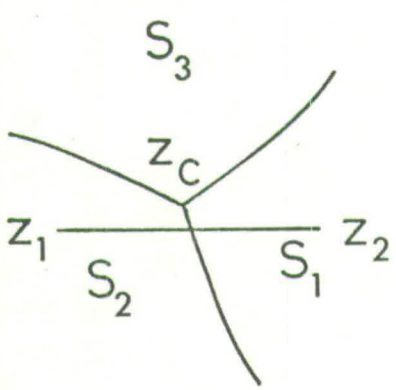

amplified eigenstate

It may be concluded from Wasow's results that sector S_3 is where the viscous, oscillatory solutions, ϕ_3 and ϕ_4, are both dominant in the sense that they are exponentially growing. Even the inviscid solution ϕ_2 must take on the nature of ϕ_3 or ϕ_4 in sector S_3. Therefore, if the z-axis crosses

S_3 as it does in the case of a damped eigenstate, an oscillatory eigenfunction should be expected.

In the Blasius case, the outer boundary point z_2 is located at infinity. Thus, the solution ϕ_4 is inadmissible since it is dominant in S_1 and does not satisfy the outer boundary condition.

Since the solution of (2.14) with appropriate boundary conditions yields a whole spectrum of eigenvalues, it is natural to attempt some kind of classification scheme. Using the expansions (2.18) Morawetz[39] contributed much to this aspect of the work, investigating three different flows: plane Couette, plane Poiseuille, and Blasius. For eigenvalues which, as $\alpha R \to \infty$, do not approach the value of U at either one of the boundary points, she reached the following conclusions:

(1) For all three flows there exist as many eigenvalues

$$c \sim c_o + \frac{c_1}{(\alpha R)^{\frac{1}{2}}} + O(\alpha R)^{-1}$$

as there are eigenvalues c_o of the inviscid problem (2.19).

(2) For plane Couette and plane Poiseuille flow there exist other eigenvalues unrelated to the inviscid problem. These satisfy $|c - c_n| < \varepsilon(\alpha R)^{-\frac{1}{2}}$ where ε is a constant and c_n is a root of

$$\mathrm{Im} \int_{z_1}^{z_2} \left[i(U(z)-c_n) \right]^{\frac{1}{2}} dz = \frac{n\pi}{(\alpha R)^{\frac{1}{2}}} \qquad n = 1,2,3 \ldots$$

As R or the domain of c increases, the number of such eigenvalues increases indefinitely and they all correspond to

damped disturbances. In the Blasius case, no such eigenvalues occur.

Finally Morawetz proved that, apart from certain excluded regions of the c-plane, no other eigenvalues exist for αR sufficiently large.

A substantial contribution was also made by Schensted [41] in her study of the temporal spectrum of the Orr-Sommerfeld equation and its adjoint

$$\left[\frac{i}{R}(D^2-\alpha^2)^2 + (\alpha U(z)-\beta)(D^2-\alpha^2) + 2\alpha\, U'(z)D\right] \chi(z) = 0 \qquad (2.21)$$

For flow between parallel walls, Schensted found the following properties:

(1) For any given boundary conditions the eigenvalues, c, of (2.14) and (2.21) are the same.

(2) The following orthogonality relation holds for suitably normalised ordinary and adjoint eigenfunctions.

$$\int_{z_1}^{z_2} \phi_j (D^2-\alpha^2)\chi_k \, dz = \int_{z_1}^{z_2} \chi_k (D^2-\alpha^2)\phi_j \, dz = \delta_{jk} .$$

(3) There is an infinite number of discrete eigenstates and the spectrum is complete in the sense that any suitable function $f(z)$ may be expanded in the form

$$f(z) = \sum_{j=1}^{\infty} a_j \phi_j(z) \quad \text{where} \quad a_j = \int_{z_1}^{z_2} f(z)(D^2-\alpha^2)\chi_j(z)\,dz.$$

Properties (1) and (2) also hold for Blasius flow since Mrs. Schensted's proofs are still valid for unbounded flows. This is not true for property (3) which depends on the interval being finite.

It is worth noting that property (1) is true even in the spatial case with α as eigenvalue, although (2) breaks down because α is non-linear in the equations.

2.6 Approximate Location of Eigenvalues of Large Modulus

Following Lord Rayleigh[57], Grohne[40] considered the solution of the Orr-Sommerfeld equation for a bounded flow at rest. In this case, (2.14) may be written in the form

$$(D^2-\alpha^2 + i\alpha RC)(D^2-\alpha^2)\phi(z) = 0$$

with boundary conditions

$$\phi = \phi' = 0 \quad \text{at} \quad z = 0, m.$$

It is found that the eigenvalues C_n are all purely imaginary and satisfy the inequality

$$\alpha^2 + \pi^2\left(\frac{n+1}{m}\right)^2 < i\alpha RC_n < \alpha^2 + \pi^2\left(\frac{n+2}{m}\right)^2 \qquad n = 0,1,2,... \tag{2.22}$$

These eigenvalues correspond to the eigenvalues c_n of Morawetz (type 2).

The importance of the above result becomes apparent when the relationship between C_n and the eigenvalues c_n of the full Orr-Sommerfeld equation for a variable velocity profile $U(z)$ is investigated. In fact, for fixed αR, Grohne shows that

$$c_n - C_n = \frac{1}{m}\int_0^m U(z)\,dz + O\left(\frac{1}{n}\right) \tag{2.23}$$

Thus, for large n (i.e. large $|c|$), the spectrum consists of a vertical line of closely spaced eigenvalues, all with real part nearly equal to the average flow velocity.

CHAPTER 3

NUMERICAL METHODS

3.1 Solution of the Blasius Equation

As discussed in section 2.3, the equation to be solved is

$$F'''(z) + F(z)\,F''(z) = 0 \qquad (3.1)$$

with initial conditions

$$F(0) = F'(0) = 0, \quad F''(0) = a,$$

where the value of a is to be chosen so that $F' \to b^2$ as $z \to \infty$.

Equation (3.1) may be written as three first order equations in the vector form

$$\underline{Y}'(z) = \underline{G}(F(z), F'(z), F''(z)) \qquad (3.2)$$

where $\underline{Y} = \begin{bmatrix} F \\ F' \\ F'' \end{bmatrix}$ and $\underline{G} = \begin{bmatrix} F' \\ F'' \\ -FF'' \end{bmatrix}$.

The system (3.2) is solved using a fourth order Runge-Kutta method. Suppose that $\underline{Y}$ is known at some point z_o. First, the following vectors are calculated:

$$\underline{k}_1 = \underline{G}(F, F', F'')$$

$$\underline{k}_2 = \underline{G}(F + \tfrac{1}{2}k_{11}, F' + \tfrac{1}{2}k_{12}, F'' + \tfrac{1}{2}k_{13})$$

$$\underline{k}_3 = \underline{G}(F + \tfrac{1}{2}k_{21}, F' + \tfrac{1}{2}k_{22}, F'' + \tfrac{1}{2}k_{23})$$

$$\underline{k}_4 = \underline{G}(F + k_{31}, F' + k_{32}, F'' + k_{33})$$

where k_{nj} denotes the jth component of $\underline{k}_n$. The components of $\underline{Y}$ at an adjacent point (z_o+h) can then be estimated from

the formula

$$\underline{Y}(z_o+h) = \underline{Y}(z_o) + \frac{h}{6}\left[\underline{k}_1 + 2\underline{k}_2 + 2\underline{k}_3 + \underline{k}_4\right] \qquad (3.3)$$

which is accurate to $O(h^5)$. However, since $O(h^{-1})$ steps are required to reach any given point, the overall method is only $O(h^4)$ accurate. Thus, the numerical value of $\underline{Y}$ at a given h is related to the true value by the expression

$$\underline{Y}_h = \underline{Y}_t + \underline{P}\, h^4 \qquad (3.4)$$

where $\underline{P}$ is a constant vector.

The following method was employed to obtain accurate numerical values for a and b. First, setting $a = 1$, formula (3.3) was used to produce a solution for $\underline{Y}$ in steps of $h = \cdot 01$. When F' reached its asymptotic value to 15 decimal places, the integration was halted and the value noted. This was repeated for $h = \cdot 005$ and the true value of $F'(\infty)$ was estimated from (3.4).

Suppose now that the solution is rescaled to $f(\eta)$, so that $f'(\infty) = 1$. Since $f(\eta) = s\,F(s\eta)$ and $F''(0) = 1$, it follows that

$$1 = s^2 F'(\infty) , \qquad f''(0) = s^3 .$$

Elimination of s gives

$$f''(0) = \left[F'(\infty)\right]^{-3/2} = \cdot 469599988361 .$$

Using this value for a, solutions were obtained as before for $h = \cdot 01, \cdot 005$. The true value of $f'(\infty)$ was estimated to be less than 10^{-12} from unity. From these solutions, the integral

$$b = \int_0^\infty (1-f'(\eta))\,d\eta = 1.216780621614$$

was evaluated using Simpson's rule.

A Blasius solution correctly scaled to the boundary layer Reynolds number (with $z = \frac{\eta}{b}$) may therefore be obtained by using

$$a = f''(0)\, b^3 = \cdot 845989418760.$$

The functions $U(z)$, $U'(z)$ and $U''(z)$ required in equations (2.14) and (2.21) are then the components of $\frac{1}{b^2}\,\underline{G}(z)$.

3.2 Solution of the Orr-Sommerfeld Equation and its Adjoint

The method used is to replace the differential equation (2.14) or (2.21) by a set of finite difference equations. This is achieved by dividing the z domain into n equal intervals of length h so that the eigenfunction ϕ becomes a vector whose components ϕ_j are the values of ϕ at the points $z = jh$ $(0 \leqslant j \leqslant n)$. The differential operators D^4, D^2 and D are represented by the following series of central difference operators:

$$\begin{aligned} h^4 D^4 \phi_j &= \left[\delta^4 - \tfrac{1}{6}\delta^6 + \tfrac{7}{240}\,\delta^8 - \ldots\right] \phi_j \\ h^2 D^2 \phi_j &= \left[\delta^2 - \tfrac{1}{12}\,\delta^4 + \tfrac{1}{90}\,\delta^6 - \ldots\right] \phi_j \qquad (3.5) \\ h\, D\, \phi_j &= \mu\left[\delta - \tfrac{1}{6}\delta^3 + \tfrac{1}{30}\,\delta^5 - \ldots\right] \phi_j \end{aligned}$$

where e.g.

$$\delta\phi_j = \phi_{j+\frac{1}{2}} - \phi_{j-\frac{1}{2}}\,, \qquad \mu\phi_j = \tfrac{1}{2}\left[\phi_{j+\frac{1}{2}} + \phi_{j-\frac{1}{2}}\right]$$

$$\delta^2\phi_j = \phi_{j+1} - 2\phi_j + \phi_{j-1}, \quad \mu\delta\phi_j = \tfrac{1}{2}\left[\phi_{j+1} - \phi_{j-1}\right] .$$

Obviously the series in (3.5) have to be truncated at some point. On the other hand, it is desirable to make the finite difference approximation as accurate as possible. In this case, a particularly efficient approach is possible using a transformation of the type first used by Noumerov[58] .

$$\phi_j = (1 + \frac{1}{6}\delta^2 - \frac{1}{720}\delta^4)v_j \quad . \tag{3.6}$$

This choice of transformation means that an overall accuracy of $O(h^4)$ can be achieved without using any difference higher than δ^4.

$$h^4D^4\phi_j = [\delta^4]\, v_j + O(h^{10}) \tag{3.7a}$$

$$h^2D^2\phi_j = [\delta^2 + \frac{1}{12}\delta^4]\, v_j + O(h^6) \tag{3.7b}$$

$$h\, D\, \phi_j = \mu\, [\delta]\, v_j + O(h^5) \quad . \tag{3.7c}$$

In fact, the relation (3.7a) is $O(h^6)$ accurate which is particularly useful for handling the highest derivative - a very sensitive quantity. It is the absence of a third derivative in (2.14) or (2.21) that makes the transformation (3.6) particularly powerful.

Using formulae (3.7) a solution is obtained first for $\underline{v}$ and then the solution for $\underline{\phi}$ is found from (3.6).

The finite difference scheme (3.7) leads to a set of (n+1) equations each involving 5 of the net points from v_{-2} to v_{n+2}. With the aid of the boundary conditions, v_{-2}, v_{-1}, v_{n+1} and v_{n+2} may all be eliminated so that the (n+1) equations may be written in the form

$$M(\lambda)\underline{v} = \underline{0} \tag{3.8}$$

where M is a complex $(n+1)\times(n+1)$ penta-diagonal matrix and λ is the eigenvalue. In case (S), $\lambda = \alpha$ and in case (T), $\lambda = c$. The eigenvector $\underline{v}$ has now only $(n+1)$ elements v_o to v_n.

Numerical Boundary Conditions

In the cases considered, the lower boundary at $z = 0$ is a rigid wall so that $\phi(0) = \phi'(0) = 0$. From (3.6) and (3.7c) it follows that

$$(1 + \tfrac{1}{6}\delta^2 - \tfrac{1}{720}\delta^4)v_o = 0 \qquad (3.9a)$$

$$\mu\delta\, v_o = 0 \quad . \qquad (3.9b)$$

Equation (3.9b) implies that $v_{-1} = v_1$ and substituting this in (3.9a) gives $v_{-2} = 474v_o + 248v_1 - v_2$.

In plane Poiseuille flow, since the velocity profile is symmetrical $\underline{\phi}$ (and therefore $\underline{v}$) may be assumed symmetrical or anti-symmetrical. Thus it is only necessary to consider half the channel width and apply the outer boundary conditions at the centre of the channel ($z = 1$). For a symmetrical eigenfunction it follows that

$$v_{n+2} = v_{n-2}, \quad v_{n+1} = v_{n-1} \qquad (3.10a)$$

whereas for an anti-symmetrical eigenfunction

$$v_{n+2} = -v_{n-2}, \quad v_{n+1} = -v_{n-1} \,. \qquad (3.10b)$$

In the Blasius case the application of (2.17) is rather more complicated. It is assumed that the components v_{n-1}, v_n, v_{n+1} and v_{n+2} all satisfy (2.17), i.e.

$$v_{n+j} = Ae^{-j\alpha h} + Be^{-j\gamma h} \qquad j = -1,0,1,2 \quad .$$

A and B are eliminated from the first two equations and substituted in the second two which become

$$v_{n+1} = (e^{-h\alpha} + e^{-h\gamma})v_n - e^{-h(\alpha+\gamma)} v_{n-1} \qquad (3.11a)$$

$$v_{n+2} = (e^{-2h\alpha} + e^{-h(\alpha+\gamma)} + e^{-2h\gamma})v_n - e^{-h(\alpha+\gamma)}(e^{-h\alpha} + e^{-h\gamma})v_{n-1} \qquad (3.11b)$$

It should be noted that equations (3.11) are still correct if $\alpha = \gamma$ although (2.17) would then become $\phi \sim (A+Bz)e^{-\alpha z}$.

In some cases $\gamma_r >> \alpha_r$ so that, since the γ term dies out rapidly with z, it is possible to apply the simpler condition $\phi \sim Ae^{-\alpha z}$ as was done by Jordinson[49]. Equations (3.11) then reduce to

$$v_{n+j} = v_n e^{-j\alpha h} \qquad j = 1,2. \qquad (3.12)$$

The point of application of the outer boundary condition should be chosen with care. If it is taken too near to the plate, the asymptotic assumption used in deriving (2.17) is wrong. If it is chosen too far out into the free stream the efficiency of the computation may be severely reduced.

The double valued function γ requires careful consideration. For every point on the complex eigenvalue plane (whether it is the α-plane or the c-plane) there exist two possible values of γ. Unless γ is purely imaginary, one of these values will have $\gamma_r > 0$ (corresponding to a bounded solution for ϕ) and the other $\gamma_r < 0$ (corresponding to an unbounded solution). It is convenient, therefore, to define the line $\gamma_r = 0$ to be a branch line and to consider only that half of the Riemann surface which has $\gamma_r \geq 0$.

On the α-plane, the branch points are located at

$$\alpha_1 = \beta + i\frac{\beta^2}{R} + O(R^{-2})$$

and $$\alpha_2 = -\beta - i(R + \frac{\beta^2}{R}) + O(R^{-2}).$$

The branch line $\gamma_r = 0$ is that portion of the hyperbola

$$\alpha_r(1 + \frac{2\alpha_i}{R}) = \beta$$

which lies above α_1 and below α_2.

On the c-plane, the only branch point is located at

$$c = 1 - \frac{i\alpha}{R} .$$

The branch line $\gamma_r = 0$ is that portion of the line $c_r = 1$ which lies below the branch point.

3.3 Solution of $M(\lambda)\underline{v} = \underline{0}$

Contour Method

This method is useful in an initial search for eigenvalues. The determinant of M is an analytic function of λ except possibly near any branch points of γ. If γ is not involved in the outer boundary condition as in (3.10) or (3.12), the determinant is completely analytic.

Consider a closed contour C which does not enclose any branch point or cross any branch line. Since $\det M$ has no poles, according to the argument theorem the number of zeros within C is given by

$$N = \frac{1}{2\pi} \oint_C d\,[\arg \det M(\lambda)] \qquad (3.13)$$

A zero of $\det M$ is an eigenvalue of (3.8). Thus if

the argument is evaluated at a sufficiently high number of points round C, the total change in argument may be estimated and the number of eigenvalues found.

It is convenient to use rectangular contours since subdivision of the region searched is then easily accomplished, allowing individual eigenvalues to be located. This approach was originally used by Dr. G.M. Thomas.

Osborne Method

This powerful iterative technique was first developed by Osborne[59]. It is basically a Newton-Raphson method for matrices so that it converges to a zero of det M in the same way as the Newton-Raphson algorithm converges to the zero of a function.

A normalising condition is required to fix the magnitude of the eigenvector. Jordinson[49] and Corner[50] have used

$$\underline{e}^t.\underline{v} = 1 \qquad (3.14)$$

where $\underline{e}^t$ is a transposed vector with mth entry unity and all others zero, m corresponding to the entry of $\underline{v}$ with maximum modulus.

Condition (3.14) is strictly incorrect since in order to preserve the $O(h^4)$ accuracy in the eigenfunction it is necessary to normalise $\underline{\phi}$ itself. Thus (3.14) should be

$$\underline{e}^t.\underline{\phi} = 1$$

or

$$\underline{s}^t.\underline{v} = 1 \qquad (3.15)$$

where

$$\underline{s}^t = \frac{1}{720}\left[0\ldots0\ -1\ 124\ \underset{\text{mth entry}}{474}\ 124\ -1\ 0\ldots0\right]$$

In (3.15) m is restricted to $2 \leqslant m \leqslant n-2$. This is unlikely to cause difficulty in practice since the maximum of $|\underline{v}|$ normally occurs at a point well within these limits.

The iterative process is designed to converge simultaneously to a single eigenvalue and its corresponding eigenvector. Suppose that the jth iteration has produced the eigenpair $\lambda^j, \underline{v}^j$. Either of the following formulae may then be used in the $(j+1)$th iteration.

$$\lambda^{j+1} = \lambda^j - \frac{1}{\underline{s}^t.\underline{x}}, \qquad \underline{v}^{j+1} = \frac{\underline{x}}{\underline{s}^t.\underline{x}} \tag{3.16a}$$

$$\lambda^{j+1} = \lambda^j - \frac{\underline{s}^t.\underline{x}}{\underline{s}^t.\underline{y}}, \qquad \underline{v}^{j+1} = \frac{\underline{y}}{\underline{s}^t.\underline{y}} \tag{3.16b}$$

where $\underline{x} = M^{-1} \frac{dM}{d\lambda} \underline{v}^j$

and $\underline{y} = M^{-1}(\frac{dM}{d\lambda} \underline{x} - \frac{1}{2} \frac{d^2M}{d\lambda^2} \underline{v}^j)$.

Equations (3.16) are due to Osborne[59] but a shorter proof is given by Corner[50]. Iteration (3.16a) is second order, and iteration (3.16b) third order but, since it is rather inefficient to compute $\frac{d^2M}{d\lambda^2}$, (3.16b) is normally used with $\underline{y} = M^{-1} \frac{dM}{d\lambda} \underline{x}$ which reduces the rate of convergence to second order (unless $\frac{d^2M}{d\lambda^2}$ is the zero matrix).

Usually, a good starting value for λ is known from other methods. However, the initial approximation to $\underline{v}$ is relatively poor - a vector with every component unity. For the first iteration, therefore, it is advisable to use (3.16b), even in its truncated form, since it is more stable with respect to this crude eigenvector approximation. Subsequent iterations are more efficiently handled by (3.16a).

The matrix inversion is performed by Gaussian elimination with partial pivoting.

LR Method

If the eigenvalue λ is linear as it is in the (T) case and if the outer boundary condition is (3.10) or (3.12), equation (3.8) can be expressed in the form

$$L\underline{v} = \lambda N\underline{v} \qquad (3.17)$$

where L and N are both pentadiagonal matrices independent of λ. Provided that N is non-singular, equation (3.17) may be written

$$M\,\underline{v} = \lambda\underline{v}$$

where $M = N^{-1}L$ is a non-sparse complex matrix and the eigenvalue problem is reduced to classical form.

The LR algorithm with shifts of origin as described by Martin & Wilkinson[60] is used to find all the eigenvalues of M. For maximum stability, the row and column norms of M are balanced and M is reduced to upper Hessenberg form before the LR algorithm is applied.

This method has the considerable advantage of producing an entire spectrum of eigenvalues in one execution.

Comparison of Numerical Methods

The general features of the three numerical methods are summarised in Table 3.1. The figures given in items 7 and 8 apply to a typical run with $n = 100$ net points and double precision arithmetic on an ICL 4-75 computer.

TABLE 3.1

Comparison of numerical methods for solving $M(\lambda)\underline{v} = 0$.

		Contour	Osborne	LR
1.	(S) or (T)	both	both	(T) only
2.	possible boundary conditions	all	all	all except (3.11)
3.	starting value required	no	yes	no
4.	number of eigenvalues produced	several	one	all
5.	number of eigenvectors produced	none	one	none
6.	accuracy of results	approximate	very accurate	accurate
7.	c.p.u. time (seconds)	50	2	500
8.	core storage (bytes)	15K	30K	200K

Excellent agreement was found between the results of the Osborne and LR methods (at least 10 significant figures) when both were used to compute the same temporal spectrum. The contour method was also found to be reliable in most cases.

In the (T) case, the LR method was always used first to produce a spectrum of eigenvalues which could then be refined (if necessary) by the Osborne method, and selected eigenvectors calculated. In the (S) case, the contour method was used to produce starting values for the Osborne method.

CHAPTER 4

RESULTS FOR SPATIALLY DEVELOPING DISTURBANCES

4.1 Introduction

This chapter is concerned exclusively with spatially developing disturbances in the Blasius boundary layer. The numerical methods described in Chapter 3 have been used to find the eigenstate spectrum over a wide range of frequency and Reynolds number. In order to illustrate the accuracy obtainable, a typical spectrum will be examined in detail in the next section. Then, the effect of variation in frequency and Reynolds number will be investigated in Section 4.3.

Only a small number of eigenstates of the Orr-Sommerfeld equation (or its adjoint) were found in any instance. However, a large number of other "eigenstates" exist which are not true eigenstates of (2.14) or (2.21). These will be discussed in Section 4.4.

The full outer boundary condition (3.11) has been used throughout. In several test cases, a considerable difference was noted when (3.12) was used instead of (3.11). This discrepancy was particularly large near $\alpha_r = \beta$.

The point of application of (3.11) was chosen far enough out into the free stream to have negligible effect on the results (say, less than 10^{-8} change in eigenvalue). This optimum position varied with Reynolds number and even among different eigenstates in the same spectrum.

For every solution (α,ϕ) of the Orr-Sommerfeld equation obtained numerically, it was found that there existed a

corresponding solution (α, χ) of the adjoint equation. This provided a useful check on the accuracy of the results and a numerical verification of the equivalence of the ordinary and adjoint eigenvalue spectra.

4.2 Study of a Typical Spectrum

The spectrum at $R = 3000$, $\beta = \cdot 24$ was found to contain the six eigenstates shown in Figure 4.1. State 1 is the fundamental eigenstate associated with the neutral stability curve. The other five states are much more heavily damped and are numbered in order of decreasing α_r. These higher eigenstates have a definite pattern on the α-plane, forming in pairs which are reflections in the line $\alpha_r = \alpha_i$. Thus, if State 2 has eigenvalue $(a + ib)$, State 3 has eigenvalue $(b + ia)$, and so on. However, a "partner" state for State 6 does not appear to exist at the present values of R and β.

Since the numerical method is $O(h^4)$ accurate, the true value α_o of the eigenvalue may be estimated from the formula

$$\alpha(h) = \alpha_o + kh^4 \qquad (4.1)$$

where $\alpha(h)$ is the numerical value of α at a given h and k is a constant. It should be noted, however, that formula (4.1) holds only for sufficiently small h.

Suppose that three numerical values $\alpha(h)$, $\alpha(ph)$, and $\alpha(qh)$ are known (with $1 < p < q$). The two more accurate results may then be used to estimate α_o. From (4.1) it follows that

$$\alpha_o = \frac{p^4\alpha(h) - \alpha(ph)}{p^4 - 1} \qquad (4.2)$$

The third result provides a useful check on the accuracy of this estimate. First, the quantity

$$r = \frac{1}{\log q}\left[\log\{\alpha(qh) - \alpha_o\} - \log\{\alpha(h) - \alpha_o\}\right] \qquad (4.3)$$

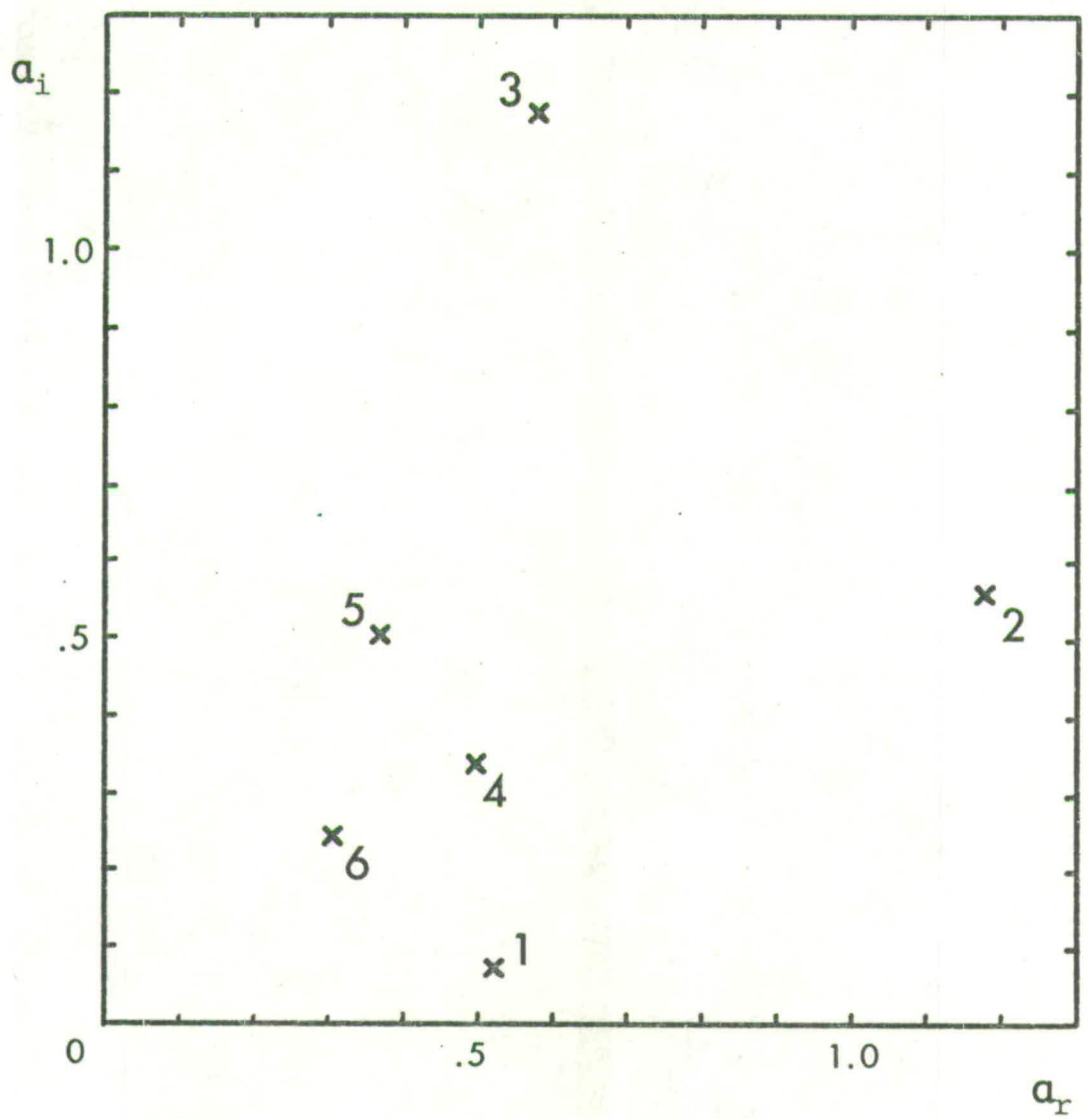

Figure 4.1 Eigenvalue Spectrum at R = 3000, β = .24 .

is calculated using the value of α_o obtained in (4.2). If $r = 4$, formula (4.1) holds exactly. Any significant deviation from $r = 4$ indicates that the net spacing is too coarse or that the eigenvalue tested does not have $O(h^4)$ behaviour.

Accurate results for the six eigenvalues at $R = 3000$, $\beta = .24$ are given in Table 4.1. Both ordinary and adjoint eigenvalues are included and, in each case, α_o has been estimated from (4.2) and checked using (4.3). There is good agreement between the ordinary and adjoint estimates but the maximum accuracy attainable varies from about 7 decimal places in the case of State 1 to only 4 or 5 decimal places in the case of State 6. As will be discussed later, this loss of accuracy in the determination of the eigenvalues of lowest α_r is almost certainly due to the existence of the spurious eigenstates.

The ordinary and adjoint eigenfunctions of the six states are shown in Figures 4.2 to 4.7. In each case, the continuous curve is the real part of the eigenfunction and the dashed curve is the imaginary part. The point of normalisation is where $\phi_r = 1$ and $\phi_i = 0$ (similarly for χ).

As can be seen from the diagrams, the χ functions are rather similar in form, varying only in the number of oscillations they possess. Since they are non-physical, they are not so important as the ϕ functions which will now be considered in detail.

State 1 is quite unique in having a very smooth, slowly varying form with its maximum well out into the free stream ($z = 1.55$). The maxima of the other five states occur closer to $z = 0$ and there is a smooth outward progression from State 2 ($z = \cdot 35$) to State 6 ($z = 1 \cdot 45$). The highly

TABLE 4.1

Blasius Spectrum at $R = 3000$, $\beta = .24$.

State	Equation	α_r	α_i	h_{min}	z_{max}
1	O.S.	.5208538	.0723599	.02	6
	Adjoint	.5208538	.0723599		
2	O.S.	1.1762618	.5592907	.02	5
	Adjoint	1.1762621	.5592917		
3	O.S.	.5781889	1.1749343	.015	5
	Adjoint	.5781888	1.1749343		
4	O.S.	.4964762	.3387088	.015	5
	Adjoint	.4964762	.3387088		
5	O.S.	.3675186	.5056801	.02	6
	Adjoint	.3675186	.5056797		
6	O.S.	.305558	.243967	.025	10
	Adjoint	.305559	.243969		

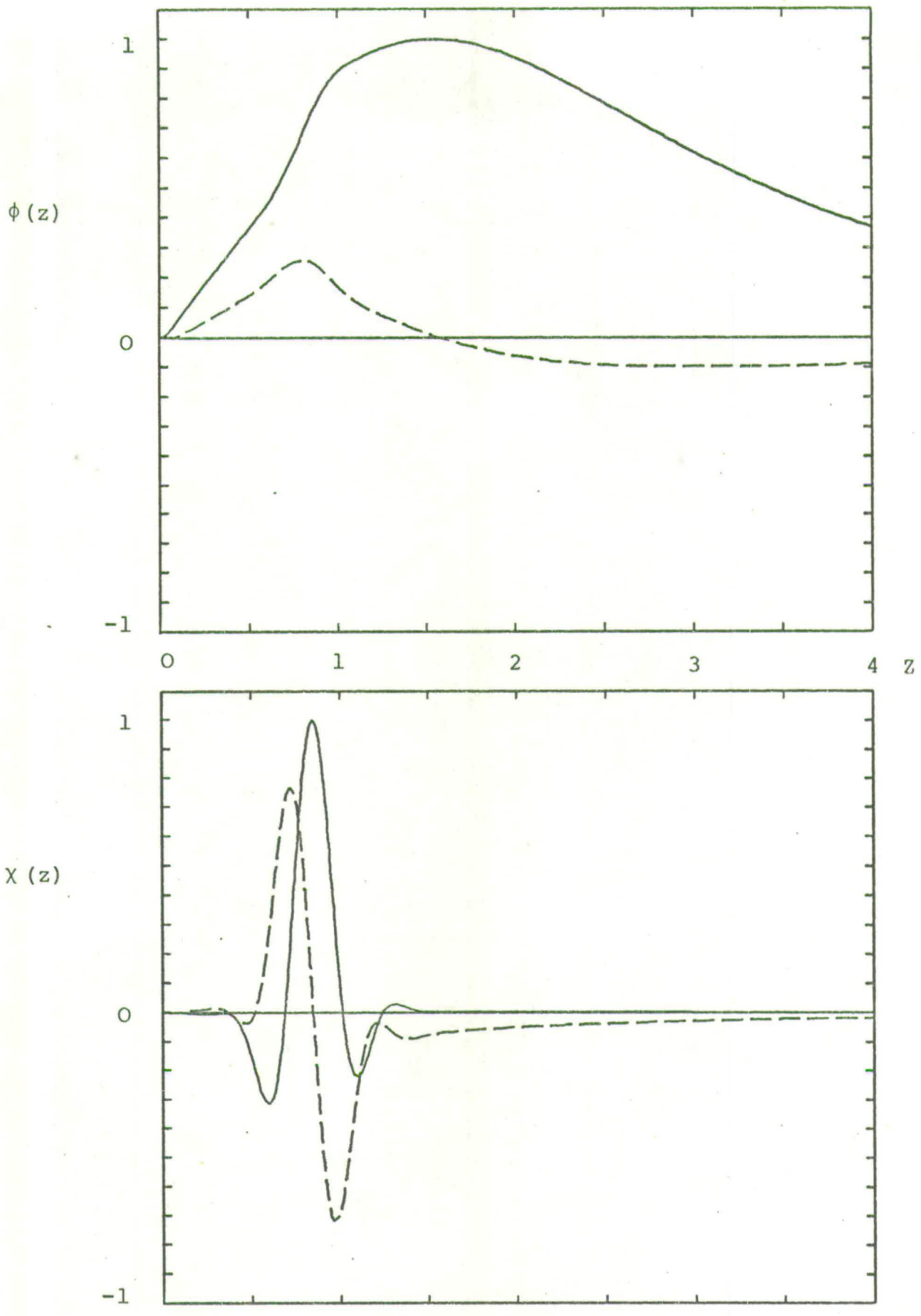

Figure 4.2 State 1 Eigenfunctions at R = 3000, β = .24 .

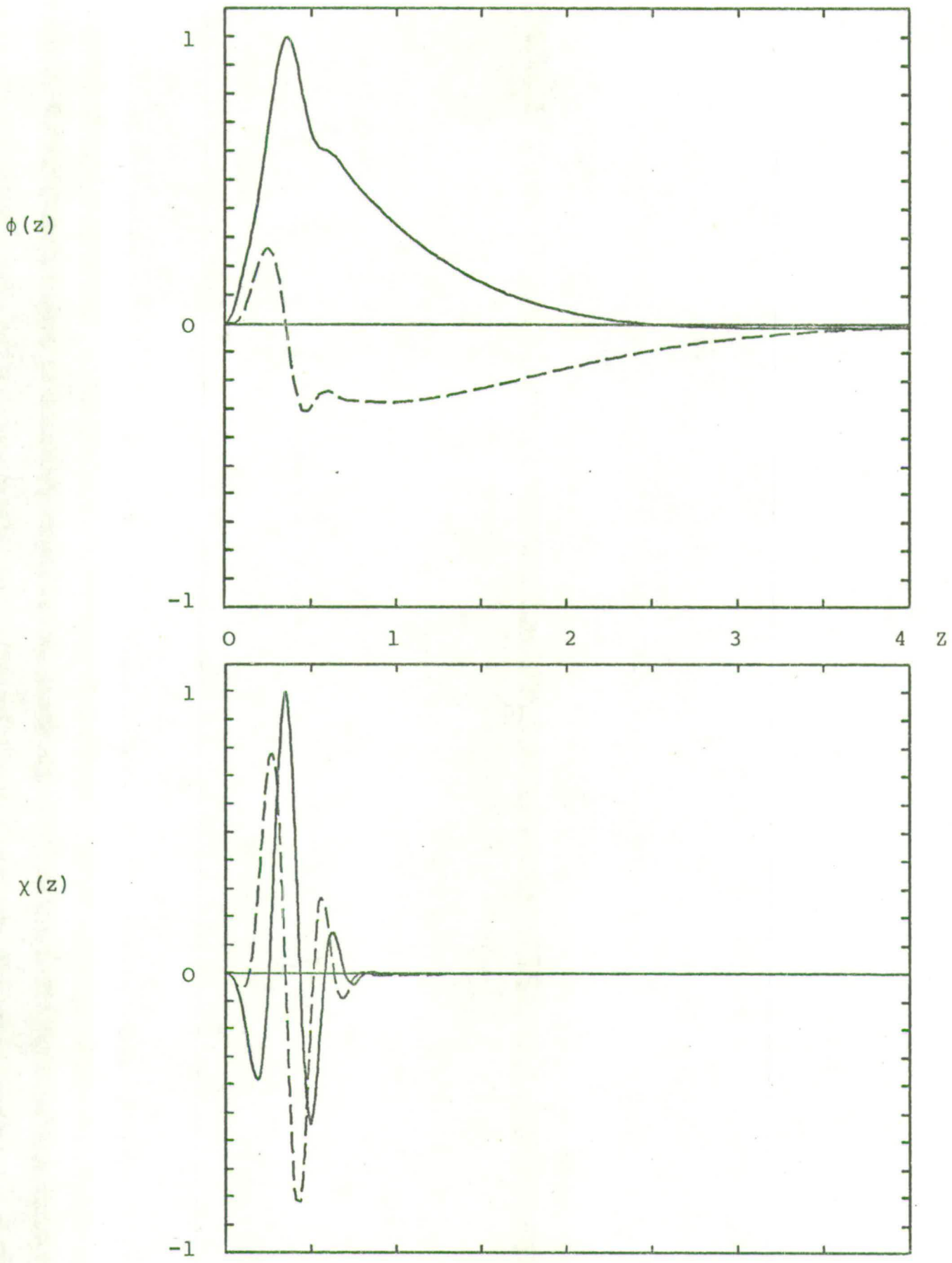

Figure 4.3 State 2 Eigenfunctions at R = 3000, β = .24 .

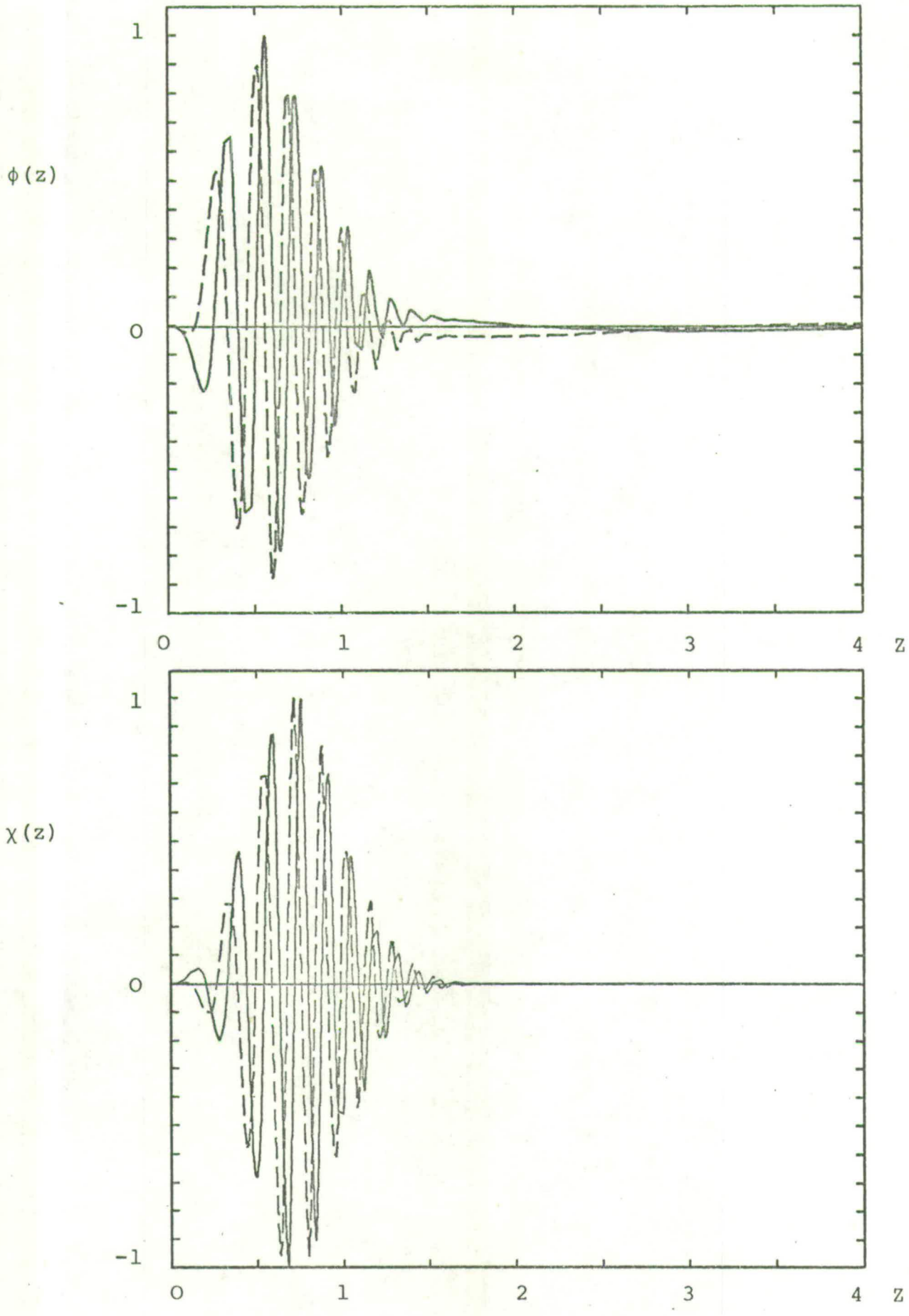

Figure 4.4 State 3 Eigenfunctions at R = 3000, β = .24 .

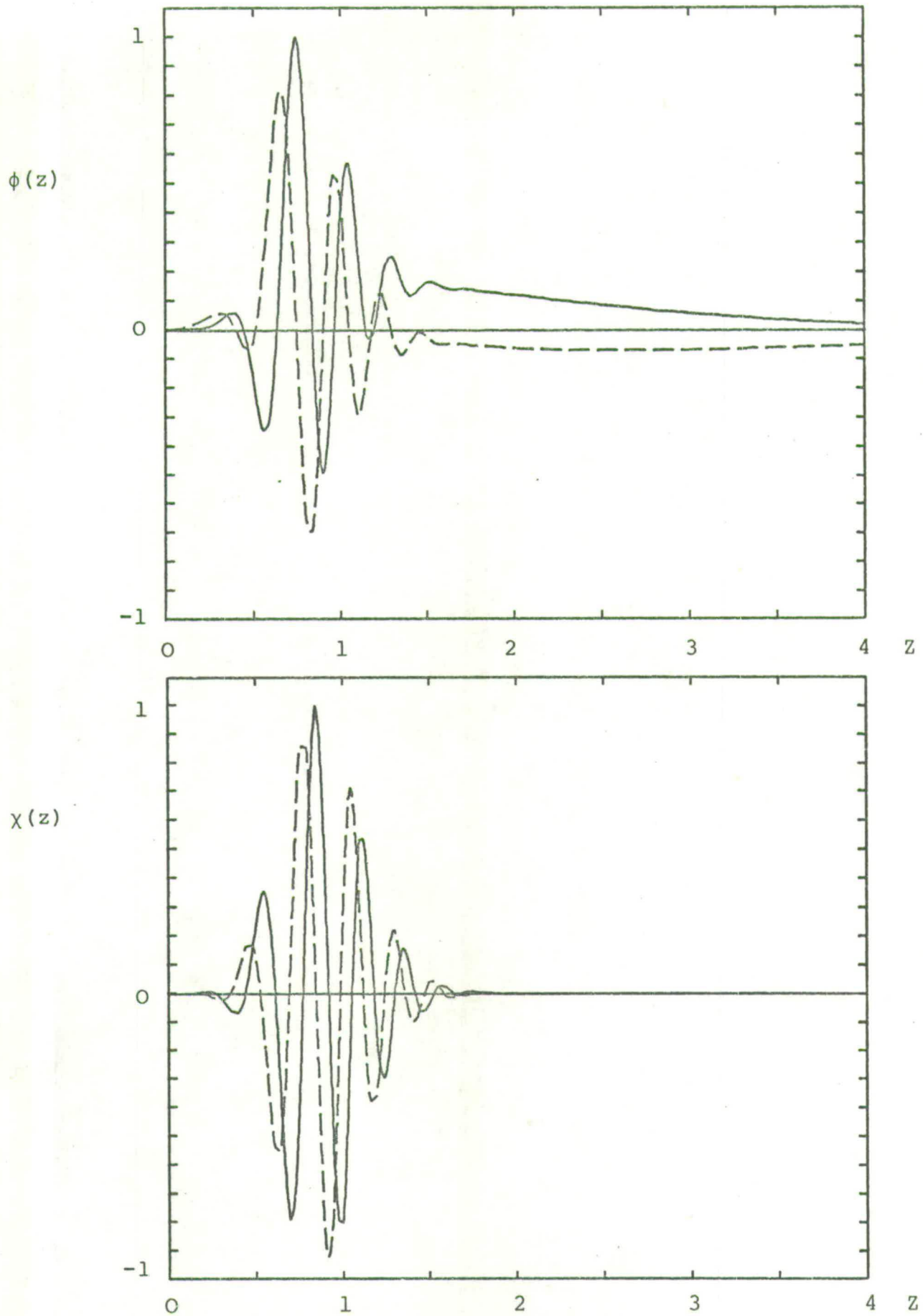

Figure 4.5 State 4 Eigenfunctions at R = 3000, β = .24.

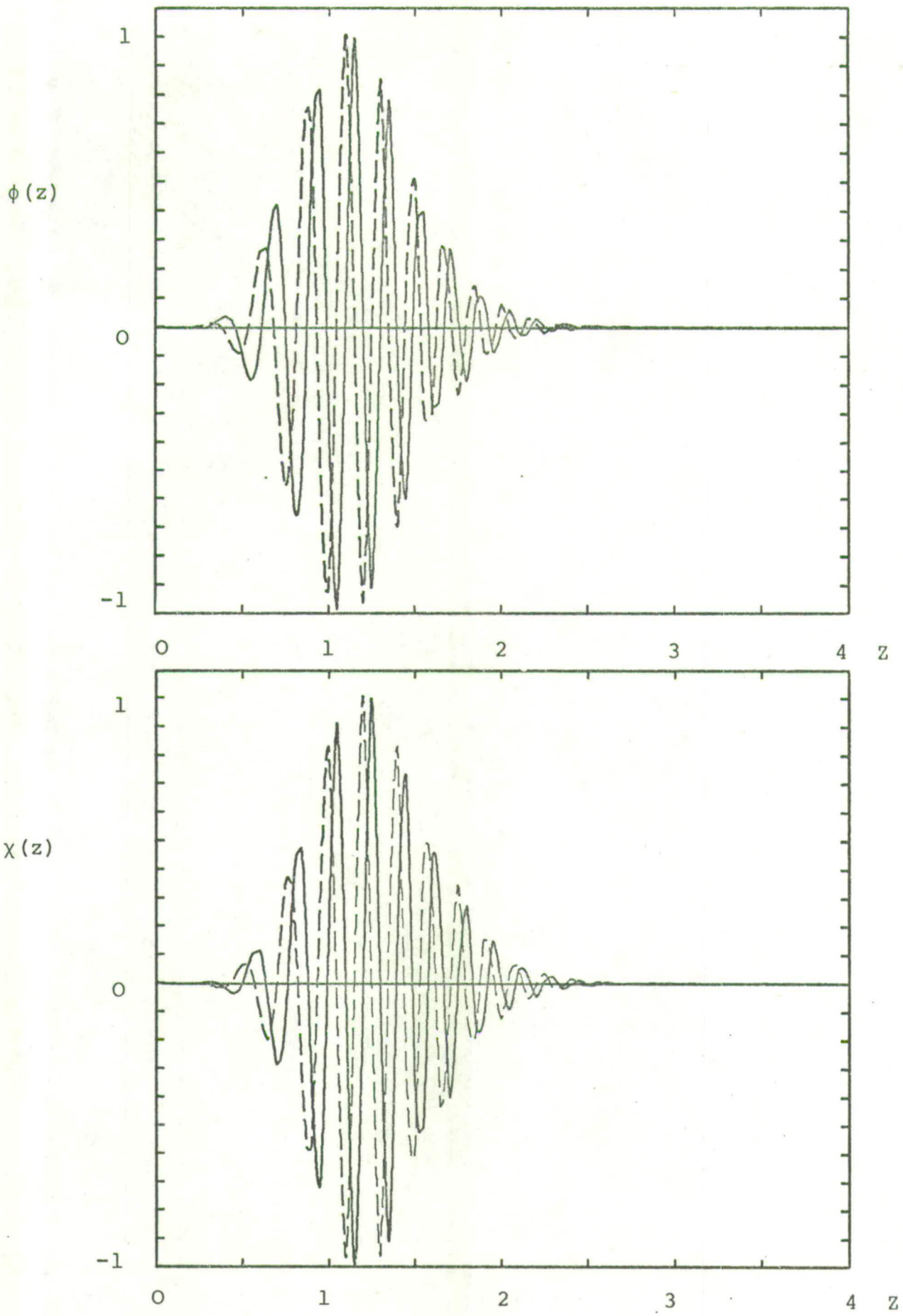

Figure 4.6 State 5 Eigenfunctions at R = 3000, β = .24.

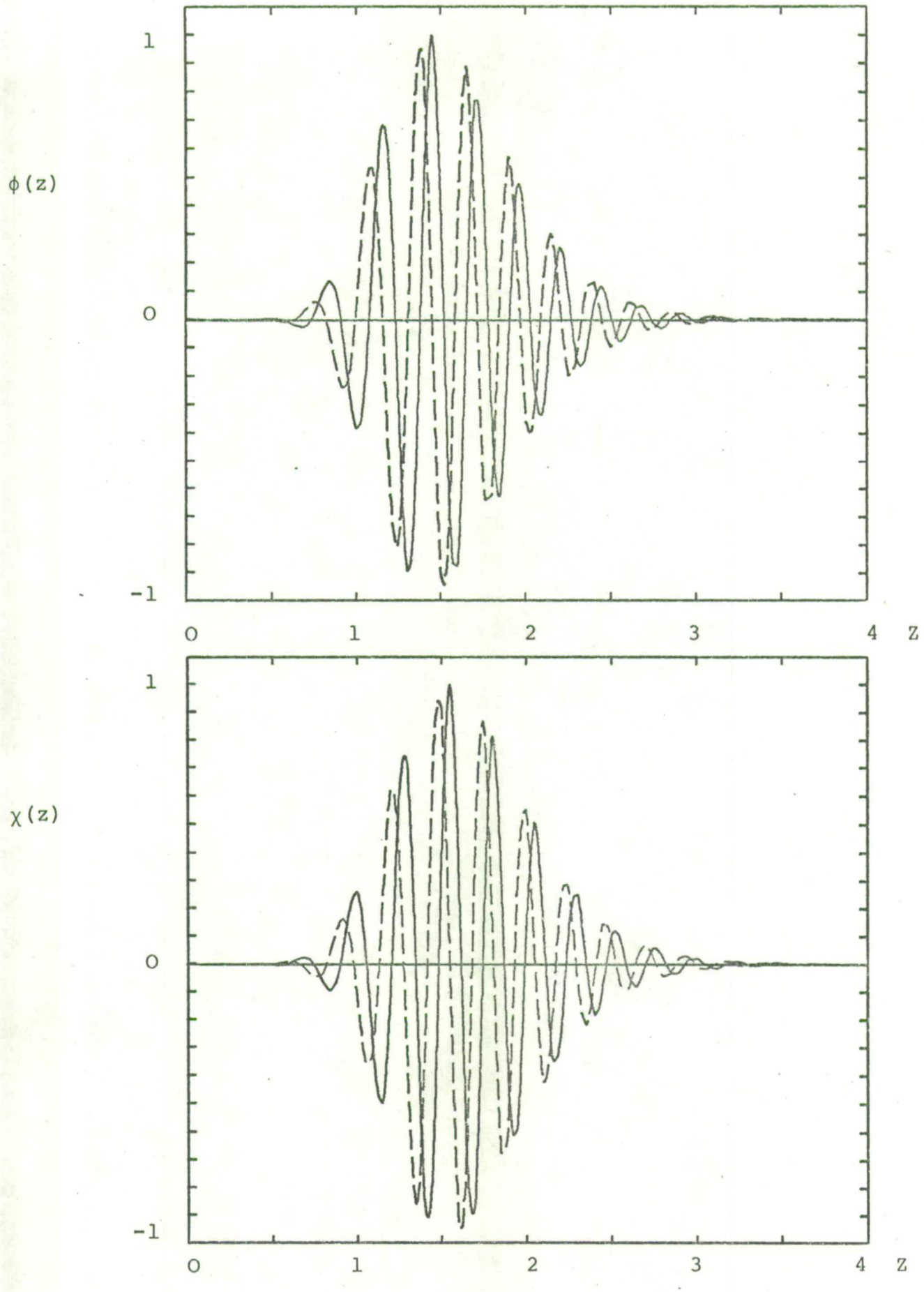

Figure 4.7 State 6 Eigenfunctions at R = 3000, β = .24.

oscillatory nature of States 3 and 5 contrasts with the less sinuous form of their "partner" states (2 and 4). State 6, however, is very similar to State 5, only it is shifted further out into the free stream.

The form of these eigenfunctions is consistent with the analytical theory discussed in Section 2.5. For the Blasius case

$$\phi = A\phi_1 + B\phi_2 + C\phi_3, \qquad (4.4)$$

a linear combination of the functions defined in (2.18) which satisfies the boundary conditions. Thus, the resultant form of ϕ depends on the relative magnitude of the constituent functions.

The highly oscillatory states have a high proportion of the viscous solution ϕ_3 or possibly ϕ_2 which, in the case of a damped eigenstate, takes on an oscillatory nature over that part of the z-axis which resides in S_3 (see Section 2.5). It appears that State 4 which changes abruptly at $z \doteq 1{\cdot}6$ to a far more slowly varying function may have a high proportion of ϕ_2 while its "partner", State 5, is purely oscillatory and probably consists mainly of ϕ_3.

Although slightly damped, State 1 is very slowly varying and betrays no viscous character. It is therefore likely to be composed almost entirely of ϕ_1. The absence of ϕ_3 is confirmed in the application of the outer boundary condition, since the inviscid condition (3.12) produces exactly the same result as the full condition (3.11).

Another interesting point emerges from a comparison with analytical theory. Assuming $U = .5714z$ (which is a good approximation to Blasius flow for $z < 1$) it is possible to

calculate, for each of the six states, the position of the critical point z_c and of the three anti-Stokes lines $Re(\alpha^{\frac{1}{2}}Q(z)) = 0$ on the complex z-plane. It turns out that for States 3 and 5 the origin of z lies in S_3 so that the positive z-axis extends over only two sectors, S_3 and S_2. The other states, however, extend over all three sectors, from S_1 through S_3 to S_2. To some extent, this may account for differences in the form of the eigenfunctions.

What is certain from the numerical evidence is that, unlike State 1, there are at least two different functions present in the higher eigenstates, one highly oscillatory and the other slowly varying.

4.3 General Structure of the Spectrum

The non-dimensional frequency parameter β is scaled relative to the boundary layer thickness δ_1 and therefore varies with x. For correlation with experiment, it is convenient to use the non-dimensional parameter

$$F = \frac{\beta}{R}$$

which is constant downstream and corresponds to the excitation frequency of the vibrating ribbon. A study of the development of the spectrum of eigenstates at constant F is thus equivalent to a hot wire moving downstream in the experiment.

Figures 4.8 illustrate the evolution of the eigenvalue spectrum in moving downstream from $R = 1000$ to $R = 5000$ at $F = 80 \times 10^{-6}$, a frequency used by Ross et al.[27] The most interesting feature is the apparent creation of eigenstates with increase in Reynolds number. The eigenvalues seem

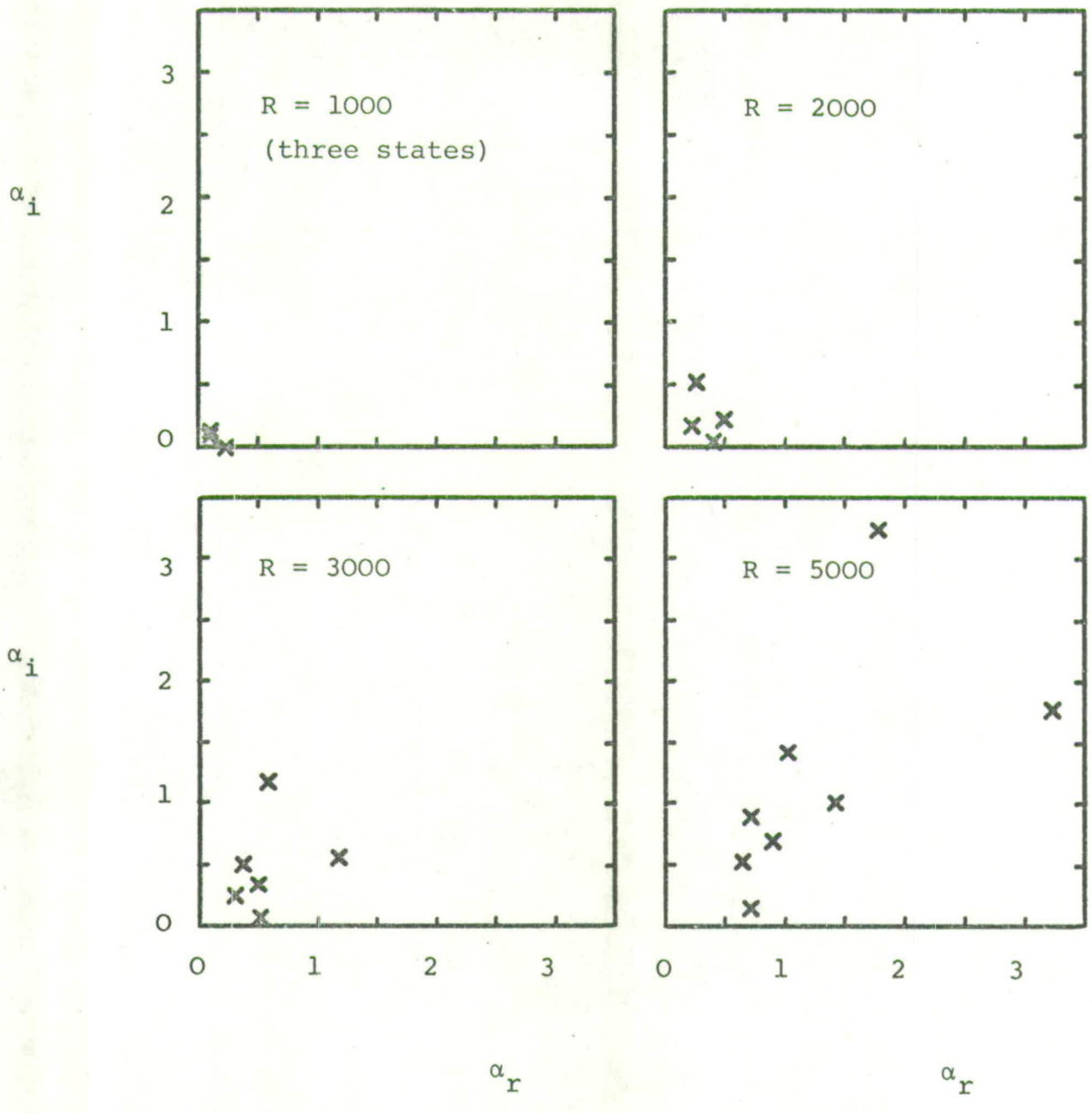

Figure 4.8 Evolution of the Eigenvalue Spectrum at $F = 80 \times 10^{-6}$

to emanate from the point $(\beta + i\beta)$ and ultimately form in pairs which are reflections in the line $\alpha_r = \alpha_i$.

Unfortunately, the numerical method does not behave well in the region of $\alpha_r = \beta$, so that newly created eigenvalues are difficult to locate and it is impossible to find the exact position of the source of eigenvalues. This difficulty increases with increase in Reynolds number or increase in the dimension of the discretisation matrix. Well-established eigenvalues, however, can be computed accurately and efficiently.

There is a considerable change in the form of the eigenfunctions as they move downstream. Figures 4.9 trace the development of State 2 from $R = 1000$ to $R = 3000$ at $F = 80 \times 10^{-6}$. At $R = 1000$ (soon after creation) the eigenfunction is highly oscillatory and stretches far out into the free stream. It then gradually contracts into the boundary layer, becoming less oscillatory until at $R = 3000$, it is a slowly varying function with its maximum very close to the plate. This behaviour suggests a mechanism by which random disturbances in the free stream might penetrate into the boundary layer and initiate natural transition to turbulence.

It should be noted that, unlike the other states, State 1 is relatively insensitive to change in Reynolds number or frequency. The eigenfunction does contract into the boundary layer but retains a similar form throughout. Only at $R = 5000$ does it show any sign of oscillatory behaviour.

The continuous variation of the eigenvalue spectrum is illustrated in Figures 4.10 to 4.12. Figure 4.10 shows the variation at $F = 80 \times 10^{-6}$ with $500 < R < 5000$, and Figure 4.11 that at $\beta = .24$ over the same range of Reynolds number. Finally,

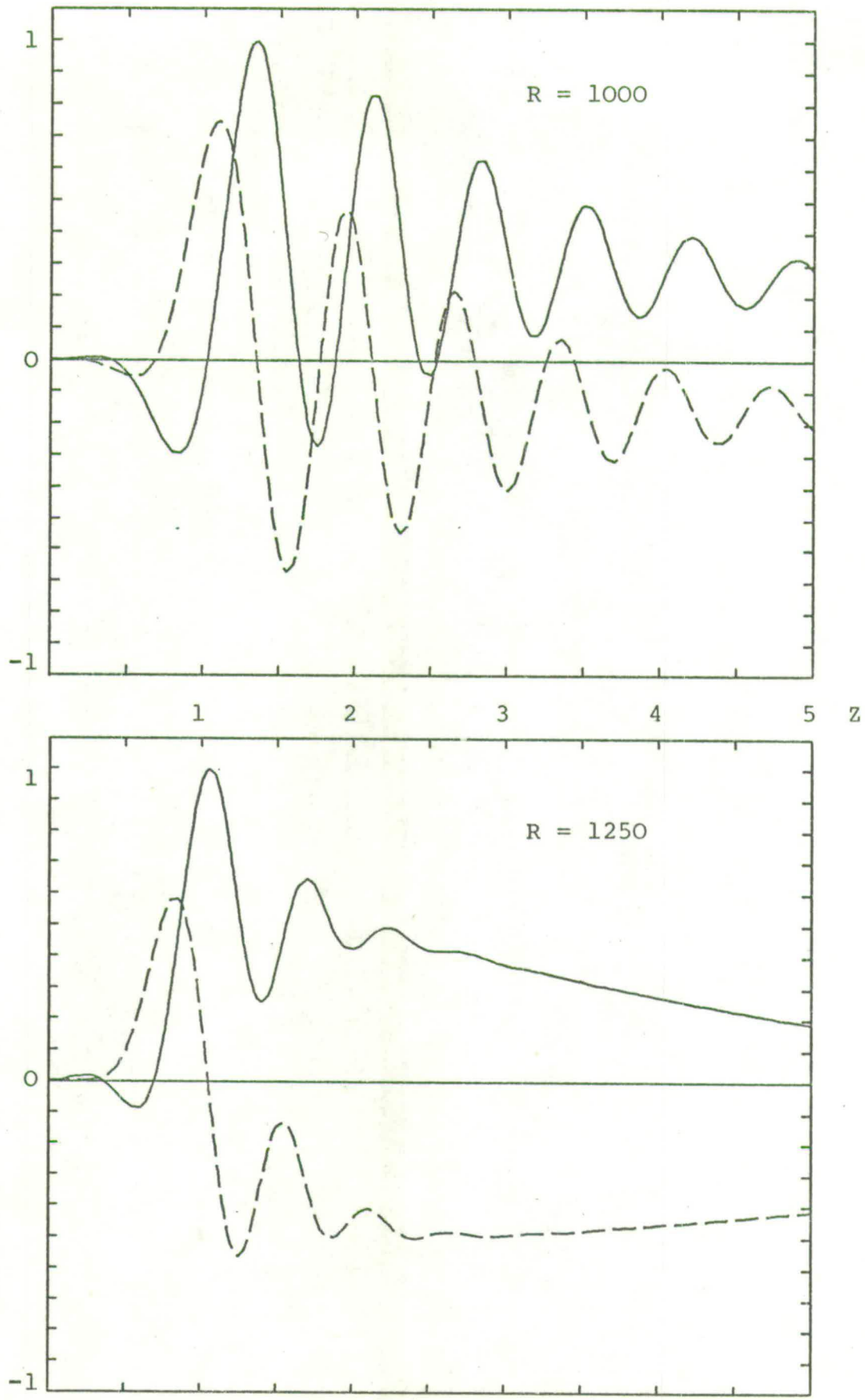

Figure 4.9 Evolution of State 2 at $F = 80 \times 10^{-6}$

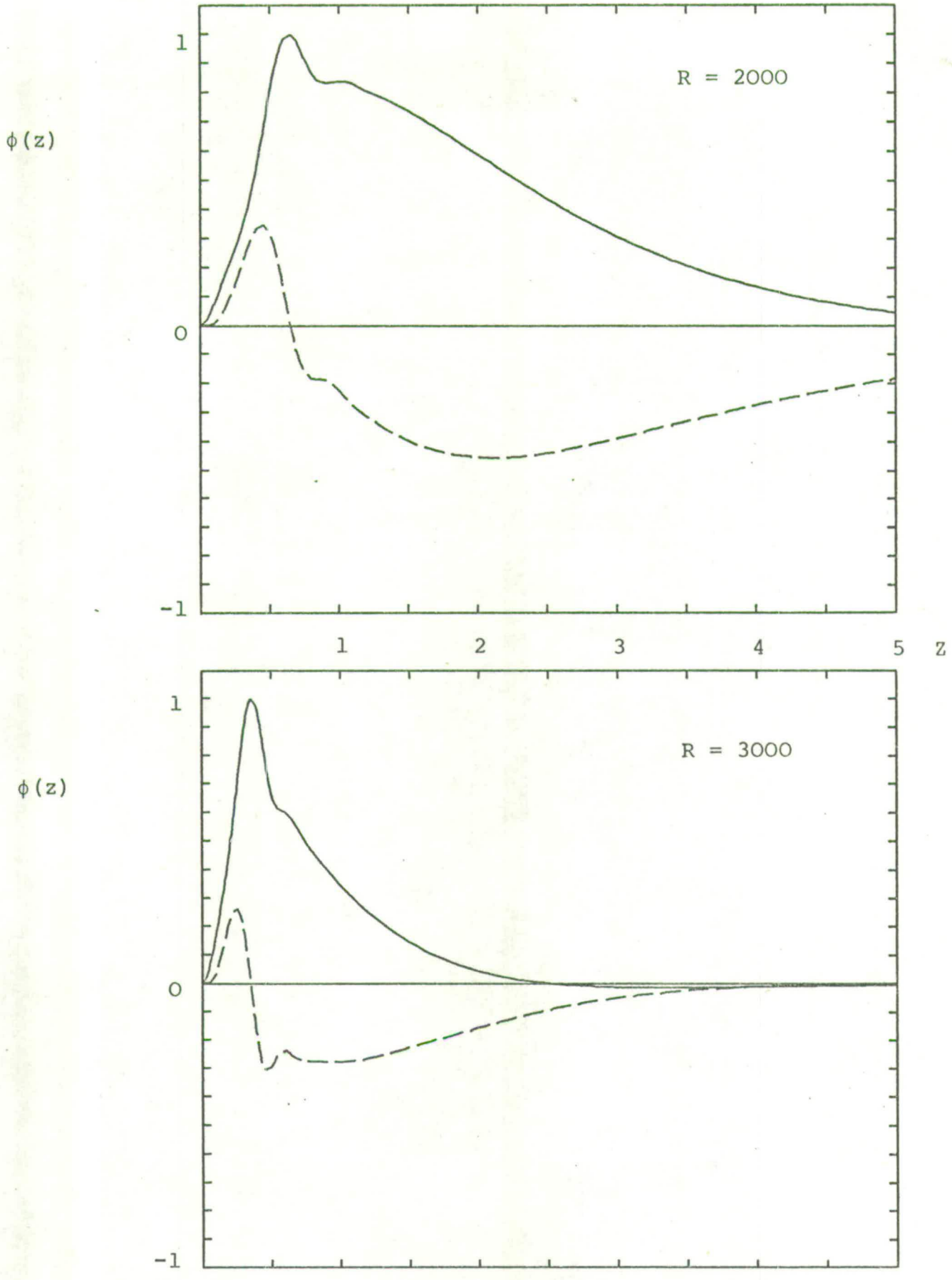

Figure 4.9 (Contd.) Evolution of State 2 at F = 80 × 10^{-6}

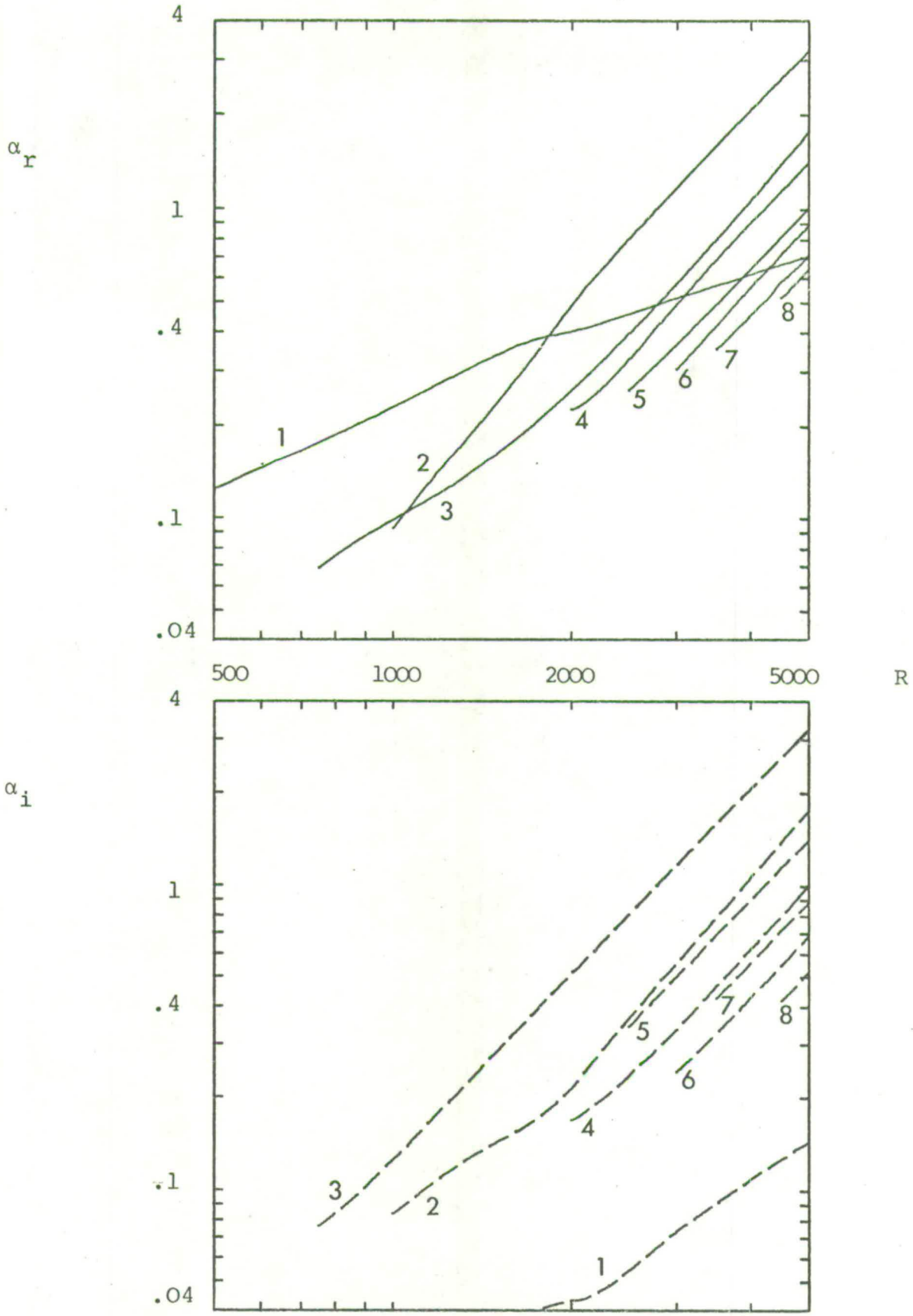

Figure 4.10 Eigenvalues at $F = 80 \times 10^{-6}$

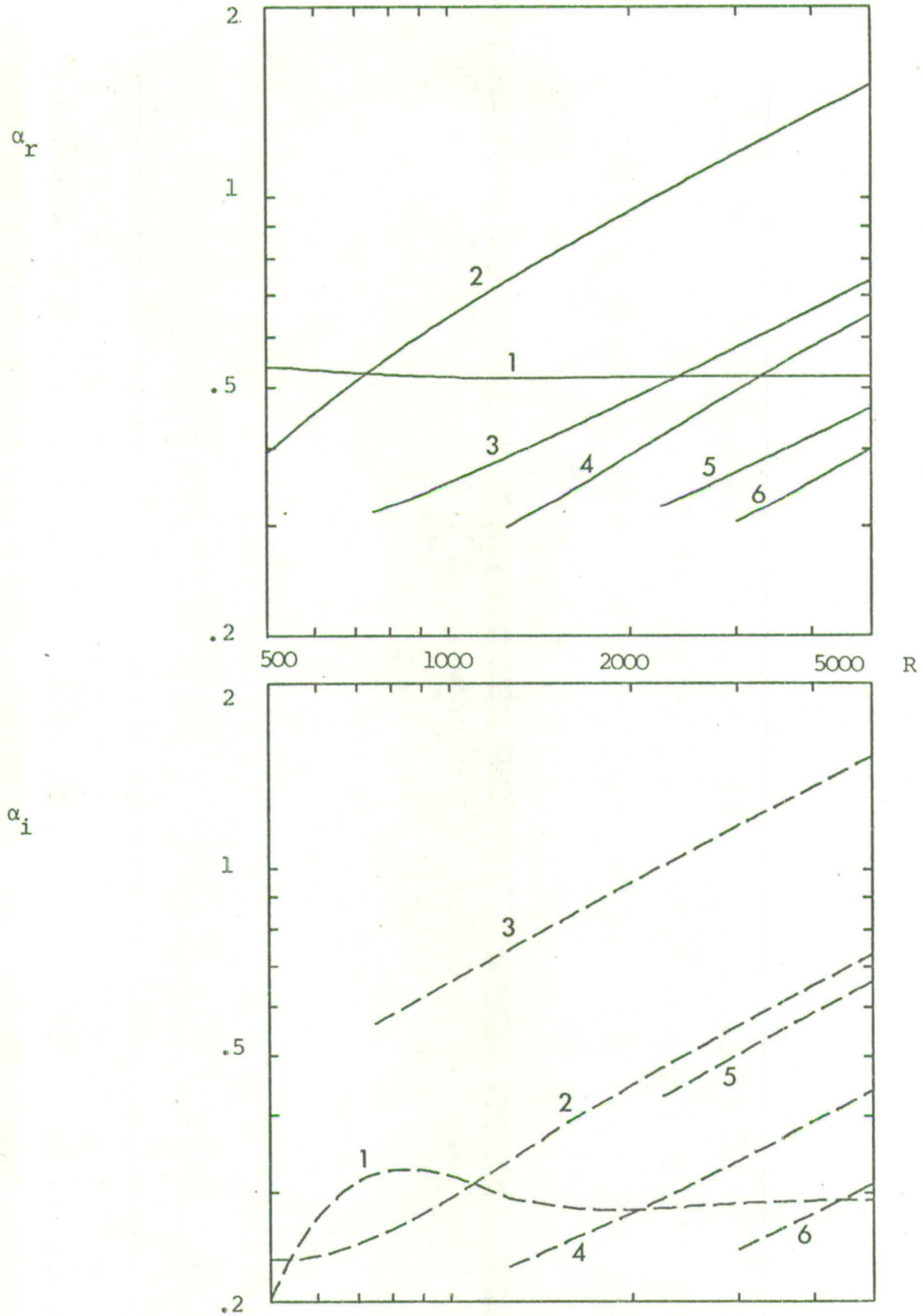

Figure 4.11 Eigenvalues at $\beta = .24$.

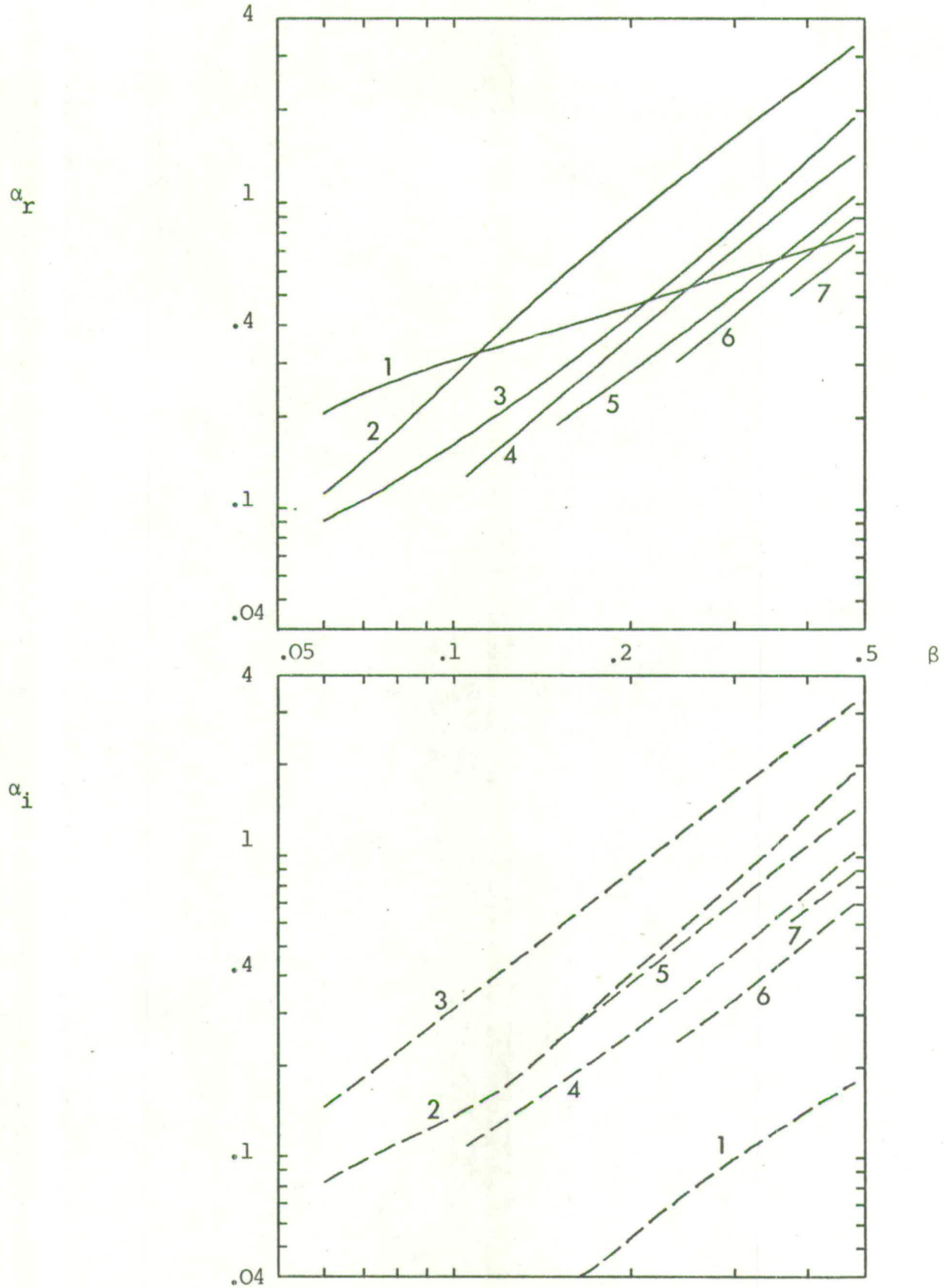

Figure 4.12 Eigenvalues at R = 3000.

the effect of change in frequency at R = 3000 is demonstrated in Figure 4.12. As before, the real part of the eigenvalue is shown as a continuous line, the imaginary part as a dashed line. In Figure 4.11 the imaginary part of State 1 has been multiplied by a factor of 4 so that it can appear on the same graph.

In each case, apart from State 1, the graphs are virtually parallel with gradients $2, \frac{1}{2}, \frac{3}{2}$ respectively. Since all scales are logarithmic, this implies that the higher eigenvalues are of the form

$$\alpha = k_j F^{3/2} R^2 = k_j \beta^{3/2} R^{1/2} \qquad (4.5)$$

where k_j is a constant which depends only on the number of the state. Thus there is a definite ratio between the eigenvalues at any given value of the parameters. Very approximately, this ratio is simply

$$\frac{k_2}{k_{2j}} = \frac{k_3}{k_{2j+1}} = j, \qquad j = 2,3,4 \ldots \qquad (4.6)$$

where k_j denotes either the real or imaginary part of the eigenvalue of the jth state. In fact, formulae (4.5) and (4.6) are more accurate if applied to $|\alpha|$ rather than α itself.

State 1 behaves quite differently and appears to have an inviscid limit at about $\alpha = \cdot 521 + \cdot 073i$ in Figure 4.11. It is therefore like the eigenvalues of Morawetz (type 1). If formula (4.5) still holds for large R, the other eigenvalues will become infinitely large in the inviscid limit and are therefore of a type excluded in the analysis of Morawetz [39].

4.4 Spurious Eigenstates

The matrix equation

$$M(\alpha)\,\underline{v} = \underline{0} \qquad (4.7)$$

has $4(n+1)$ eigenvalues (not necessarily distinct) on the complex α-plane. If the full outer boundary condition (3.11) involving the double-valued parameter γ has been used, equation (4.7) has $8(n+1)$ eigenvalues over the entire Riemann surface.

Some of these eigenvalues are true eigenvalues of the original differential equation while the others are purely algebraic solutions of (4.7). Obviously, the numerical methods described in Chapter 3 produce both types of solution and it is necessary to distinguish between them. The most reliable method of doing this is to vary the net spacing h. Only true eigenvalues satisfy equation (4.1) for sufficiently small h.

Algebraic eigenvalues found at $R = 3000$, $\beta = \cdot 24$ for $h = \cdot 1$ and $h = \cdot 05$ appear in Figure 4.13 along with the true eigenvalues of States 1, 4, 5 and 6. All the eigenvalues shown lie on the physical half of the Riemann surface ($\gamma_r \geq 0$) and the branch line is approximately the line $\alpha_r = \beta$ (with $\alpha_i > 0$) in this region of the α-plane.

The algebraic eigenvalues form a large Y-shaped array, the position of which is extremely sensitive to change in h. The stem and left branch of the Y are close to the branch line and have very closely spaced eigenvalues, particularly when α_i is small. The right branch, however, is relatively sparse in eigenvalues and stretches beyond the limits of the graph. Figure 4.14 is the lower part of Figure 4.13 on a more suitable scale.

In comparing the two results at different h, it is worth

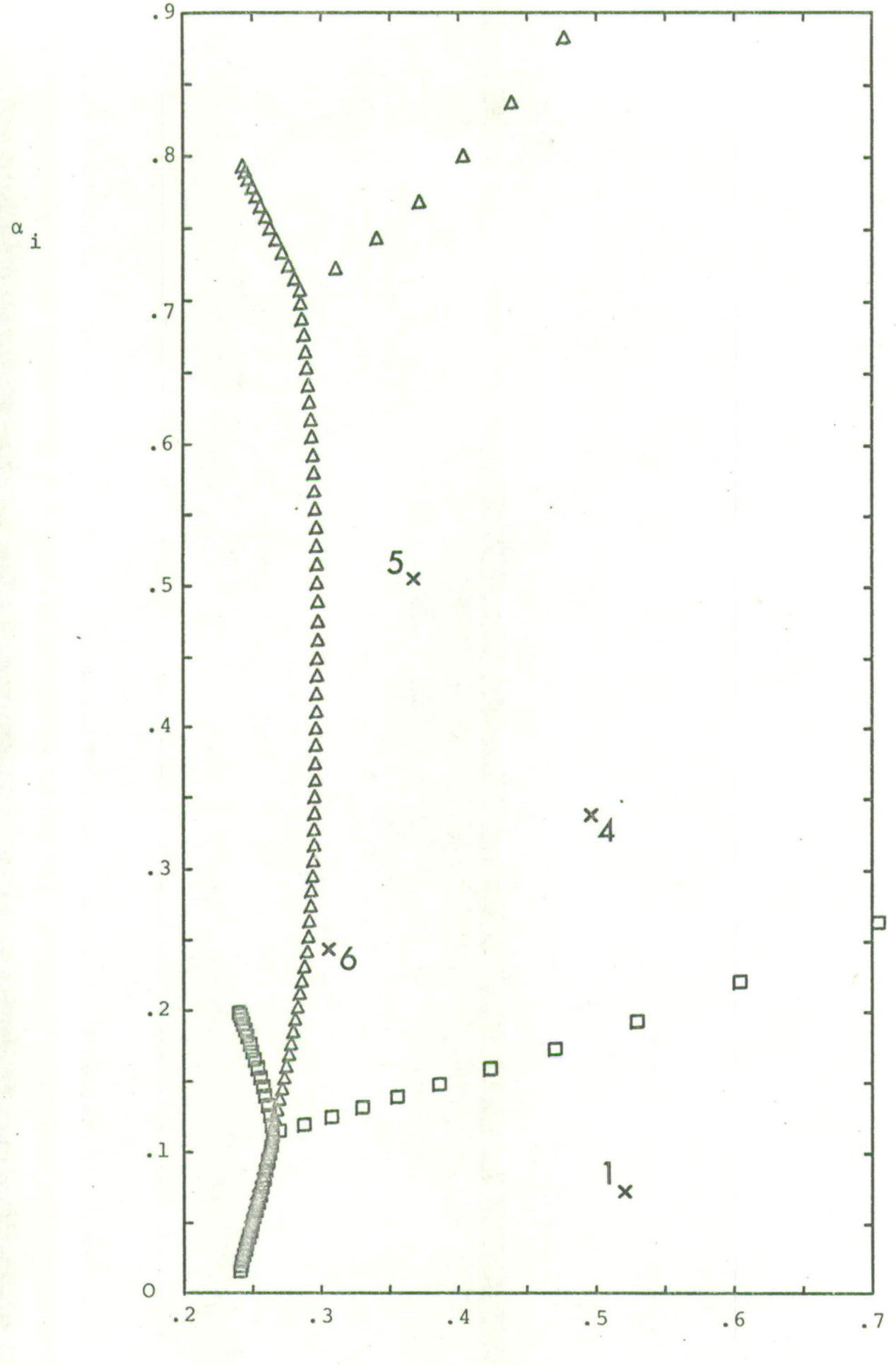

Figure 4.13 Algebraic Eigenvalues at R = 3000, β = .24

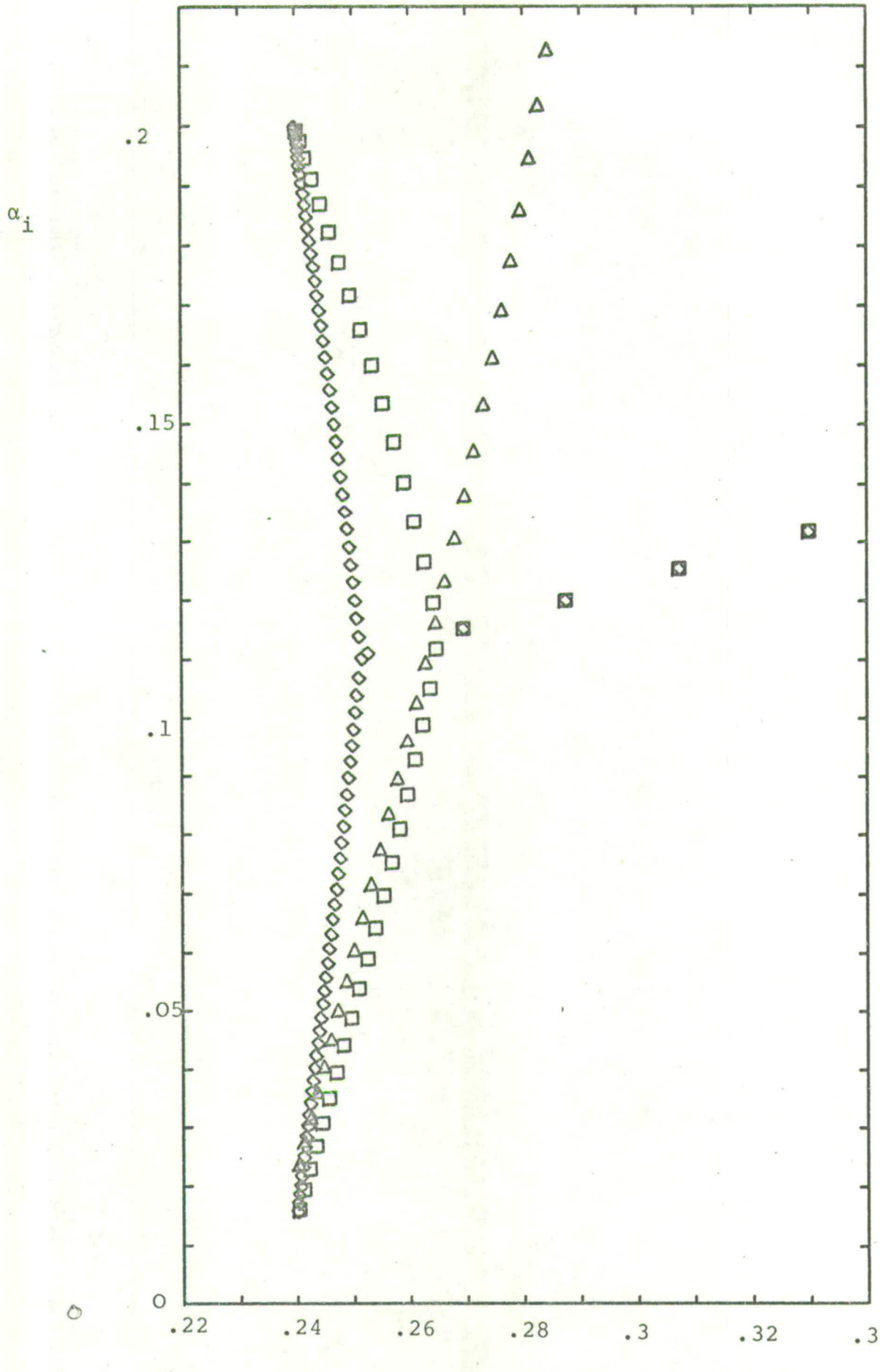

Figure 4.14 Algebraic Eigenvalues at R = 3000, β = .24

△ h = .05, z_{max} = 6

□ h = .1, z_{max} = 6

◇ h = .1, z_{max} = 12.

noting the following points:

(i) The spacing of eigenvalues on the stem is the same in both cases.

(ii) The stem eigenvalues move a little to the left when h is halved.

(iii) The imaginary part of the last eigenvalue on the left branch jumps from $\cdot 2$ to $\cdot 8$ when h is halved. Thus, there is $O(h^{-2})$ behaviour in the branch eigenvalues.

In both the results for Figure 4.13, the point of application of the outer boundary condition (3.11) was fixed at $z_{max} = 6$. It turns out that the algebraic eigenvalues are also sensitive to change in z_{max}. This is illustrated in Figure 4.14 which shows an additional set of results at $h = \cdot 1$ but with $z_{max} = 12$.

A comparison of the two results at $h = \cdot 1$ leads to the following conclusions:

(i) The spacing of eigenvalues on the stem and the left branch halves when z_{max} is doubled.

(ii) The distance of the stem and the left branch from the line $\alpha_r = \beta$ halves when z_{max} is doubled.

(iii) The branch eigenvalues are relatively insensitive to change in z_{max} compared with change in h.

The branch eigenvalues appear to be completely spurious, representing a breakdown in the resolution of the finite difference process. If a true eigenstate is too oscillatory to be represented at a given h, the right branch passes below the position of its eigenvalue, so that it does not appear in the spectrum. As h is decreased, however, the branch rapidly

rises up and the true eigenvalue is revealed. For example, the spectrum at $R = 3000$, $\beta = \cdot 24$, and $h = \cdot 05$ does not contain State 3 which has the highest number of oscillations per unit z. At $h = \cdot 04$, however, all six states appear.

The stem eigenvalues, on the other hand, may have some degree of physical significance, since they are similar to the infinite set of eigenvalues found in bounded flows (Morawetz, type 2). This possibility will be fully discussed in Section 5.5, where precisely the same question arises in the (T) case.

Considering the high density of algebraic eigenvalues near $\alpha_r = \beta$, it is hardly surprising that neither of the numerical methods works well in this region. Since $\det M(\alpha)$ is highly oscillatory, the Contour method requires a very fine grid of points in the α-plane and so is rather inefficient. The Osborne method converges very slowly to stem eigenstates (about 10 iterations instead of 2 or 3) unless a very good initial approximation to the eigenvalue is available. In the case of a true eigenstate close to the stem (as with State 6 at $R = 3000$, $\beta = \cdot 24$) the rate of convergence is slightly better, but there is a definite ceiling to the level of accuracy which is low when the eigenvalue is very close or when h is small. Even increasing z_{max} does not help since, although the stem moves to the left, the density of stem eigenvalues increases. It is as if the presence of the stem prevents the true eigenvalue taking up its proper position.

CHAPTER 5

RESULTS FOR TEMPORALLY DEVELOPING DISTURBANCES

5.1 Introduction

This chapter is concerned with temporally developing disturbances in plane Poiseuille and Blasius flow. The LR method has been used successfully to compute the eigenvalue spectrum in both cases. The results for a typical plane Poiseuille spectrum will be presented in the next section together with selected eigenfunctions obtained by the Osborne method.

The remainder of the chapter is devoted to the Blasius boundary layer. In Section 5.3, accurate results for a particular spectrum will be given. Then the orthogonality properties of the eigenfunctions will be discussed, and finally, the behaviour of spurious eigenstates will be described in Section 5.5.

In the Blasius case, the LR method is restricted to the simple outer boundary condition (3.12). Thus, it was always necessary to refine the results by using the Osborne method with the full outer boundary condition (3.11). As in the spatial case, the point of application of (3.11) or (3.12) was chosen far enough out into the free stream so that the eigenvalue was insensitive to further increase in z_{max} compared with change in h.

In every case, the accuracy of the eigenvalues obtained was checked by calculating the corresponding solution of the adjoint equation (2.21).

5.2 Plane Poiseuille Spectrum

Although the spectrum of the Orr-Sommerfeld equation for plane Poiseuille flow is well known, it was considered useful to apply the same numerical method to this typical bounded flow for direct comparison with the results for unbounded Blasius flow. In addition, it was hoped that there would be good agreement with previous results for the plane Poiseuille spectrum like those of Grosch and Salwen[45] or Orszag[46], thus confirming the accuracy of the present methods. Only symmetrical disturbances (i.e. disturbances with a symmetrical eigenfunction) are discussed here and the appropriate outer boundary condition is therefore (3.10a).

The eigenvalue spectrum at $R = 10{,}000$, $\alpha = 1$ was calculated using the LR method with $h = \cdot 01$. The first 32 eigenvalues are shown in Figure 5.1 and listed in Table 5.1. These are all true eivenvalues and indeed, many more were found with $c_r \doteq {}^2/_3$ and $c_i < -1$. Since a comparison with the adjoint results suggests that the eigenvalues shown are accurate to about 4 decimal places, further refinement is considered unnecessary. There is also excellent agreement with the results of Orszag.

The eigenvalues lie in a Y-shaped configuration on the c-plane, with the stem of the Y positioned at $c_r \doteq {}^2/_3$ and the branches going towards $c_r = 0$ and $c_r = 1$. The left branch is split into two lines of eigenvalues which appear to be paired like those found in Chapter 4, but in not such an obvious way. Eigenvalues on the right branch and the stem are more closely spaced.

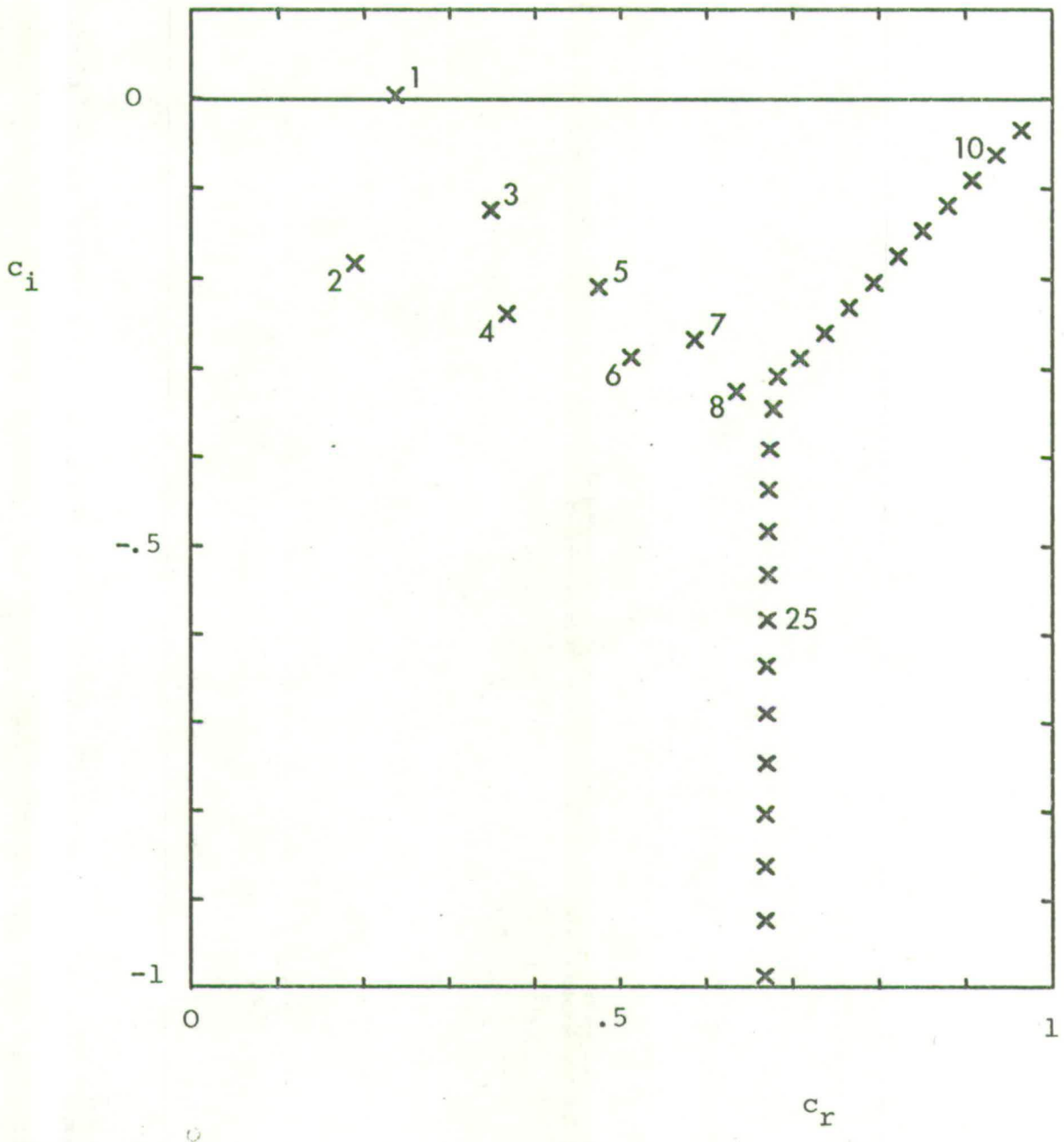

Figure 5.1 Plane Poiseuille Spectrum at R = 10,000, α = 1

TABLE 5.1

The First 32 Symmetrical States of the Plane Poiseuille Spectrum at $R = 10{,}000$, $\alpha = 1$ $(h = .01)$

State	c_r	c_i	State	c_r	c_i	State	c_r	c_i
1	.23753	.00373	9	.96464	-.03519	20	.67765	-.34381
2	.19007	-.18283	10	.93635	-.06325	21	.67453	-.38986
3	.34910	-.12453	11	.90806	-.09131	22	.67322	-.43576
4	.36852	-.23887	12	.87976	-.11938	23	.67234	-.48313
5	.47490	-.20880	13	.85146	-.14743	24	.67161	-.53214
6	.51298	-.28672	14	.82315	-.17549	25	.67098	-.58283
7	.58723	-.26729	15	.79484	-.20355	26	.67045	-.63521
8	.63621	-.32535	16	.76653	-.23162	27	.66999	-.68931
			17	.73816	-.25974	28	.66959	-.74513
			18	.70894	-.28772	29	.66925	-.80269
			19	.68292	-.30775	30	.66896	-.86199
						31	.66870	-.92302
						32	.66848	-.98580

The stem eigenvalues agree well with the approximate formulae of Grohne (see Section 2.6). Substitution of the Poiseuille profile (2.7) in equation (2.23) with $m = 2$ gives

$$c_r = \frac{1}{2} \int_0^2 z(2-z)\,dz = {}^2/_3 \,. \qquad (5.1)$$

Since State 32 (symmetrical) corresponds to $n = 62$ in Grohne's notation for the complete spectrum, inequality (2.22) becomes

$$-1.011 < c_i < -.979 \qquad (5.2)$$

and the imaginary part of State 32 does, in fact, lie within these limits.

From analytical work, it is known that the stem eigenvalues are infinite in number, so that Figure 4.1 shows a very small part of the total spectrum. Obviously, a given size of discretisation matrix can only represent a certain number of eigenstates and this is inversely proportional to the net spacing h. As was found by Grosch and Salwen, the numerical model eventually breaks down and the stem of eigenvalues splits into two spurious branches, rather like those discussed in Section 4.4.

The Osborne method was used to calculate some of the eigenfunctions. Figure 5.2 shows States 4 and 5, which are very similar except that State 5 is shifted further out towards the centre of the channel ($z = 1$). For comparison, two line eigenstates are illustrated in Figure 5.3. State 10 has almost all its amplitude near $z = 1$, while State 25 has a relatively small region of rapid oscillations near the critical layer.

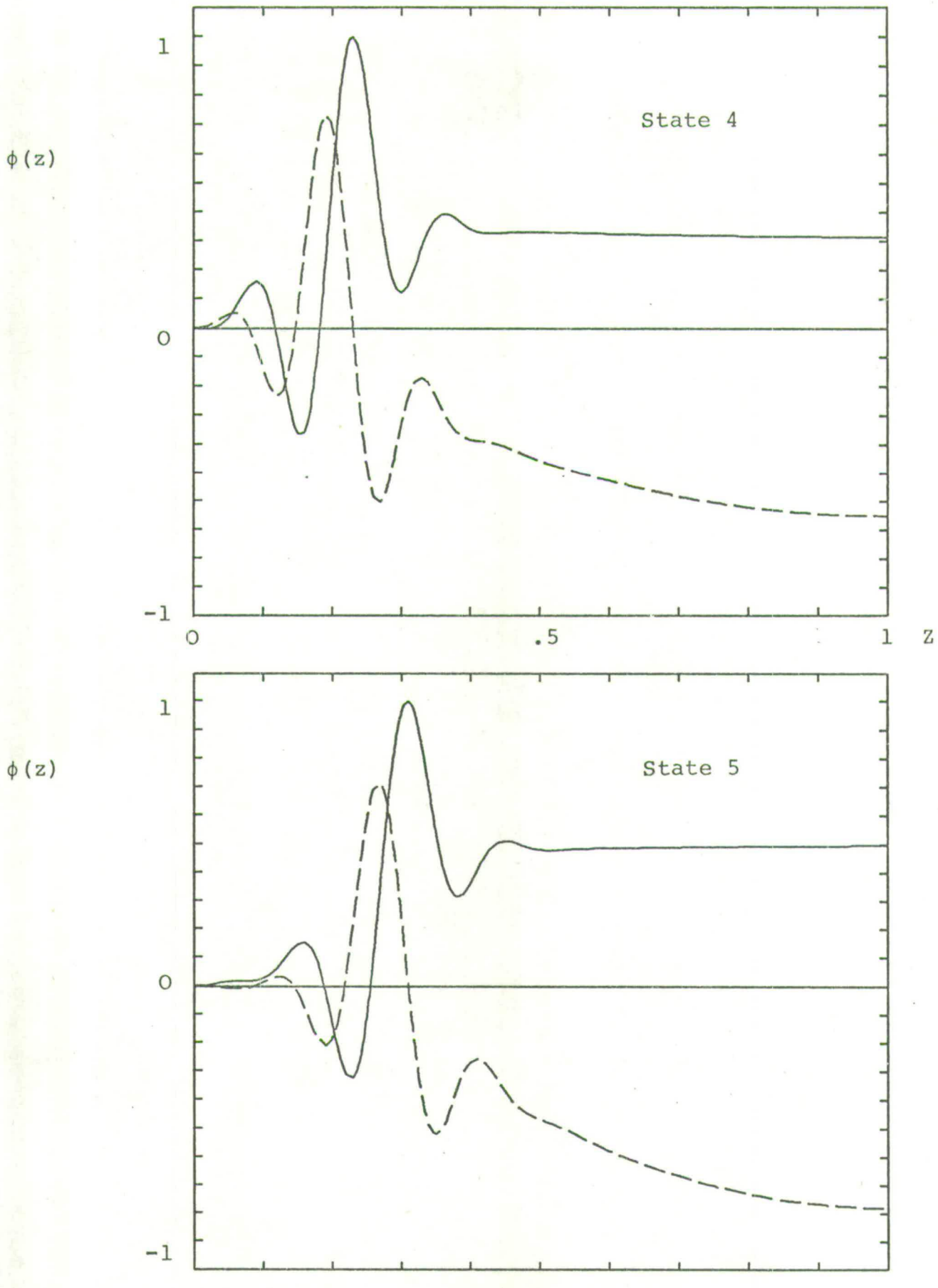

Figure 5.2 Eigenfunctions at R = 10,000, α = 1.

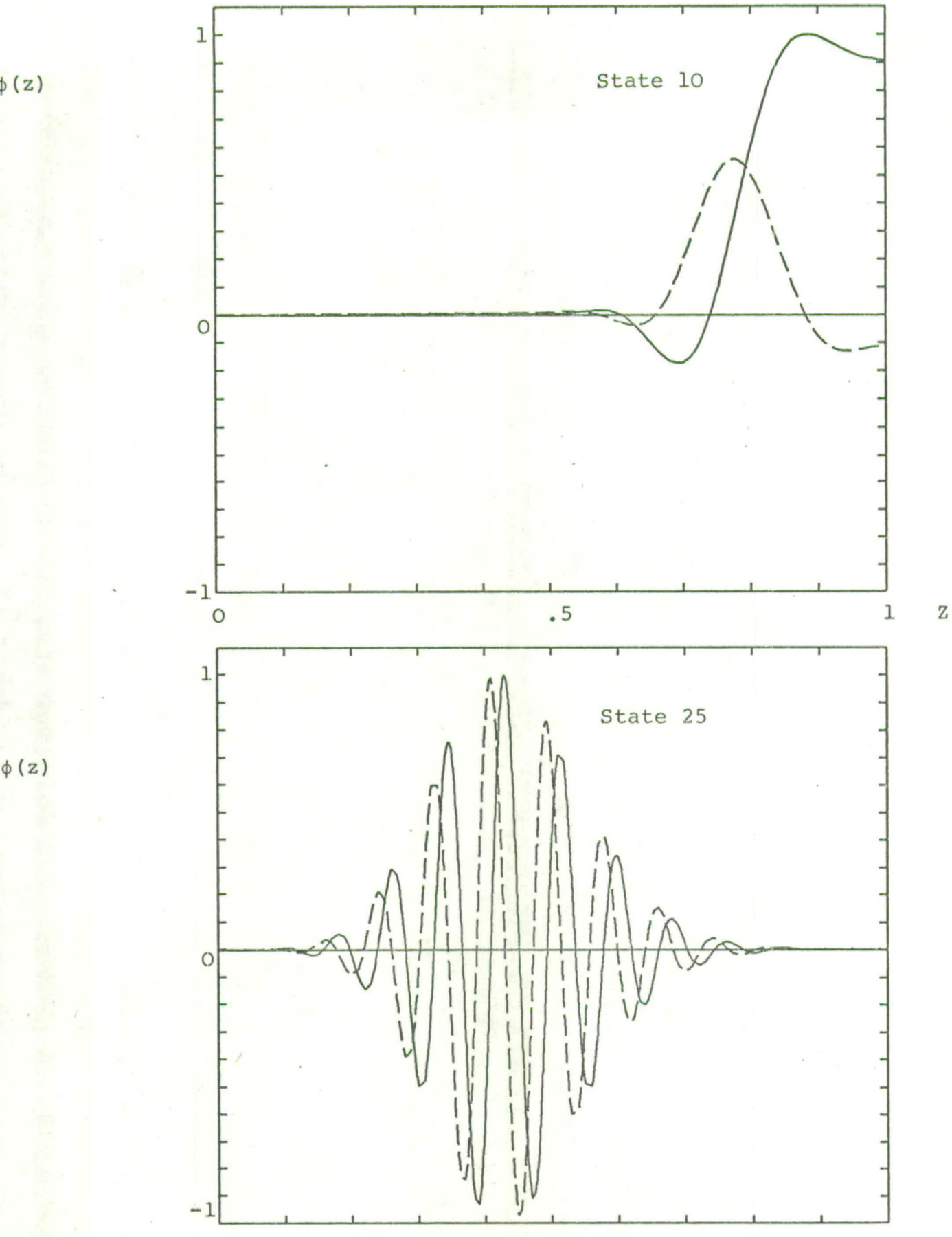

Figure 5.3 Eigenfunctions at R = 10,000, α = 1.

5.3 Blasius Spectrum

Following Jordinson[49], the eigenstate spectrum of Blasius flow at $R = 998$, $\alpha = .308$, was thoroughly investigated. The LR method was used to provide good starting values for the Osborne method and seven true eigenstates were found. These are illustrated in Figure 5.4 which looks very much like a fragment of the plane Poiseuille spectrum (Figure 5.1) except that the eigenvalues are shifted more towards $c_r = 1$. The eigenstates are numbered in order of increasing c_r except for State 1 which is the fundamental eigenstate associated with the neutral stability curve.

Compared with the spatial case (Figure 4.1), the pattern of these higher eigenstates is not quite so simple to formulate. Certainly, they lie along two definite lines on the c-plane which appear to converge near $c_r = 1$, one line through the even states and the other through the odd states (excluding State 1). However, there is no simple relationship between the eigenvalues of "partner" states.

Since equations (4.1), (4.2) and (4.3) apply equally well to the temporal eigenvalue c, the method of Section 4.2 was used to obtain accurate estimates of the ordinary and adjoint eigenvalues which appear in Table 5.2. A much higher level of accuracy was achieved than in the spatial case, ranging from 9 decimal places (State 1) to 6 decimal places (State 7). This was almost certainly due to the lower Reynolds number but the linearity of the eigenvalue might also have helped. States 1, 2, 4 and 6 were originally found by Jordinson[49] and there is very good agreement with the more recent results of Davey[52]

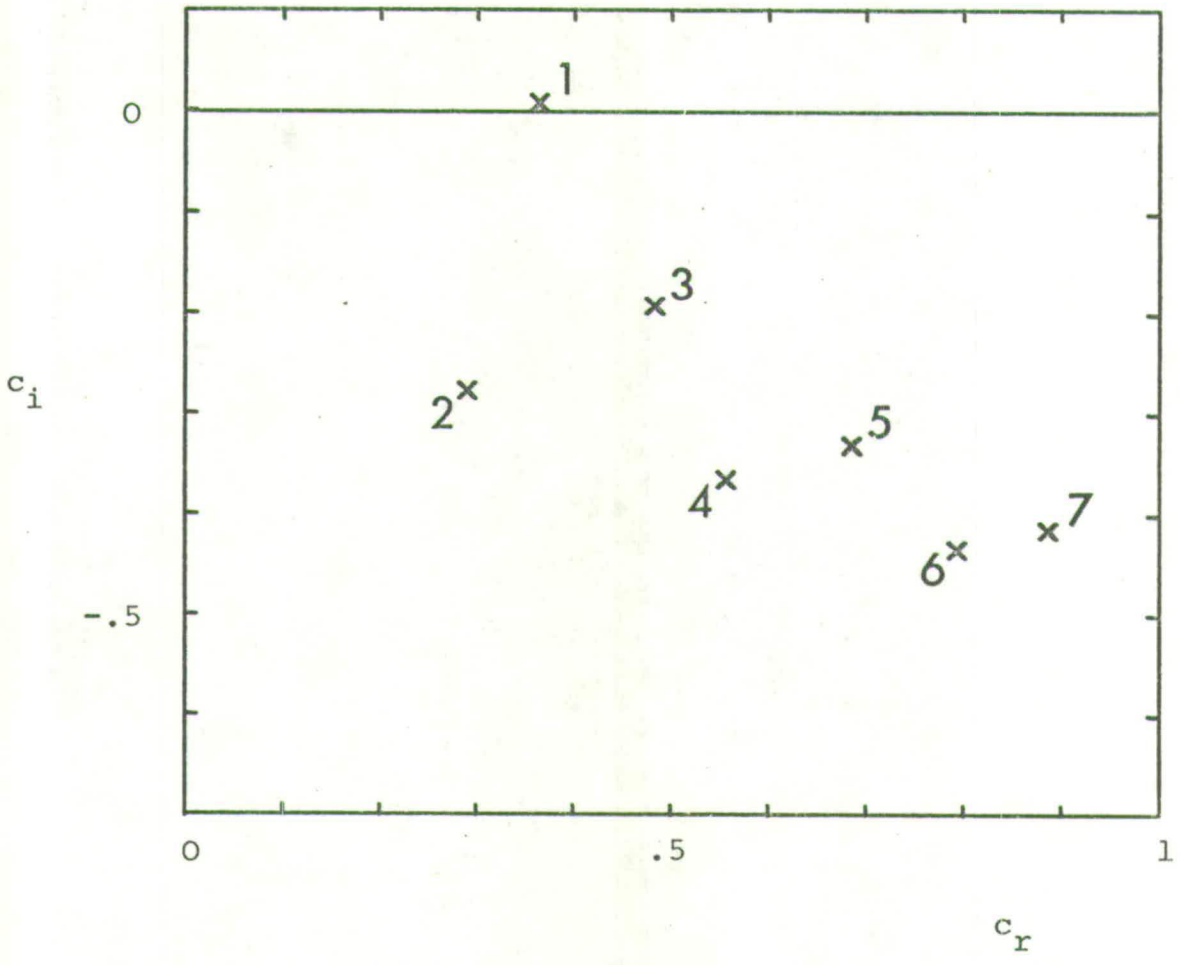

Figure 5.4 Blasius Spectrum at R = 998, α = .308.

TABLE 5.2

Blasius Spectrum at R = 998, α = .308.

State	Equation	c_r	c_i	h_{min}	z_{max}
1	O.S.	.364121290	.007962505	.01	6
	Adjoint	.364121289	.007962505		
2	O.S.	.289724306	-.276873857	.01	6
	Adjoint	.289724306	-.276873857		
3	O.S.	.483943904	-.192082409	.01	6
	Adjoint	.483943903	-.192082409		
4	O.S.	.55722135	-.36535147	.01	6
	Adjoint	.55722135	-.36535147		
5	O.S.	.68628783	-.33078588	.01	6
	Adjoint	.68628783	-.33078587		
6	O.S.	.7936877	-.4340984	.02	7
	Adjoint	.7936877	-.4340983		
7	O.S.	.887408	-.414760	.02	10
	Adjoint	.887409	-.414761		

and Mack[51] obtained by explicit methods.

The ordinary and adjoint eigenfunctions of the seven states are shown in Figures 5.5 to 5.11. As before, the continuous line is the real part of the eigenfunction and the dashed line is the imaginary part.

As a whole, the ϕ functions are very similar to those found in the spatial case, if the difference in Reynolds number is taken into account. An exception is State 3 which looks very much like State 1 with its maximum well out into the free stream ($z \doteqdot 2$). The other states have their maximum amplitude closer to the plate but there is an outward progression from $z \doteqdot .7$ (State 2) to $z \doteqdot 1.8$ (State 7). Apart from this shift outwards, States 4 and 5 are virtually identical and States 6 and 7 are also very similar.

As far as comparison with analytical theory is concerned, it is clear that both a viscous, oscillatory function and an inviscid, slowly varying function are present in the higher eigenstates. In addition, approximate calculations indicate that the even states reside in only two sectors of the complex z-plane (S_3 and S_2) while the odd states (apart from State 1) extend over all three sectors (cf. Section 4.2).

5.4 Orthogonality Properties

So far, only the accuracy of the eigenvalue has been investigated. The orthogonality properties of the temporal eigenfunctions (discussed in Section 2.5) provide a useful check on the accuracy of the ordinary and adjoint functions obtained numerically. Using the results of Section 5.3, the following integrals were evaluated by Simpson's Rule.

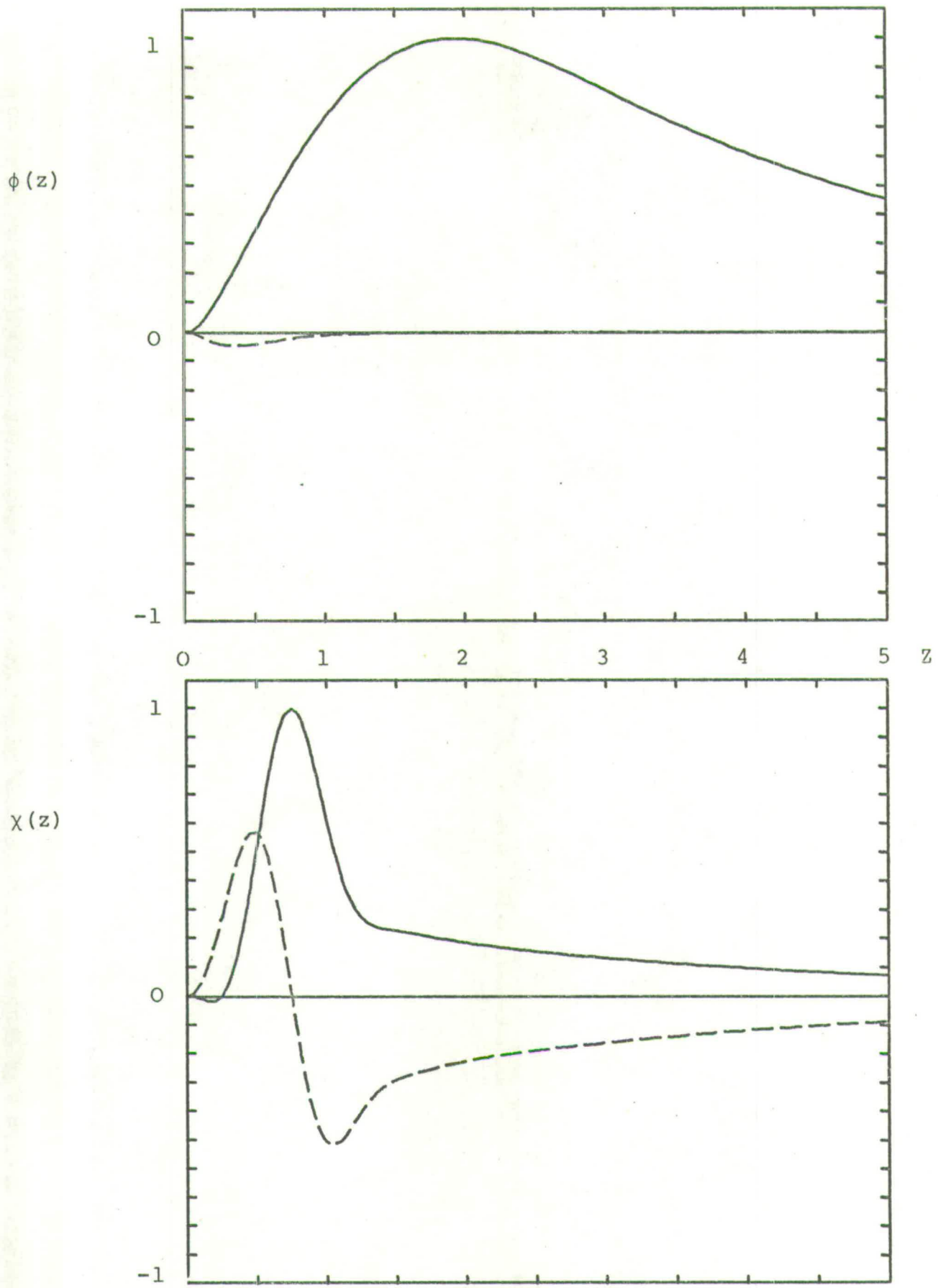

Figure 5.5 State 1 Eigenfunctions at R = 998, α = .308.

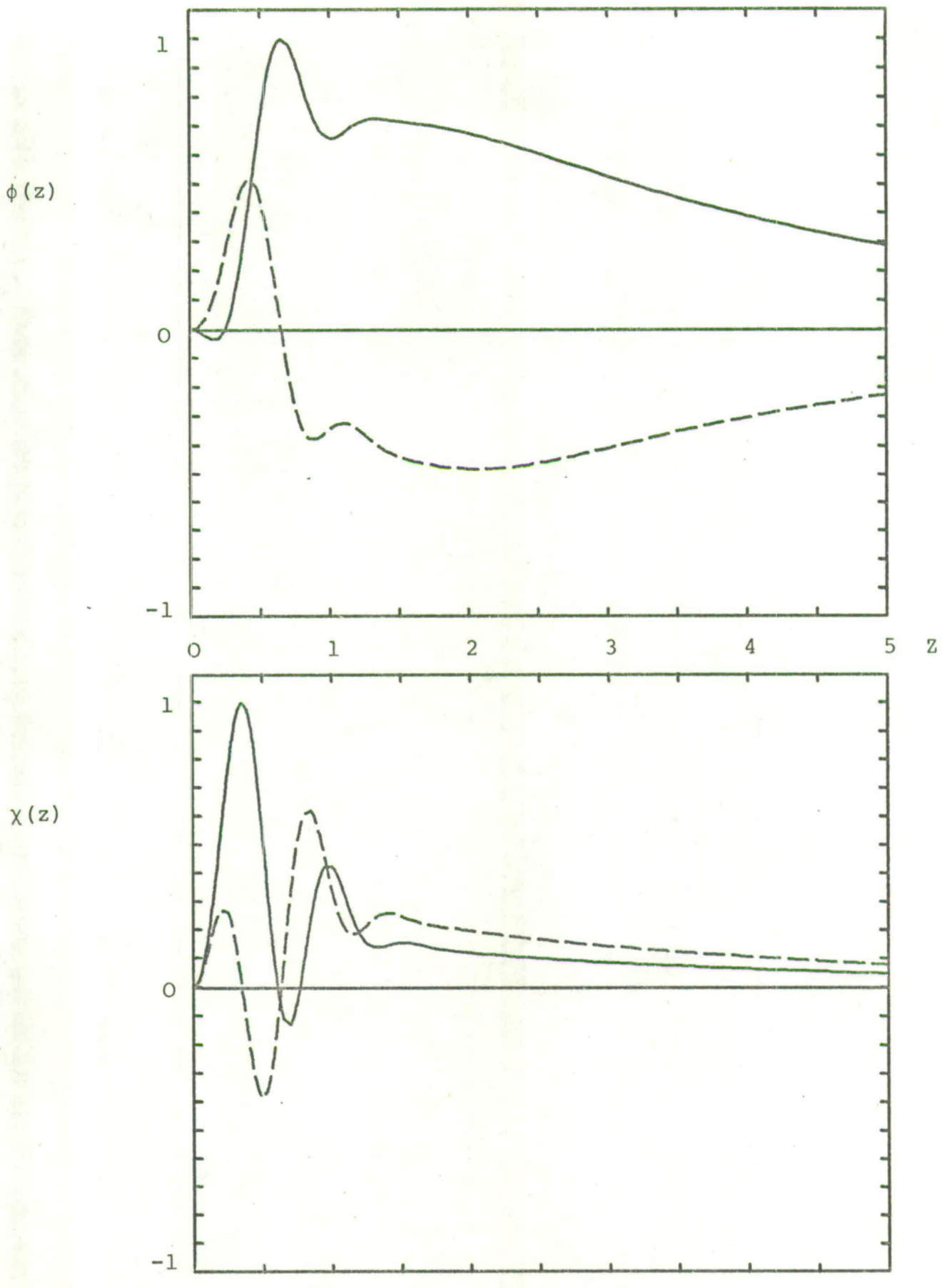

Figure 5.6 State 2 Eigenfunctions at R = 998, α = .308.

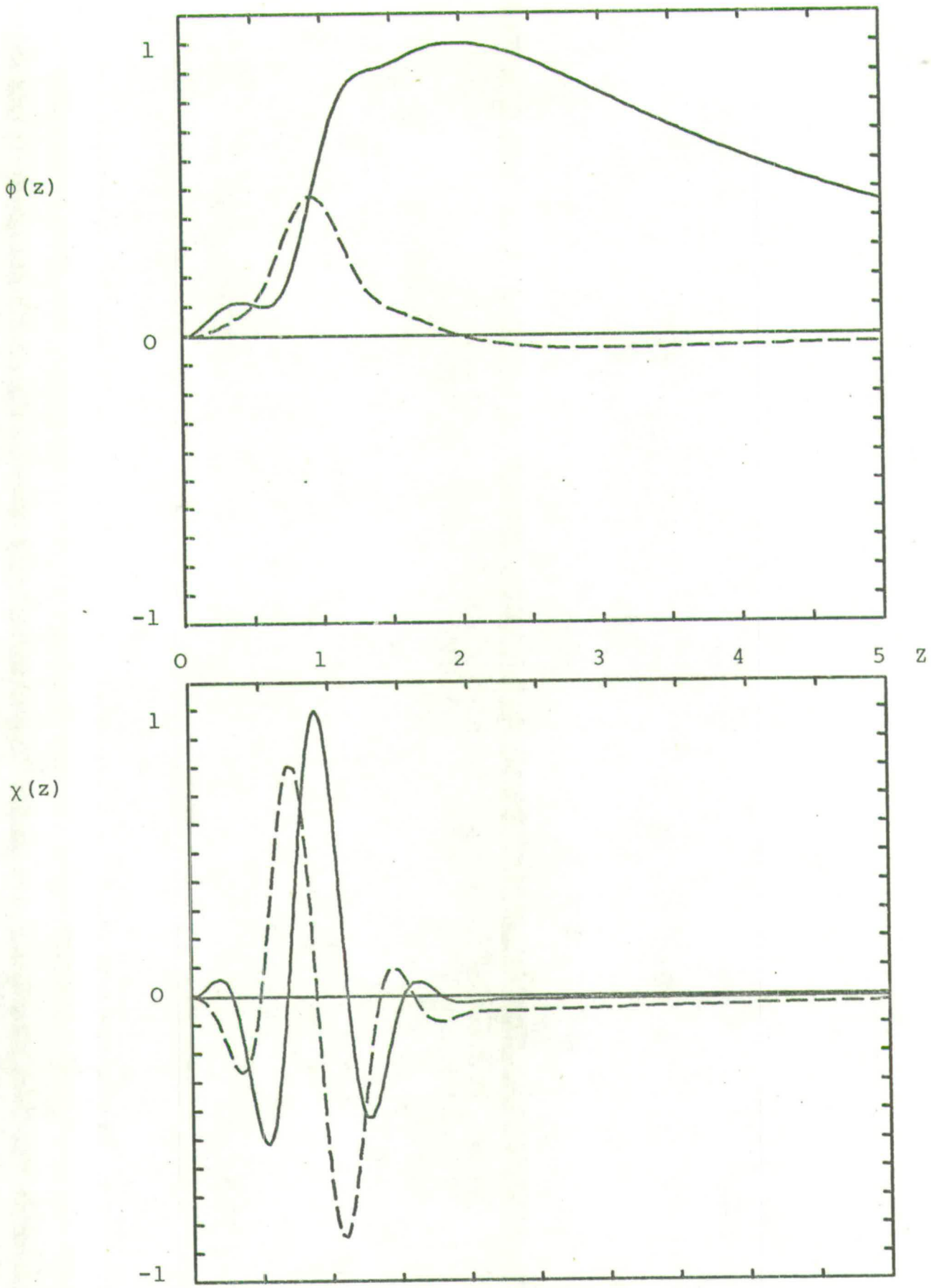

Figure 5.7 State 3 Eigenfunctions at R = 998, α = .308.

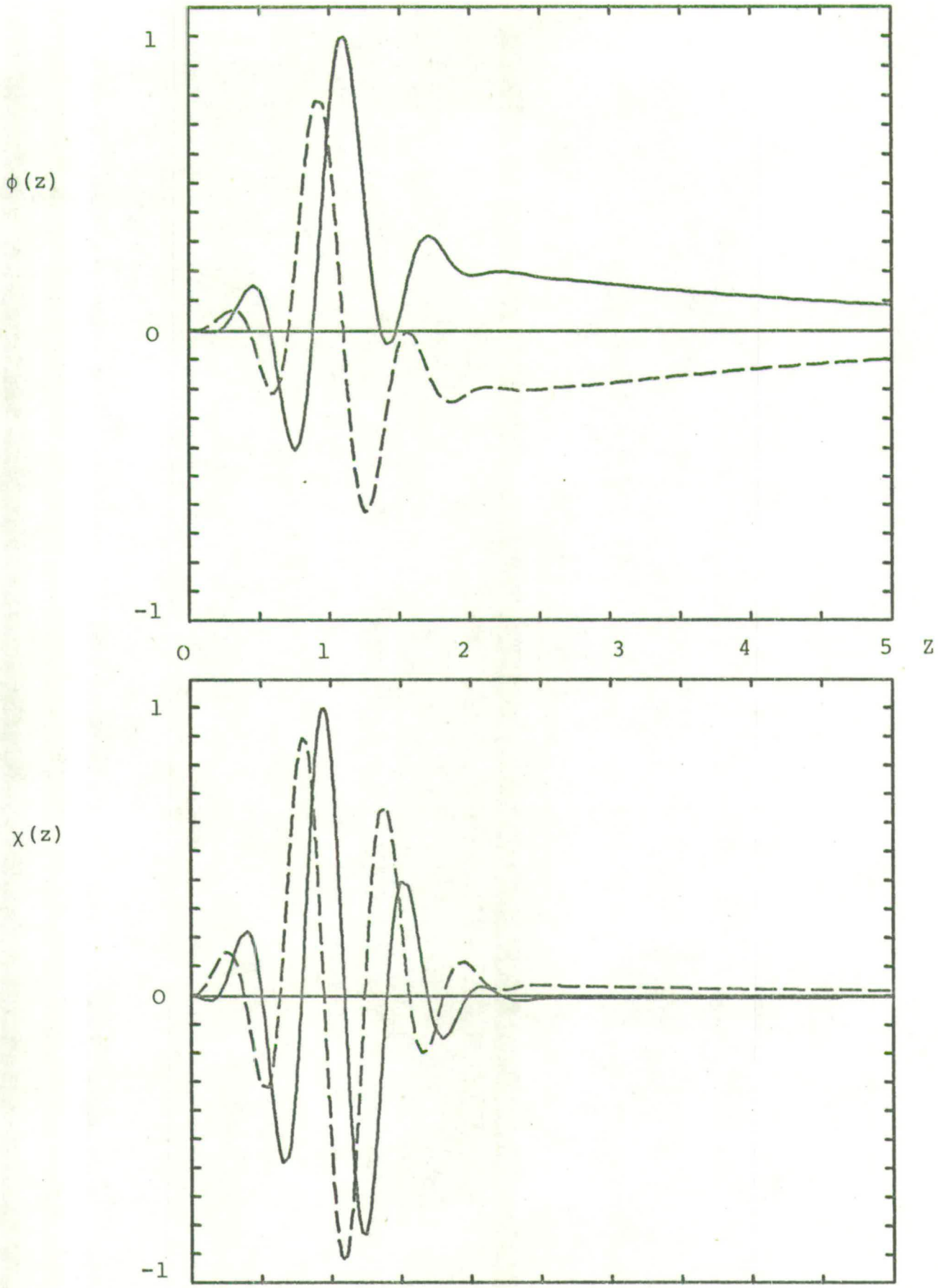

Figure 5.8 State 4 Eigenfunctions at R = 998, α = .308 .

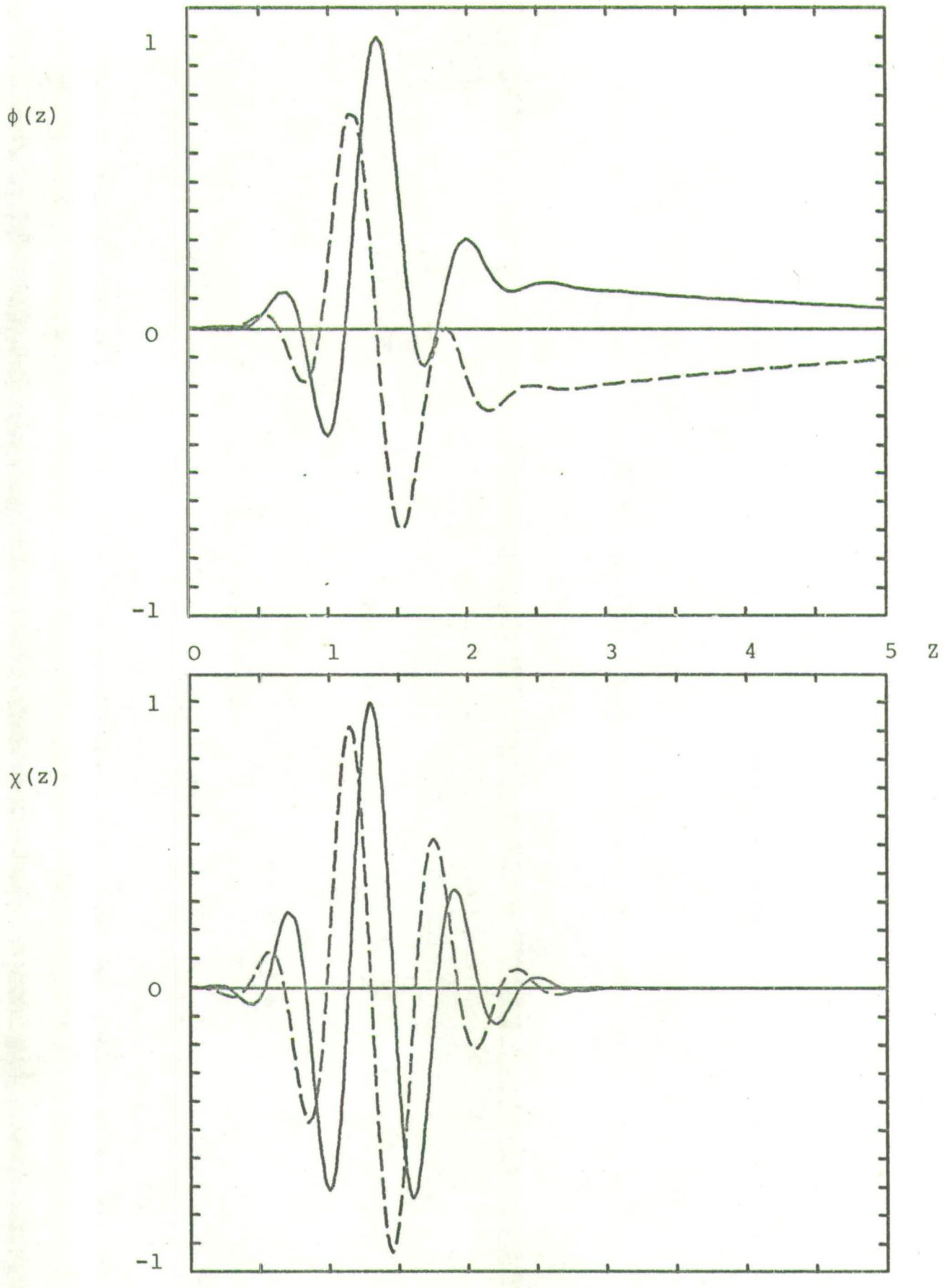

Figure 5.9 State 5 Eigenfunctions at R = 998, α = .308 .

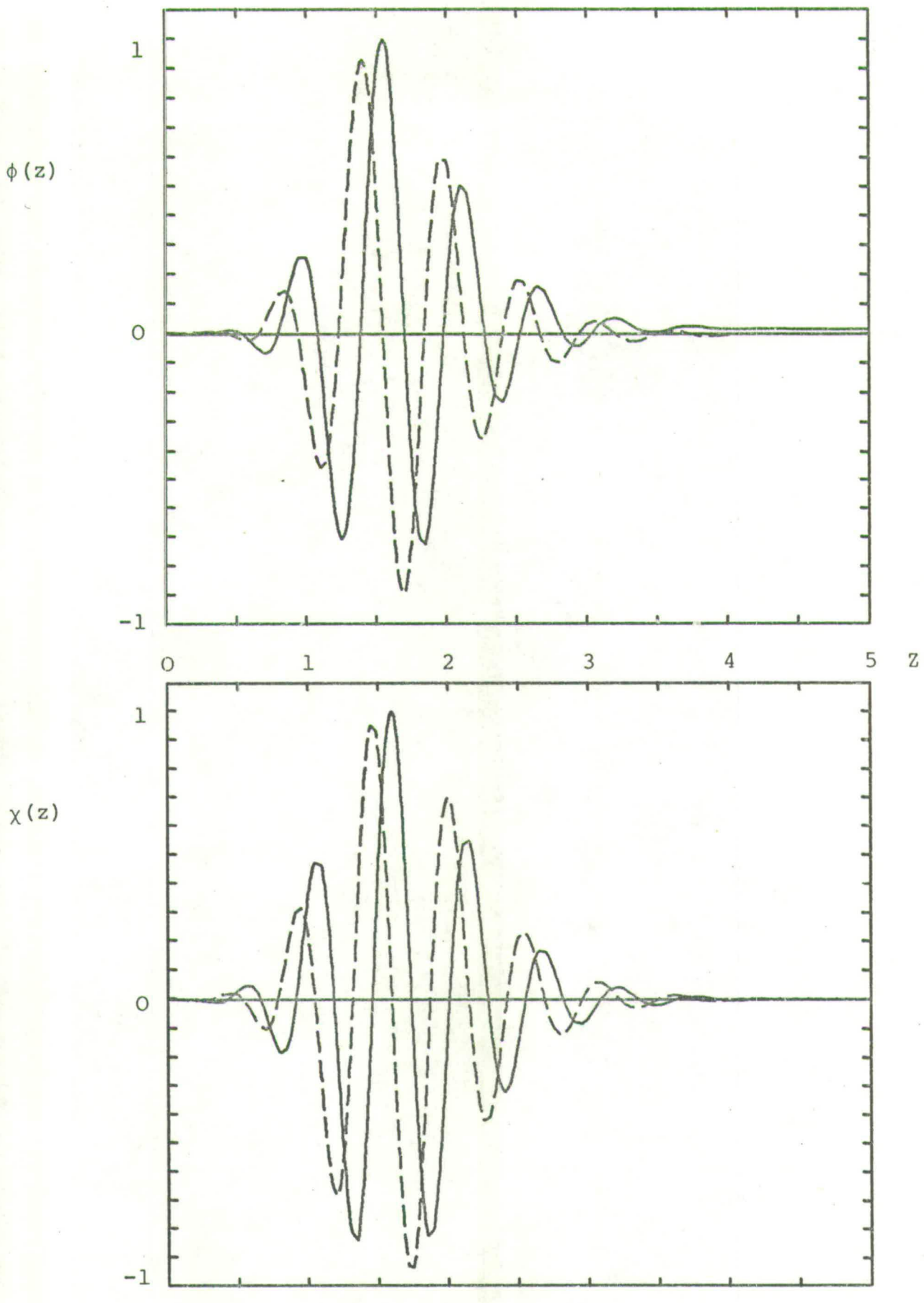

Figure 5.10 State 6 Eigenfunctions at R = 998, α = .308 .

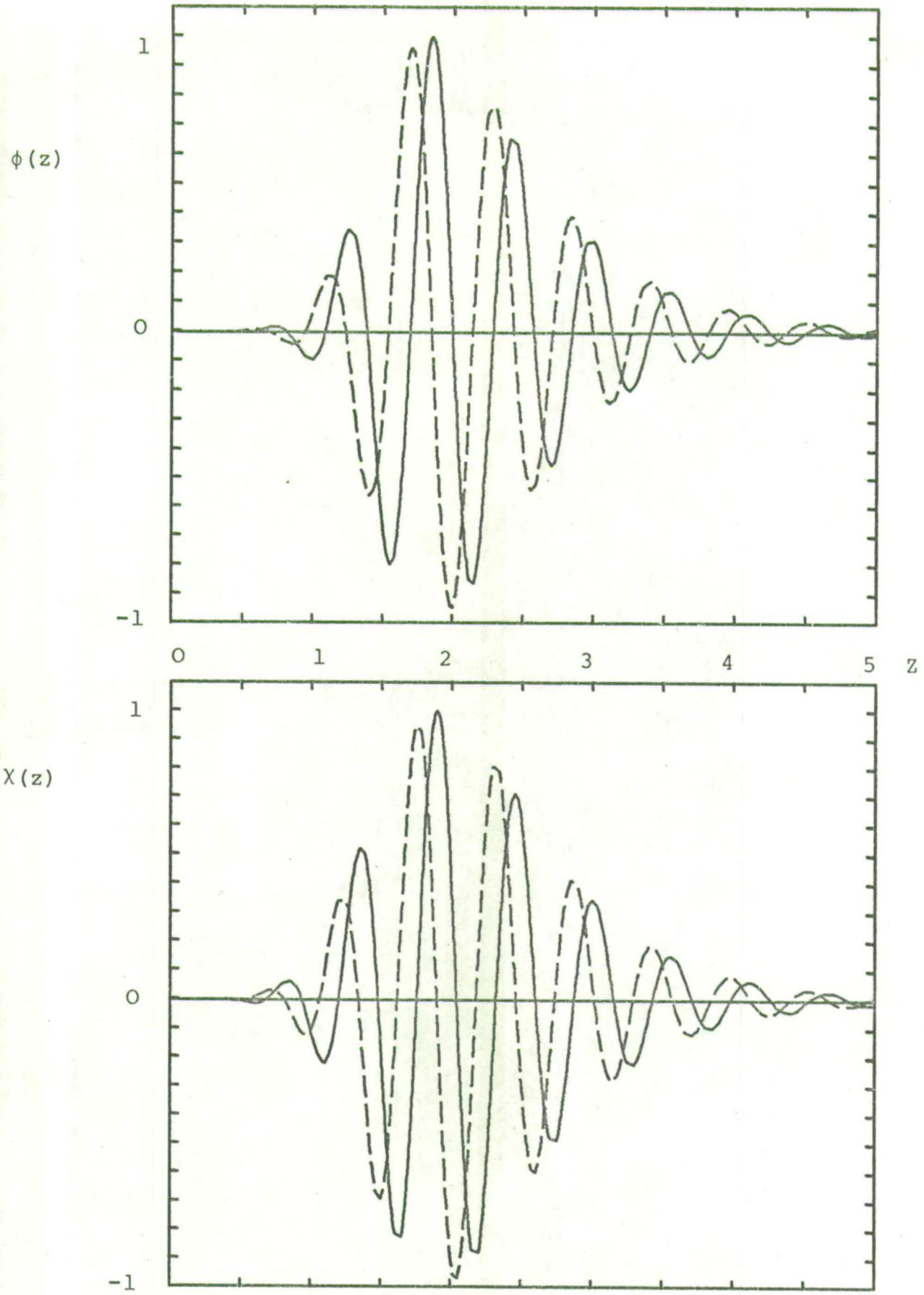

Figure 5.11 State 7 Eigenfunctions at R = 998, α = .308 .

$$I_{jk} = \int_0^{12} \phi_j(z)\{D^2 - \alpha^2\}\chi_k(z)\,dz \qquad (5.3a)$$

$$J_{jk} = \int_0^{12} \chi_j(z)\{D^2 - \alpha^2\}\phi_k(z)\,dz\ . \qquad (5.3b)$$

All 49 combinations of j and k $(1 \leqslant j \leqslant 7,\ 1 \leqslant k \leqslant 7)$ were investigated with $h = .05$ and $z_{max} = 12$. In every case, integrals with $j \neq k$ were found to be several orders of magnitude smaller than integrals with $j = k$. Also, the relation

$$I_{kk} \doteq J_{kk} \qquad k = 1, \ldots, 7 \qquad (5.4)$$

was found to be accurate to 4 or 5 significant figures.

For simplicity, the original normalisation (3.15) of ϕ and χ was adhered to in equations (5.3) and the values obtained in (5.4) were all found to be $O(h^4)$ accurate. Integrals with $j \neq k$ became much smaller as h was decreased.

Results for $|I|$ and $|J|$ with all combinations of States 1, 6 and 7 are given in Table 5.3. For ease of presentation, the normalisation has been changed so that

$$|I_{jk}|' = \frac{|I_{jk}|}{|I_{jj}|^{\frac{1}{2}}|I_{kk}|^{\frac{1}{2}}} \qquad j, k = 1, 6, 7$$

and similarly for J.

The ordinary and adjoint eigenfunctions in the spatial spectrum at $R = 3000$, $\beta = .24$ were also tested for orthogonality by evaluating the integrals (5.3). As expected, no numerical evidence of orthogonality was found.

TABLE 5.3

Magnitude of the Orthogonality Integrals I_{jk}, J_{jk} for States 1, 6, and 7 at R = 998, α = .308 (Blasius)

| I |

j \ k	1	6	7
1	1	.000184	.000156
6	.000005	1	.000577
7	.000131	.001763	1

| J |

j \ k	1	6	7
1	1	.000141	.000258
6	.000336	1	.002110
7	.000191	.000519	1

5.5 Spurious Eigenstates

As in the spatial case, the matrix equation

$$M(c)\ \underline{v} \quad = \quad \underline{0}$$

possesses eigenvalues which are not true eigenvalues of the original differential equation (together with the appropriate boundary conditions). In the plane Poiseuille case, only a small number of eigenvalues do not exhibit $O(h^4)$ behaviour and so are purely algebraic. This constrasts with the Blasius case in which many spurious eigenvalues occur. Those found by the LR method at $R = 998$, $\alpha = .308$ for $h = .1$ and $h = .05$ ($z_{max} = 6$) appear in Figure 5.12.

If the Osborne method is used with the full outer boundary condition (3.11), a similar pattern of algebraic eigenvalues is found on the physical half of the Riemann surface ($\gamma_r \geq 0$). The branch line is located at $c_r = 1$ with $c_i < -\frac{\alpha}{R}$.

In addition to those shown in Figure 5.12, there is a highly spurious eigenvalue with $c_r \doteq 0$ and c_i large and positive (e.g. $c_i = 15.6$ at $h = .05$). In fact, the imaginary part of this eigenvalue is always double that of the most highly damped eigenvalue on the line (but inverted in sign). Kurtz[20] also found an eigenvalue with this behaviour.

The pattern of algebraic eigenvalues on the c-plane is similar to the line of closely spaced eigenvalues found in plane Poiseuille flow (Figure 5.1) except that the asymptotic value of c_r is about $5/6$ rather than $2/3$. Even the spurious branching effect at the bottom of the line is the same.

Figure 5.13 is the upper part of Figure 5.12 on a more suitable scale. The effect of change in h with z_{max} constant

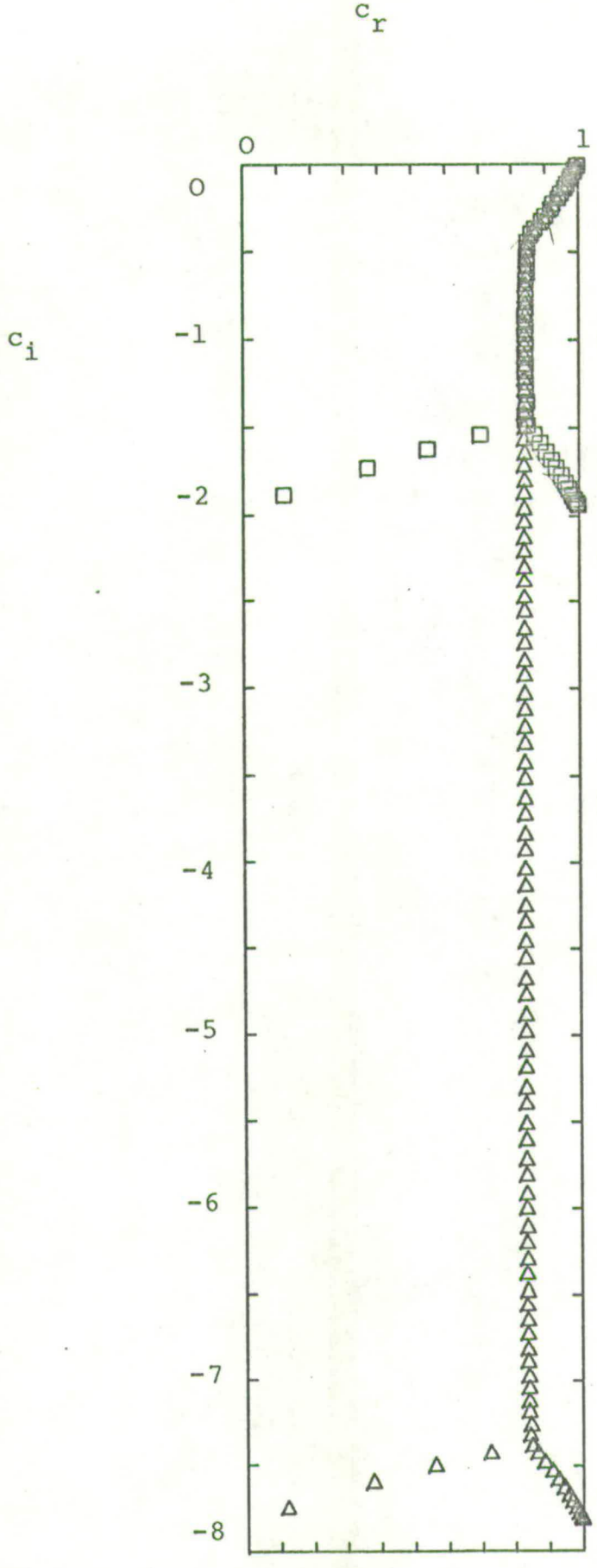

Figure 5.12 Algebraic Eigenvalues (Blasius) at R = 998, α = .308.

△ h = .05, z_{max} = 6.

□ h = .1 , z_{max} = 6.

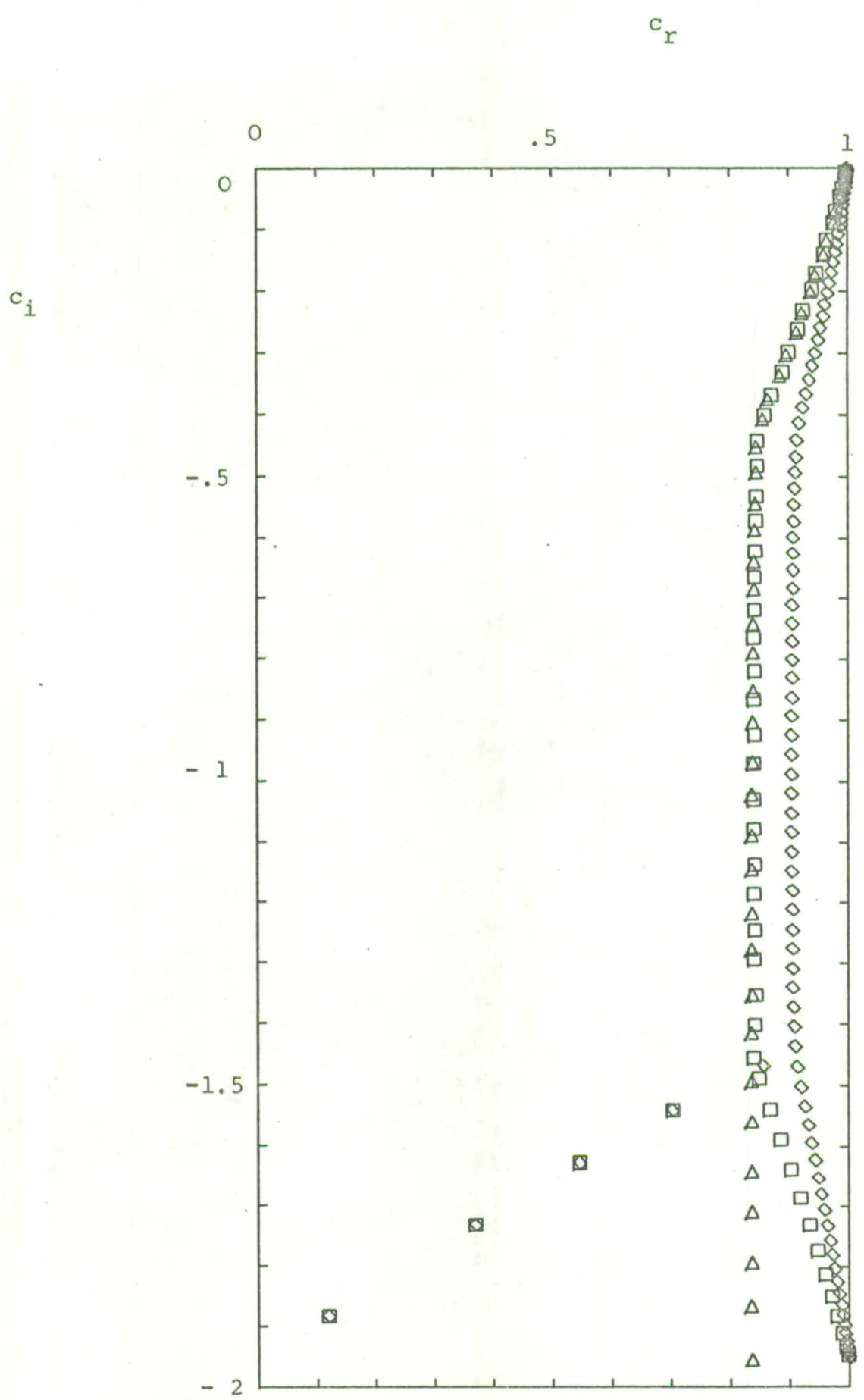

Figure 5.13 Algebraic Eigenvalues (Blasius) at R = 998, α = .308.

△ h = .05, z_{max} = 6

□ h = .1, z_{max} = 6

◇ h = .1, z_{max} = 12

is as follows:

(i) The spacing of eigenvalues is unaltered.

(ii) The position of the vertical line is unchanged.

(iii) The imaginary part of the most highly damped eigenvalue jumps from 1.95 to 7.8 when h is halved. This is $O(h^{-2})$ behaviour.

Another series of results at $h = .1$ but with $z_{max} = 10$ is also shown in Figure 5.13. The effect of change in z_{max} at $h = .1$ is as follows:

(i) The spacing of the vertical family of eigenvalues decreases as z_{max} increases.

(ii) The vertical line moves to $c_r \doteqdot .9$.

(iii) Apart from the changes in (i) and (ii), the pattern of eigenvalues is relatively unchanged.

A comparison of the above observations with those made in Section 4.4 suggests that the nature of the spurious eigenstates found in the Blasius spectrum in the (S) case and in the (T) case is virtually identical. A reason for their existence will now be proposed.

Consider symmetrical flow in a wide channel where the velocity profile is composed of two Blasius profiles both truncated at $z = z_{max}$ (where $z_{max} \geq 6$). The discontinuity in the velocity derivatives at the centre of the channel would be negligible but this point is not essential to the argument. The stability problem for symmetrical disturbances in this flow situation would be exactly the same as for pure Blasius flow except for the outer boundary condition which would be (3.10a) rather than (3.11) or (3.12).

Since it is a flow between parallel walls, the analysis of Grohne (Section 2.6) is applicable. Since $m = 2z_{max}$, (2.23) becomes

$$c_r = \frac{1}{z_{max}} \int_0^{z_{max}} \{1 - (1 - U)\} dz \doteq 1 - \frac{1}{z_{max}} . \qquad (5.5)$$

Thus, in the temporal spectrum, a vertical line of eigenvalues would be expected with $c_r = {}^5/6$ ($z_{max} = 6$) or $c_r = .9$ ($z_{max} = 10$) and the distance of this line from $c_r = 1$ would be halved if z_{max} were doubled.

If $R = 998$, $\alpha = .308$ and $m = 12$, the imaginary part of State 30 (symmetrical) which corresponds to $n = 58$ in Grohne's notation, would satisfy

$$- .803 < c_i < - .776 \qquad (5.6)$$

Also, since $c_i = k \frac{n^2}{m^2}$ (where k is a constant), if m were doubled, double the number of states would be required before the same value of c_i would be reached. This means that the spacing $\frac{2kn}{m^2}$ at a given c_i would be halved if m were doubled.

All the above spectral features of the hypothetical flow exist in the algebraic eigenvalues of the Blasius spectrum at $R = 998$, $\alpha = .308$. If $z_{max} = 6$, State 30 of the complete spectrum has $c_r = .839$, $c_i = - .792$, and this is completely consistent with (5.5) and (5.6). Thus, the algebraic eigenstates found in the Blasius case are essentially channel flow solutions which are tolerated by the outer boundary condition. This highlights a weakness in the finite difference method and a need for careful checking of solutions at various values of h and z_{max}. Only eigenstates with $O(h^4)$ behaviour and insensitivity to change in z_{max} are true boundary layer solutions.

5.6 General Structure of the Spectrum

In addition to the typical spectrum discussed in Section 5.3, other results were obtained at various Reynolds numbers and wave numbers for comparison with Mack[51].

One of the interesting features discovered by Mack is the switch in identity between States 1 and 3 at $\alpha = .308$, $R > 4000$ (in the present non-dimensionalisation). This behaviour was confirmed and the results are shown in Figure 5.14. The real parts of the eigenvalues come together at $R \doteq 4000$ and then diverge. However it is State 3 which remains relatively constant (suggesting the existence of an inviscid limit) while State 1 suddenly begins to decrease towards $c_r = 0$. The imaginary parts of the eigenvalues actually intersect but it is again State 3 which appears to have an inviscid limit while State 1 decreases gradually towards $c_i = 0$.

Thus for $R > 5000$, it is State 3 which appears to be the fundamental eigenstate while State 1 has the behaviour of a higher eigenstate. For classification purposes, it is more convenient to rename the two states above the cross-over region so that State 1 is always the fundamental eigenstate. This convention is used in Figure 5.14.

The effect of variation in R at constant α is illustrated in Figure 5.15 while Figure 5.16 shows the effect of variation in α at constant R. In both cases, the imaginary part of State 1 is not shown since it is very small. It is apparent from these diagrams that the higher temporal eigenvalues are approximately proportional to the quantity $(\alpha R)^{-1/3}$. As α or R is increased, more eigenvalues appear near $c_r = 1$ and move over towards the origin.

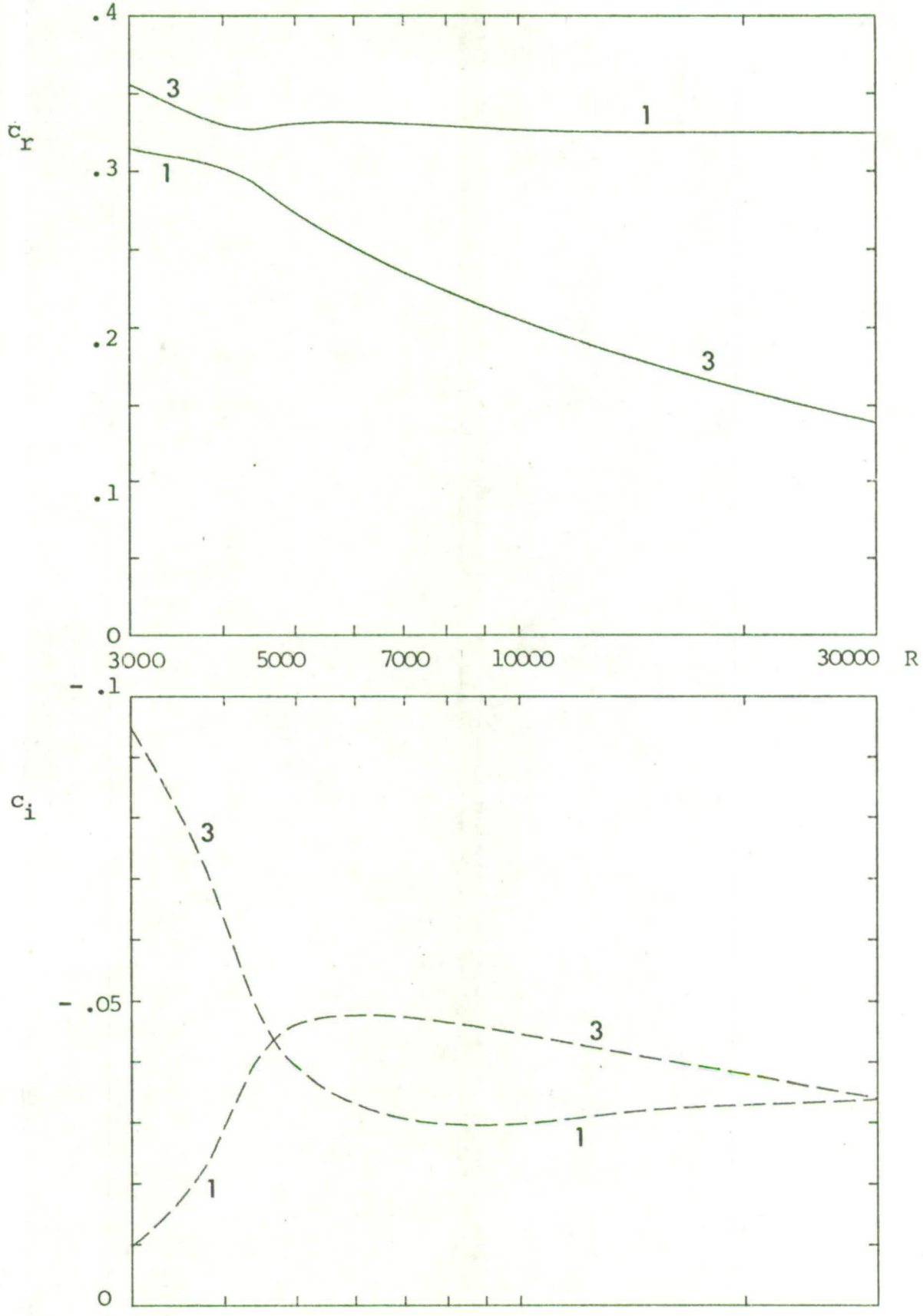

FIGURE 5.14 Switch in identity between States 1 and 3 at $\alpha = .308$, $3000 \leq R \leq 30{,}000$.

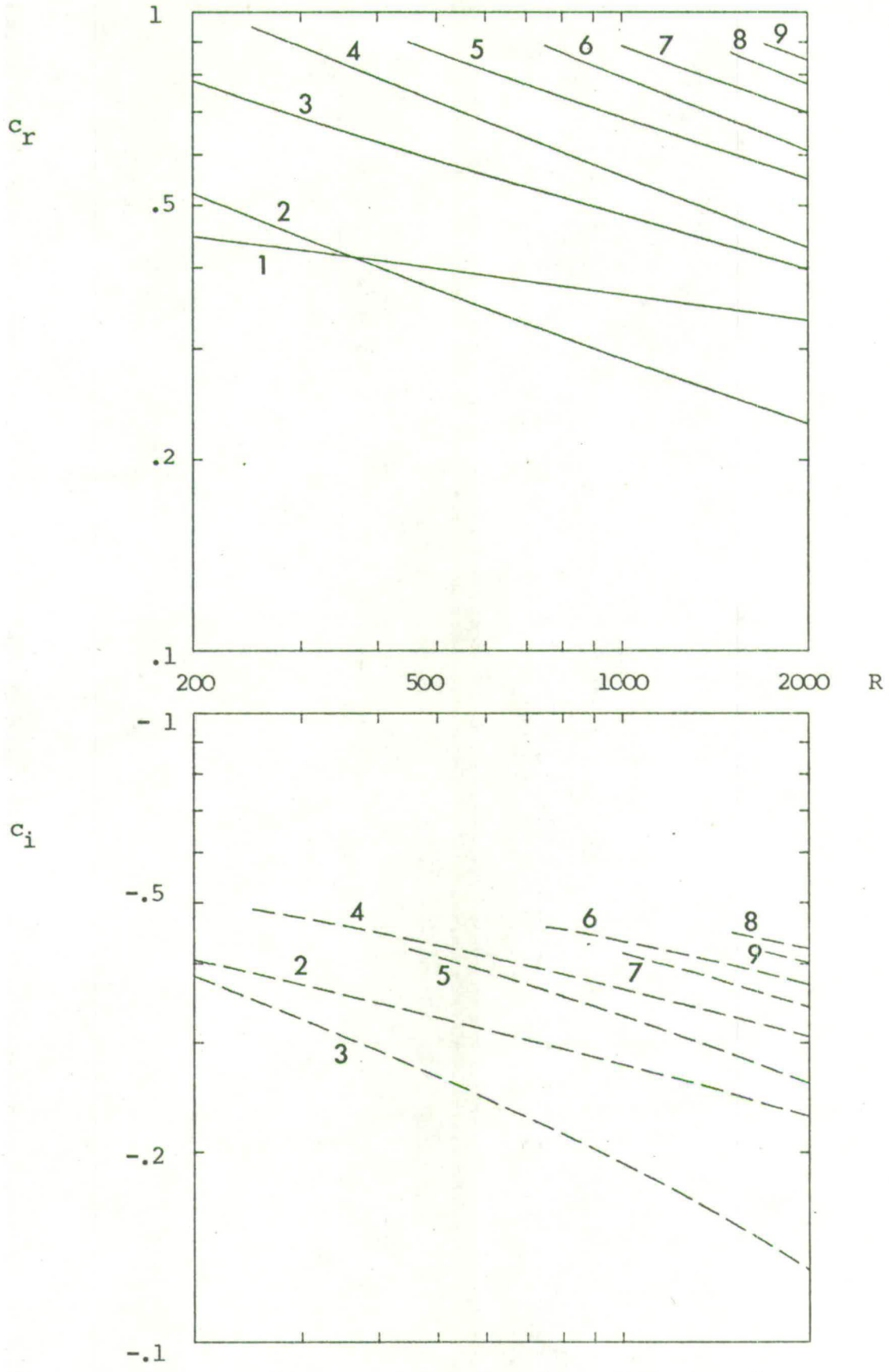

FIGURE 5.15 Eigenvalues at $\alpha = .308$.

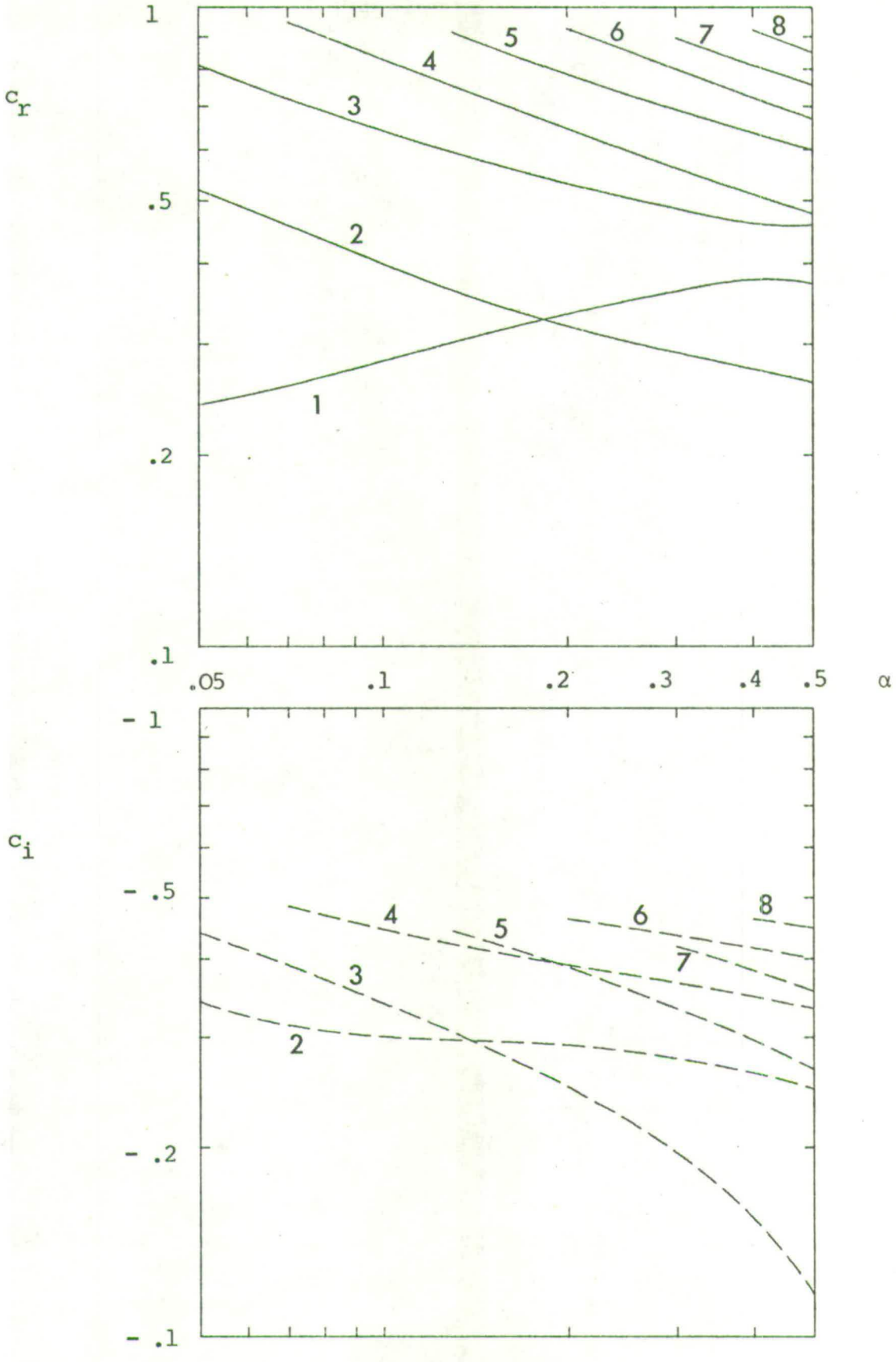

FIGURE 5.16 Eigenvalues at R = 998.

In the temporal case, there appears to be no simple formula corresponding to equation (4.6) which gives the relative magnitudes of spatial eigenvalues. The temporal eigenstates seem to be far more numerous than the spatial eigenstates at the same Reynolds number, although it is difficult to make a direct comparison since the number of states also depends on α or β.

Mack experienced difficulty in obtaining solutions for high order eigenstates at high Reynolds numbers. Similar difficulty was found with the Osborne method. For example, at $R = 17{,}200$, $\alpha = .308$ no true state was found above State 15. This was the same point at which Mack's method appeared to break down.

CHAPTER 6

AN ALTERNATIVE APPROACH TO THE SPECTRUM PROBLEM

6.1 Introduction

So far, the spectrum problem has been solved directly by the use of numerical methods. While this approach has many advantages, it was thought that a more analytical method would provide a valuable comparison with previous results and would not have the disadvantage of producing a large number of spurious eigenstates. Evidence for the existence of a continuous spectrum in addition to the small number of discrete states in the Blasius case might also be found by an analytical approach, whereas a numerical method, being inherently discrete, would fail.

The first difficulty to be overcome is the Blasius profile itself, for which there is no uniformly valid analytical expression. The only way round this difficulty is to use an artificial boundary layer profile composed of straight line segments or simple polynomial curves. The following profile was chosen.

$$U(z) = \begin{cases} 1 & (z \geq 1) \\ z & (0 \leq z \leq 1) \end{cases} \qquad (6.1)$$

Even this simple profile requires a considerable amount of analysis. First, the Orr-Sommerfeld equation is solved in each of the upper and lower regions of the flow. Then the upper and lower solutions are matched at the common boundary, $z = 1$. This approach was used by Esch[61], who studied the stability of a shear layer with a piecewise linear profile.

6.2 Mathematical Analysis

In the upper region of the flow (6.1), the Orr-Sommerfeld equation reduces to

$$(D^2-\gamma^2)(D^2 - \alpha^2)\phi(z) = 0$$

where

$$\gamma^2 = \alpha^2 + i\alpha R(1 - c)$$

with general solution

$$\phi = Ae^{-\alpha z} + Be^{-\gamma z} + A_1e^{\alpha z} + B_1e^{\gamma z} .$$

As before, assuming $\alpha_r, \gamma_r \geq 0$, the exponentially growing solutions do not satisfy the outer boundary condition $\phi = \phi' = 0$. Therefore $A_1 = B_1 = 0$ and the upper solution is

$$\phi = Ae^{-\alpha z} + Be^{-\gamma z} . \tag{6.2}$$

In the lower region of the flow (6.1), the equation to be solved is

$$\left[D^2 - \alpha^2 - i\alpha R(z-c)\right](D^2 - \alpha^2)\phi(z) = 0. \tag{6.3}$$

Again, $e^{\pm\alpha z}$ are solutions and so are

$$F(z) = \int_0^z f(\xi) \frac{\sinh\alpha(z-\xi)}{\alpha} d\xi \tag{6.4a}$$

$$G(z) = \int_0^z g(\xi) \frac{\sinh\alpha(z-\xi)}{\alpha} d\xi \tag{6.4b}$$

where $f(z)$, $g(z)$ are independent solutions of

$$\left[D^2 - \alpha^2 - i\alpha R(z-c)\right]y(z) = 0$$

which may be written

$$\left[\frac{d^2}{d\zeta^2} + \zeta\right]y(\zeta) = 0 \tag{6.5}$$

where

$$\zeta = (\alpha R)^{1/3}\left[i(z-c) + \frac{\alpha}{R}\right] . \qquad (6.6)$$

Equation (6.5) is Stokes' equation which has the independent solutions

$$f(\zeta) = (\tfrac{2}{3})^{1/3}\, \zeta^{\frac{1}{2}}\, J_{-1/3}(\tfrac{2}{3}\zeta^{3/2}) \qquad (6.7a)$$

$$g(\zeta) = (\tfrac{2}{3})^{1/3}\, \zeta^{\frac{1}{2}}\, J_{1/3}(\tfrac{2}{3}\zeta^{3/2}) \qquad (6.7b)$$

where $J_\nu(z)$ denotes the Bessel function of the first kind of rder ν.

The general solution of (6.3) is thus:

$$\phi = a\,F(z) + b\,G(z) + a_1 e^{\alpha z} + b_1 e^{-\alpha z} .$$

The lower boundary condition $\phi(0) = \phi'(0) = 0$ is already satisfied by both F and G, which implies that $a_1 = b_1 = 0$ and that the lower solution is

$$\phi = a\,F(z) + b\,G(z) \qquad (6.8)$$

where F and G are determined from (6.4), (6.6) and (6.7).

The solutions (6.2) and (6.8) must match at the common boundary, $z = 1$. However, the derivatives of U are discontinuous at $z = 1$ and this is dealt with in the following manner. The functions ϕ, ϕ', ϕ'' are assumed continuous at $z = 1$ and ϕ''' discontinuous such that

$$\lim_{\varepsilon \to 0} \int_{1-\varepsilon}^{1+\varepsilon} [\text{Equation (2.14)}]\,dz = 0 \qquad (6.9)$$

Since

$$\int_{1-\varepsilon}^{1+\varepsilon} U''\phi \, dz = \left[U'\phi\right]_{1-}^{1+} - \int_{1-\varepsilon}^{1+\varepsilon} U'\phi' \, dz$$

$$= -\phi(1-\varepsilon) - \left[U\phi'\right]_{1-\varepsilon}^{1+\varepsilon} + \int_{1-\varepsilon}^{1+\varepsilon} U\phi'' \, dz,$$

equation (6.9) implies that

$$\lim_{\varepsilon \to 0} \left[\phi'''(1+\varepsilon) - \phi'''(1-\varepsilon)\right] = i\alpha R\, \phi(1).$$

Thus the matching conditions at $z = 1$ are as follows:

$$Ae^{-\alpha} + Be^{-\gamma} = a\,F(1) + b\,G(1) \tag{6.10a}$$

$$-\alpha Ae^{-\alpha} - \gamma Be^{-\gamma} = a\,F'(1) + b\,G'(1) \tag{6.10b}$$

$$\alpha^2 Ae^{-\alpha} + \gamma^2 Be^{-\gamma} = a\,F''(1) + b\,G''(1) \tag{6.10c}$$

$$-\alpha^3 Ae^{-\alpha} - \gamma^3 Be^{-\gamma} = a\,F'''(1) + b\,G'''(1) + i\alpha R\{aF(1) + b\,G(1)\}. \tag{6.10d}$$

Equations (6.10) may be considered as a homogeneous system in the four unknowns A, B, a, b. For non-trivial solutions it is necessary that the following relation should be satisfied.

$$\begin{vmatrix} -1 & -1 & F(1) & G(1) \\ \alpha & \gamma & F'(1) & G'(1) \\ -\alpha^2 & -\gamma^2 & F''(1) & G''(1) \\ \alpha^3 & \gamma^3 & F'''(1)+i\alpha RF(1) & G'''(1)+i\alpha RG(1) \end{vmatrix} = 0.$$

Using the identities

$$F''(z) = \alpha^2 F(z) + f(z), \qquad G''(z) = \alpha^2 G(z) + g(z),$$

$$F'''(z) = \alpha^2 F'(z) + f'(z), \qquad G'''(z) = \alpha^2 G'(z) + g'(z),$$

the above relation may be written

$$(\alpha-\gamma)\begin{vmatrix} f(1) + (\alpha+\gamma)\{F'(1)+\alpha F(1)\} & g(1)+(\alpha+\gamma)\{G'(1)+\alpha G(1)\} \\ f'(1)+\gamma f(1) + i\alpha R\, F(1) & g'(1)+\gamma g(1) + i\alpha R\, G(1) \end{vmatrix} = 0 \qquad (6.11)$$

Thus the original eigenvalue problem has been reduced to equation (6.11) where the determinant is a highly complicated function of α, c and R. Note that $F(1)$, $G(1)$, $f(1)$, $g(1)$ and their derivatives are all functions of α, c and R through the transformation (6.6). It is useful to think of equation (6.11) in the form

$$S(\alpha, c, R) = 0 \ .$$

6.3 Methods for the Solution of the Determinantal Equation

It had been hoped that an obvious singularity would exist in equation (6.11) corresponding to a continuous spectrum of eigenvalues (e.g. at $c_r = 1$ or $\gamma_r = 0$). Unfortunately, the only singularity seems to be $\gamma = \alpha$ which is inadmissible since it is assumed that $e^{-\alpha z}$ and $e^{-\gamma z}$ are independent solutions of the upper region.

In order to find discrete zeros of the determinant, it is necessary to resort to numerical methods. The first step is the calculation of the functions $f(\zeta)$, $g(\zeta)$ and their derivatives. This is done by evaluating a finite number of terms in their Bessel series, which are as follows:

$$\begin{aligned} f(\zeta) &= A_o + A_1\zeta^3 + A_2\zeta^6 + \ldots\ldots + A_m\,\zeta^{3m} + \ldots \\ g(\zeta) &= \zeta(B_o + B_1\zeta^3 + B_2\zeta^6 + \ldots + B_m\,\zeta^{3m} + \ldots) \\ f'(\zeta) &= -\zeta^2(C_o + C_1\zeta^3 + C_2\zeta^6 + \ldots + C_m\,\zeta^{3m} + \ldots) \\ g'(\zeta) &= D_o + D_1\zeta^3 + D_2\zeta^6 + \ldots + D_m\,\zeta^{3m} + \ldots \end{aligned} \qquad (6.12)$$

where

$$A_o = .93043671693 \qquad A_m = -\frac{A_{m-1}}{(3m-1)\,3m}$$

$$B_o = .67829872514 \qquad B_m = -\frac{B_{m-1}}{3m(3m+1)}$$

$$C_o = \tfrac{1}{2}A_o \qquad C_m = -\frac{C_{m-1}}{3m(3m+2)}$$

$$D_o = B_o \qquad D_m = -\frac{D_{m-1}}{(3m-2)\,3m} \quad .$$

In each case, as many terms as necessary are taken in order to make the result accurate to eight decimal places. It should be noted that, using (6.6)

$$f'(z) = \frac{df}{dz} = i(\alpha R)^{1/3}\frac{df}{d\zeta} = i(\alpha R)^{1/3} f'(\zeta)$$

and similarly for $g'(z)$.

The series (6.12) were previously used by Aiken et al.[62] to tabulate the modified Hankel functions of order one-third which are related to the functions f and g as follows:

$$h_1(\zeta) = g(\zeta) + \frac{i}{\sqrt{3}}\{g(\zeta) - 2f(\zeta)\}$$

$$h_2(\zeta) = g(\zeta) - \frac{i}{\sqrt{3}}\{g(\zeta) - 2f(\zeta)\} \quad .$$

The program which was written to evaluate the series (6.12) was tested by choosing several values of ζ and calculating $h_1(\zeta)$, $h_2(\zeta)$, $h_1'(\zeta)$ and $h_2'(\zeta)$ for comparison with Aiken's tables. In every case, there was complete agreement.

The problem of evaluating the determinant in equation (6.11) will now be considered. Assume that α and R have been given fixed positive values so that the determinant is a function only of the complex variable c. For a particular value of c it

will be necessary to sum the four series (6.12) at the point $\zeta = (\alpha R)^{1/3}[i(1-c) + \frac{\alpha}{R}]$ giving the values $f(1)$, $g(1)$, $f'(1)$ and $g'(1)$ required in (6.11). However, the integrals (6.4) have to be evaluated by some numerical means so that the values $f(jh)$, $g(jh)$, $f'(jh)$ and $g'(jh)$ (where $j = 0,1,2, \ldots n$; $h = \frac{1}{n}$) are required to produce $F(1)$, $G(1)$, $F'(1)$ and $G'(1)$. Simpson's Rule was found to be adequate for these integrations. Usually $n = 50$ or $n = 100$ was used.

It should be noted that the above procedure only evaluates the determinant at a particular point on the c-plane and does not produce what is really required, i.e. zeros of the determinant. The approximate location of zeros could be found by the Contour Method (Section 3.3) but this would be excessively time-consuming (involving about 10,000 summations). An iterative method capable of converging towards individual zeros would be far more efficient. However, most iterative methods would require the derivative (with respect to c) of the determinant and this would be very tedious to evaluate.

The following method was devised and found to function successfully. First, the determinant S is evaluated at two points close together on the c-plane. The derivative $\frac{dS}{dc}$ is then estimated from the formulae:

$$\left(\frac{dS}{dc}\right)_r = \frac{1}{2}\left(\frac{\Delta S_r}{\Delta c_r} + \frac{\Delta S_i}{\Delta c_i}\right)$$
$$\left(\frac{dS}{dc}\right)_i = \frac{1}{2}\left(\frac{\Delta S_i}{\Delta c_r} - \frac{\Delta S_r}{\Delta c_i}\right) \qquad (6.13)$$

where $\Delta c_r = c_r$ (second point) $- c_r$ (first point), etc.

This approximate derivative is then used in the quasi-Newton iterative process

$$c^{j+1} = c^j - \frac{S^j}{(\frac{dS}{dc})^j} . \qquad (6.14)$$

Thus, two evaluations of the determinant are required for every iteration. Starting values c^o may be obtained by using the LR Method (as described in Chapter 3) to solve the Orr-Sommerfeld equation for the profile (6.1) rather than the Blasius profile. Alternatively, random starting values may be used.

6.4 Results

The temporal spectrum of the artificial flow (6.1) was studied in detail at $\alpha = .54$, $R = 1750$. These values were chosen deliberately so that this case-study could be compared directly with the Blasius spectrum at $\alpha = .308$, $R = 998$ (Section 5.3).

Since the initial gradient of the profile (6.1) is 1 compared with .5714 in the Blasius case, the Blasius values of α and R must be increased in the same proportion (about 1.75) in order to make the eigenvalue problem equivalent. To prove this, consider the Orr-Sommerfeld equation for the lower region of the artificial flow (6.1):

$$\left[\frac{d^2}{dz^2} - \alpha^2 - i\alpha R(z-c)\right]\left[\frac{d^2}{dz^2} - \alpha^2\right]\phi(z) = 0 . \qquad (6.15)$$

Suppose that the normal coordinate is stretched to y (where $z = .5714y$) and $U(y) = .5714y$. In new coordinates the equation is

$$\left[\frac{d^2}{dy^2} - \bar{\alpha}^2 - i\bar{\alpha}\bar{R}(.5714y - c)\right]\left[\frac{d}{dy^2} - \bar{\alpha}^2\right]\phi(y) = 0 \qquad (6.16)$$

A choice of $\bar{\alpha} = .5714\alpha$, $\bar{R} = .5714R$ makes equations (6.15) and (6.16) identical. The vertical scaling of (6.16) is the same as that of the Blasius boundary layer for low z. It should be noted that the above analysis applies equally well to the adjoint equation.

The LR method was used to produce an ordinary and an adjoint spectrum of the artificial flow (6.1) at $\alpha = .54$, $R = 1750$ with $h = .02$ and $z_{max} = 2$. In contrast to all previous results the ordinary and adjoint solutions did not agree. Obviously, this was due to the inherent discontinuity in $U'(z)$ and $U''(z)$ at $z = 1$. Since $U'(z)$ is non-zero for $z < 1$ and has only a finite discontinuity at $z = 1$, it was thought that the adjoint solution (using U and U') would be a better representation of the true spectrum than the ordinary solution (using U and U''). This was confirmed by the fact that States 1, 2 and 3 of Figure 5.4 all appeared in the adjoint solution (to a fair approximation).

In addition, many of the states found in the adjoint solution were found to be good starting values for the solution of equation (6.11) using the iterative process (6.14). The approximate derivatives in (6.13) were calculated by taking $\Delta c_r = \Delta c_i = .0001$ and this was found to give quite rapid convergence. For example, a determinant of initial modulus 10^4 could become one of modulus 10^{-8} in less than 10 iterations. The rate of convergence was somewhere between linear and quadratic. Using $h = .02$ in the numerical integration to evaluate $F(1)$, $G(1)$, $F'(1)$ and $G'(1)$ produced relatively accurate results with a c.p.u. time of less than a second per iteration. With this choice of h, over 400 Bessel series were summed in each iteration.

The discrete states found at $\alpha = .54$, $R = 1750$ appear in the first part of Table 6.1 and are illustrated in Figure 6.1. Only the first three states (of lowest c_r) match those of Figure 5.4. States 4 and 5 have much more negative c_i than their Blasius counterparts.

In addition, two completely new types of eigenvalue were found, denoted A and B states. The eigenvalues of these states ultimately move towards $c_r = 1$ as R is increased. This behaviour is quite contrary to that of the other eigenvalues in the spectrum and also that of the temporal Blasius eigenvalues, all of which move towards $c_r = 0$ as R is increased (except State 1 which has an inviscid limit).

For comparison, the artificial spectrum at $\alpha = .54$, $R = 5000$ is given in Table 6.1 and Figure 6.2. There are seven ordinary states, three A states, and three B states. The A states appear to lie on one curved line through the point $(c_r = 1, c_i = 0)$, the B states on another. In fact, it is reasonable to suppose that for each pair of ordinary states there exists a pair of "mirror" states, one A state and one B state. Again, State 1 is the exception. The other twelve states may be divided into three quadruplets as follows:

a) 2, 3, A1, B1
b) 4, 5, A2, B2
c) 6, 7, A3, B3 .

In each group the A state is the "mirror" image of the odd numbered state and the B state that of the even state. In fact, for sufficiently large R it appears that

$$c_r \text{ (A state)} = 1 - c_r \text{ (odd state)},$$
$$c_r \text{ (B state)} = 1 - c_r \text{ (even state)}.$$

The mirror states are apparently caused by the discontinuity

TABLE 6.1

Eigenvalue Spectra at $\alpha = .54$.

	R = 1750		R = 5000	
State	c_r	c_i	c_r	c_i
1	.40700	.03219	.39406	.00673
2	.29076	-.28600	.20599	-.21134
3	.45677	-.18660	.32224	-.07632
4	.57998	-.50176	.3769	-.2877
5	.6095	-.6658	.4749	-.2286
6			.545	-.419
7			.562	-.506
A1	.56571	-.12943	.70823	-.09128
A2	.50176	-.39063	.5276	-.1984
A3			.499	-.354
B1	.71621	-.44186	.79864	-.31451
B2	.631	-.835	.6355	-.3972
B3			.57	-.61

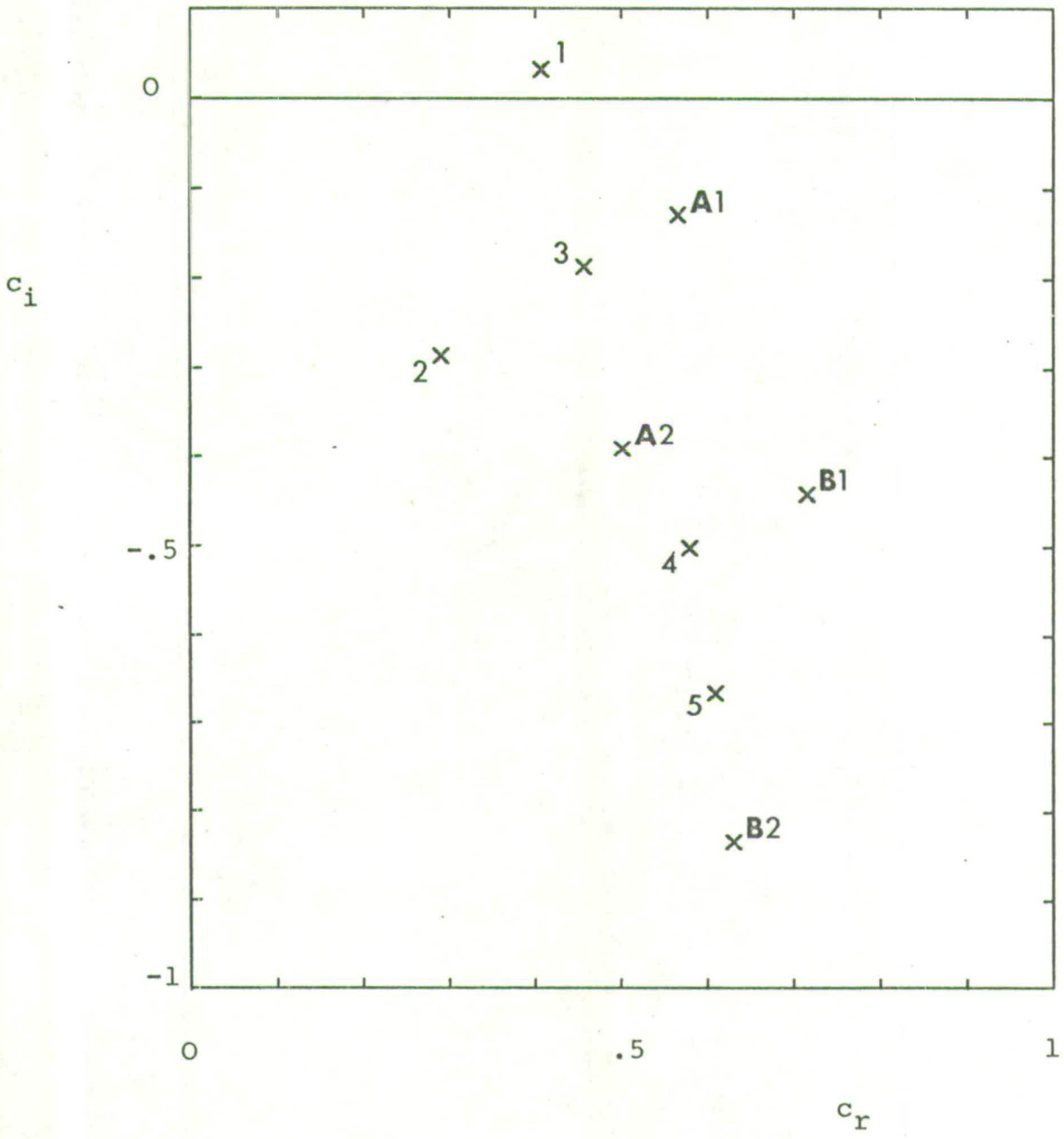

Figure 6.1 Eigenvalue Spectrum at R = 1750, α = .54.

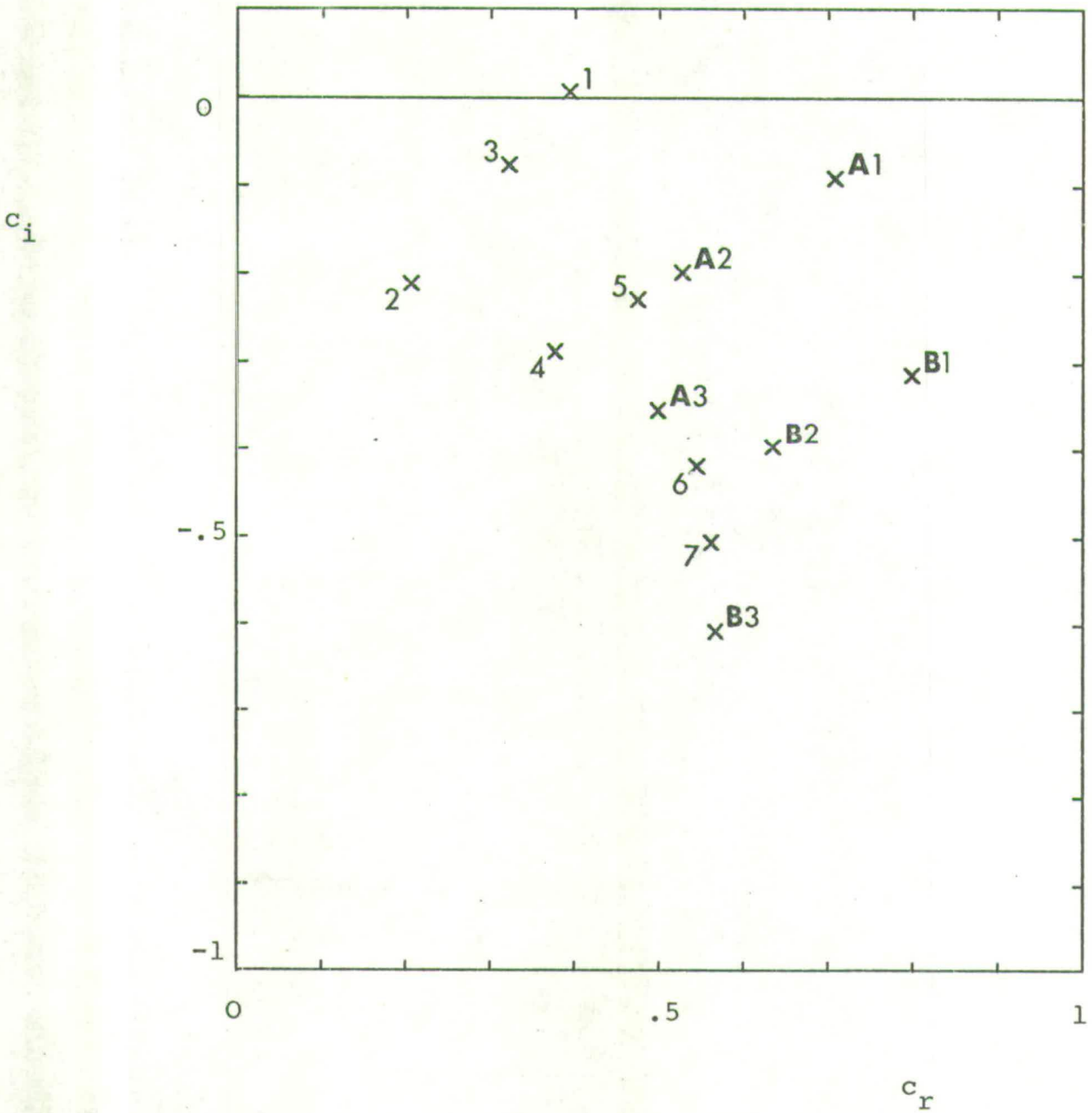

Figure 6.2 Eigenvalue Spectrum at R = 5000, α = .54

in the profile derivatives at $z = 1$. A reference to this kind of phenomenon is made by Betchov and Criminale[63].

The most important feature of these results, however, is that despite a completely different approach to the problem, the artificial states of low order ($c_r < .5$) are very similar to the low order Blasius states. Since those states have most of their amplitude close to $z = 0$ where the artificial profile is virtually the same as the Blasius profile, one would expect good agreement between the two sets of results. The fact that such agreement has been achieved points to the correctness and accuracy of both procedures.

The other significant fact is that there is no evidence of a continuous spectrum (or indeed any line of closely spaced eigenvalues) despite the fact that the present method considers the entire semi-infinite flow. Since numerical analysis has been used to evaluate the determinant in (6.11), this lack of evidence is not conclusive but is, nevertheless, a strong indication of the true nature of the spectrum.

CHAPTER 7

CONCLUSIONS

7.1 Summary

(a) Features common to both the spatial and temporal Blasius Spectra

(1) The eigenvalue spectrum is discrete and finite.

(2) The fundamental eigenstate (State 1) has the following properties:

(i) It appears to exist at all positive values of R and β (or α).

(ii) It may be damped or amplified.

(iii) It has an inviscid limit which it approaches as $R^{-\frac{1}{2}}$.

(iv) Its eigenfunction is slowly varying.

(3) The higher eigenstates have the following properties:

(i) The number of states increases as R and β (or α) are increased. Thus every state has a threshold below which it does not exist.

(ii) They are all highly damped.

(iii) None of the higher eigenstates has an inviscid limit.

(iv) On threshold, the eigenfunctions are highly oscillatory and extend far out into the free stream. As R and β (or α) are increased, they become less oscillatory and contract into the boundary layer.

(b) Features peculiar to the spatial Blasius spectrum:

(1) The higher eigenvalues lie on two imaginary lines in the α-plane which are reflections in the line $\alpha_r = \alpha_i$ and seem to converge near the point $(\beta + i\beta)$. For every

eigenvalue (a + ib) on the upper line, there is an eigenvalue (b + ia) on the lower line.

(2) For sufficiently large values of R and β, the higher eigenvalues are proportional to $\beta^{3/2} R^{\frac{1}{2}}$ and would thus become infinitely large in the inviscid limit.

(3) The eigenfunctions appear to have no orthogonality properties.

(c) Features peculiar to the temporal Blasius spectrum:

(1) The higher eigenvalues lie on two imaginary lines in the c-plane which converge near the point (1- ·5i) and extend back towards the origin. There is no simple relationship between eigenvalues.

(2) For sufficiently large values of R and α, the higher eigenvalues are proportional to $(\alpha R)^{-1/3}$ and would thus become vanishingly small in the inviscid limit.

(3) All the eigenfunctions have the orthogonality properties discussed in Section 5.4.

(4) There is a change in identity between States 1 and 3 (see Section 5.6)

(d) Comparison with the temporal plane Poiseuille spectrum:

(1) The Blasius spectrum is very similar to the finite number of states in the plane Poiseuille spectrum with $c_r < \frac{2}{3}$. These states have most of their amplitude near the walls of the channel.

(2) The infinite semi-vertical line of closely spaced eigenvalues is critically dependent upon the finite width of the flow. The eigenfunctions of these states have most of their amplitude in the centre of the channel and the critical layer.

(e) Comparison with the artificial boundary layer spectrum:

(1) Although this is a very poor approximation to Blasius flow, the spectrum is not dissimilar to the temporal Blasius spectrum, especially for the states of low order.

(2) In addition, "mirror" states exist which move towards $c_r = 1$ as R is increased. These are thought to be spuriously generated by the discontinuity in the profile derivatives.

(3) Although the entire semi-infinite flow is considered, there is no evidence of a continuous spectrum.

7.2 Comparison with the Spectrum of the Schrödinger Equation

There are some interesting similarities between the spectrum of the Orr-Sommerfeld equation and that of the much simpler Schrödinger equation which has been widely studied in the field of Quantum Mechanics.

Consider the one-dimensional Schrödinger equation

$$\left[-\frac{\hbar^2}{2m}\frac{d^2}{dz^2} + V(z) - E \right] \psi(z) = 0 \qquad (7.1)$$

in the case of the infinite square well potential

$$
\begin{aligned}
V(z) &\to \infty, && z < 0 \\
V(z) &= 0, && 0 \leq z \leq 2 \\
V(z) &\to \infty, && z > 2 \ .
\end{aligned}
\tag{7.2}
$$

The boundary conditions are simply

$$\psi(0) = \psi(2) = 0.$$

It is well known* that the energy spectrum is discrete and infinite. In this case, the energy eigenvalues are

$$E_n = \frac{\pi^2 \hbar^2}{8m} n^2 , \qquad n = 1,2,3, \ldots$$

with the corresponding eigenfunctions

$$\psi_n = \sin \frac{n\pi z}{2} \ .$$

This solution is remarkably similar to the plane Poiseuille spectrum discussed in Section 5.2 where, for large n, the real part of the eigenvalue is constant and the imaginary part is proportional to n^2. The finite width of the potential well corresponds to the finite width of the plane Poiseuille flow and in both cases the eigenfunctions are bound states, confined between parallel walls.

Now consider equation (7.1) applied to the potential

$$
\begin{aligned}
V(z) &\to \infty, && z < 0 \\
V(z) &= 0 && 0 \leq z \leq 1 \\
V(z) &= V_o && z > 1
\end{aligned}
\tag{7.3}
$$

---

* C.f. Matthews: "Introduction to Quantum Mechanics", McGraw-Hill.

with boundary conditions

$$\psi(0) = 0 \tag{7.4a}$$

$$\psi \to 0 \quad \text{as} \quad z \to +\infty \tag{7.4b}$$

The solution in this case is more complicated. For $E < V_o$, the eigenfunctions are given by

$$\psi(z) = \sin kz \qquad 0 \leq z \leq 1 \tag{7.5a}$$

$$\psi(z) = (\sin k)e^{-\kappa(z-1)} \qquad z > 1 \tag{7.5b}$$

where

$$k^2 = \frac{2mE}{\hbar^2}, \qquad \kappa^2 = \frac{2m(V_o-E)}{\hbar^2} \tag{7.6}$$

and

$$k \cot k = -\kappa . \tag{7.7}$$

The transcendental equation (7.7) alsc gives the eigenvalues. If E is nearly equal to V_o, (7.7) is approximately

$$\cot k = 0$$

so that $k = (2n-1)\frac{\pi}{2}$ and the energy eigenvalues are again proportional to n^2. However, since V_o is finite, the number of discrete states is also finite.

If $E > V_o$, the solution is

$$\psi(z) = \sin k_1 z \qquad 0 \leq z \leq 1 \tag{7.8a}$$

$$\psi(z) = A \sin(k_2 z - \varepsilon) \qquad z > 1 \tag{7.8b}$$

where

$$k_1^2 = \frac{2mE}{\hbar^2}, \qquad k_2^2 = \frac{2m(E-V_o)}{\hbar^2}$$

and the constants A and ε are determined by the continuity conditions at $z = 1$. There is no restriction on k_1 or k_2 and so the energy spectrum is continuous above $E = V_o$. It

should be noted that, strictly speaking, the eigenfunction (7.8) does not satisfy the outer boundary condition (7.4b) but it is bounded at infinity. It may be argued that this kind of solution is physically uninteresting anyway and that the main result is the existence of a finite number of bound states with non-zero amplitude outside the potential well.

Exactly the same features are apparent in the spatial or temporal spectrum of the Orr-Sommerfeld equation for Blasius flow. Only a finite number of eigenstates appear to exist but this number may be increased by increasing the Reynolds number R in the same way as the number of Schrödinger states may be increased by raising the potential V_o. Also, the Blasius states become more oscillatory and extend farther out into the free stream as the order of the state increases and this behaviour also occurs in the Schrödinger case since the wave number k of the eigenfunction increases and the exponential decay factor κ decreases as n increases.

No evidence for the existance of a continuous spectrum has been found in the Blasius case. However, if a continuous spectrum did exist, it would be very similar to the one in the Schrödinger example. The eigenfunctions would certainly be infinite in extent with little amplitude in the boundary layer itself compared with the free stream, where they would be purely sinusoidal in form. An infinite line of eigenvalues would occur on both the c-plane and the α-plane along the lines corresponding to $\gamma_r = 0$. (The actual position of these lines is given at the end of Section 3.2).

The similarity between the Blasius results and the simpler Schrödinger case discussed above is of some assistance in the physical explanation of the nature of the Blasius spectrum. It suggests that the few Blasius states which have been found are

the only ones which can be trapped within the boundary layer at a given Reynolds number and frequency (or wave number). In the Schrödinger case, there is a definite energy barrier above which no bound states are found. By analogy, there must be a similar barrier in the Blasius case, more difficult to define. For instance, there may be a limit in the phase velocity of the disturbance above which the wave would be travelling too fast in comparison with the slower mass of fluid in the boundary layer.

7.3 Final Remarks

The aim of this work has been to provide a thorough numerical investigation into the nature of the spectrum of the Orr-Sommerfeld equation for Blasius flow. Many new and hitherto unknown results have been obtained and, although no single study can be exhaustive, it is believed that most of the features of the spectrum which are capable of investigation by numerical methods have been discovered. While it is recognised that the accuracy of the results in certain cases could be improved, it is thought that in general other currently available numerical methods would be no more reliable than the present methods. This points to the desirability of using analytical methods in future work. There are two areas where further research would be particularly useful:

(1) The existence of a continuous spectrum.

(2) The structure of the spectrum near the source of eigenvalues.

The importance of the higher eigenstates in the non-linear development of the disturbance should not be underestimated. This has already been demonstrated in the case of plane Poiseuille flow by the remarkable work of Pekeris and Shkoller[33]. A similar eigenstate interaction model could be developed for Blasius flow but difficulties concerning the changing Reynolds number and the incompleteness of the spectrum would have to be resolved.

REFERENCES

1. Rayleigh, Lord 1880 Scientific Papers 1, 474-87, Cambridge.
2. Reynolds, O. 1883 Phil. Trans. 174, 935-82.
3. Lorentz, H.A. 1896 Collected Papers 4, 15-35, Nijhoff (1937).
4. Prandtl, L. 1904 Tech. Memor. nat. adv. Comm. Aero., Wash. No. 452.
5. Taylor, G.I. 1923 Phil. Trans. A223, 289-343.
6. Heisenberg, W. 1924 Tech. Memor. nat. adv. Comm. Aero., Wash. No. 1291.
7. Tollmien, W. 1929 Tech. Memor. nat. adv. Comm. Aero., Wash., No. 609.
8. Schlichting, H. 1933 Nachr. Ges. Wiss. Göttingen, Math.-phys. Kl., 181-208.
9. Schlichting, H. 1935 Tech. Memor. nat. adv. Comm. Aero., Wash. No. 1265.
10. Taylor, G.I. 1938 Proc. 5th Int. Congr. Appl. Mech., 294-310.
11. Lin, C.C. 1945 Quart. appl. Math. 3, 117-42, 218-34, 277-301.
12. Schubauer, G.B. & Skramstad, H.K. 1947 J. Res. Nat. Bur. Stand. 38, 251.
13. Tollmien, W. 1947 Z. angew. Math. Mech. 25/27, 33-50, 70-83.
14. Wasow, W. 1948 Ann. Math. (2) 49, 852-71..
15. Wasow, W. 1950 Ann. Math. 52, 350-61.
16. Wasow, W. 1953 Ann. Math. 58, 222-52.
17. Lin, C.C. 1955 "The Theory of Hydrodynamic Stability." Cambridge.
18. Thomas, L.H. 1953 Phys. Rev. (2) 91, 780-3.
19. Shen, S.F. 1954 J. aero. Sci. 21, 62-4.
20. Kurtz, E.F. 1961 Ph.D. Thesis, M.I.T.
21. Kaplan, R.E. 1964 Ph.D. Thesis, M.I.T.
22. Gaster, M. 1962 J. Fluid Mech. 14, 222-4.
23. Watson, J. 1962 J. Fluid Mech. 14, 211-21.
24. Michalke, A. 1964 J. Fluid Mech. 19, 543-56.

REFERENCES (Contd.)

25. Michalke, A. 1965 J. Fluid Mech. 23, 521-44.

26. Jordinson, R. 1970 J. Fluid Mech. 43, 801-11.

27. Ross, J.A., Barnes, F.H., Burns, J.G. & Ross, M.A.S. 1970 J. Fluid Mech. 43, 819-32.

28. Barry, M.D.J. & Ross, M.A.S. 1970 J. Fluid Mech. 43, 813-8.

29. Stuart, J.T. 1965 Appl. Mech. Rev. 18, 523-31.

30. Ross, M.A.S. 1973 AGARD Lecture Series No. 64, Paper 7.

31. Meksyn, D. & Stuart, J.T. 1951 Proc. Roy. Soc. A208, 517-26.

32. Stuart, J.T. 1960 J. Fluid Mech. 9, 353-70.

33. Pekeris, C.L. & Shkoller, B. 1969 J. Fluid Mech. 39, 611-27.

34. Bouthier, M. 1972 Journal de Mécanique 11, 599-621.

35. Ling, C-H & Reynolds, W.C. 1973 J. Fluid Mech. 59, 571-91.

36. Gaster, M. 1974 J. Fluid Mech. 66, 465-80.

37. Corner, D., Barry, M.D.J. & Ross, M.A.S. 1974 Aero. Res. Council Current Papers No. 1296.

38. Stewartson, K. & Stuart, J.T. 1971 J. Fluid Mech. 48, 529-45.

39. Morawetz, C.S. 1952 J. rat. Mech. Anal., Indiana Univ. 1, 579-603.

40. Grohne, D. 1954 Tech. Memor. nat. adv. Comm. Aero. , Wash., No. 1417.

41. Schensted, I.V. 1961 Ph.D. Thesis, University of Michigan.

42. Eckhaus, W. 1965 "Studies in Non-Linear Stability Theory", Springer-Verlag, Berlin.

43. Gallagher, A.P. & Mercer, A.McD. 1964 J. Fluid Mech. 18, 350-2

44. Gallagher, A.P. 1974 J. Fluid Mech. 65, 29-32.

45. Grosch, C.E. & Salwen, H. 1968 J. Fluid Mech. 34, 177-205.

46. Orszag, S.A. 1971 J. Fluid Mech. 50, 689-703.

47. Davey, A. & Drazin, P.G. 1969 J. Fluid Mech. 36, 209-18.

48. Salwen, H. & Grosch, C.E. 1972 J. Fluid Mech. 54, 93.

49. Jordinson, R. 1971 Phys. Fluids 14, 2535-7.

REFERENCES (Contd.)

50. Corner, D. 1973 Ph.D. Thesis, University of Edinburgh.

51. Mack, L.M. 1974 (private communication).

52. Davey, A. 1974 (private communication).

53. Jones, C.W. & Watson, E.J. 1963 "Laminar Boundary Layers", Oxford.

54. Blasius, H. 1908 Tech. Memor. nat. adv. Comm. Aero., Wash. No. 1256.

55. Pretsch, J. 1941 Jb. dtsch. Luftfahrtf. 1, 158-75.

56. Freymuth, P. 1966 J. Fluid Mech. 25, 683-704.

57. Rayleigh, Lord 1892 Scientific Papers 3, 575-84. Cambridge.

58. Noumerov, B.V. 1924 Mon. Not. R. Astr. Soc. 84, 180-6.

59. Osborne, M.R. 1967 SIAM J. Appl. Math. 15, 539-57.

60. Martin,R.S. & Wilkinson, J.H. 1968 Num. Math. 12, 369-76.

61. Esch, R.E. 1957 J. Fluid Mech. 3, 289-303.

62. Aiken, H.H. 1945 "Tables of the Modified Hankel Functions of Order One-Third and of their Derivatives", Harvard.

63. Betchov, R. & Criminale, W.O. "Stability of Parallel Flows", Academic Press.